


12
p.s.

DISTRIBUTION STATEMENT A
Approved for public release;
Distribution Unlimited


 D D C
 RECEIVED
 NOV 18 1977
 RECEIVED
 A

12

6 BEHAVIOR OF ELECTRIC POTENTIAL FIELDS
OVER RANDOMLY LAYERED EARTH MODELS.

9 Doctoral thesis,

11 19 Apr 77

12 122p.

DISTRIBUTION STATEMENT A
Approved for public release
Distribution Unlimited

By

10 Chong Yan/Lee

15 N00014-76-C-0750 new

DDC
RECEIVED
NOV 18 1977
A

A Thesis submitted to the Faculty and the Board of Trustees of the Colorado School of Mines in partial fulfillment of the requirements for the degree of Doctor of Philosophy in Geophysics.

Signed: Chong Yan Lee
Chong Yan Lee

Golden, Colorado

Date: April 19, 1977

Approved: George V. Keller
George V. Keller
Thesis Advisor and
Head of Department

Golden, Colorado

Date: April 19, 1977

No. to Section		<input checked="" type="checkbox"/>
Diff. Section		<input type="checkbox"/>
Availability Codes		
SPECIAL		
A		

Letter on file

ABSTRACT

Solutions are derived for the potential distributions over one-layer and two-layer random conductivity earth models for the direct current resistivity method. The random potential due to a stationary Gaussian random conductivity function is non-Gaussian and non-stationary. The ensemble and sample statistics of the random potential fields are examined.

The potential field due to dipole excitation is more sensitive to variations in conductivity in the subsurface than that due to monopole excitation. Random variations in conductivity at depth are difficult to detect.

Representative curves of the apparent resistivity and kernel functions are presented to show the effects of a random conductivity profile on them. These effects are appreciable and result in significant errors in the interpretation of resistivity data. However, noise of this kind is difficult to distinguish from the signal itself, especially in the presence of measurement noise. Nevertheless, variations in the conductivity profile should be recognized as an additional source of error in the interpretation of resistivity data.

CONTENTS

	<u>Page</u>
ABSTRACT.	iii
ILLUSTRATIONS	vi
ACKNOWLEDGEMENTS	ix
INTRODUCTION.	1
THE RANDOM CONDUCTIVITY PROBLEM	3
Statement of the Problem.	3
Boundary Conditions	6
Properties of the Random Function	7
General Solution.	10
Reduction to the One-Layer Case	12
THE ONE-LAYER CASE.	14
Monopole and Dipole Potentials.	14
Ensemble Statistics	16
Sample Statistics	18
Sample Realizations	27
Sensitivity to Resistivity Variations	40
Anisotropy.	44
Case I	45
Case II.	49
Macro-anisotropy	49
THE TWO-LAYER CASE.	51
Sample Realizations	52
Kernel function.	52

	<u>Page</u>
Apparent resistivity.	66
Ensemble Statistics.	78
Sample Statistics.	82
Effect on Interpretation of Data	82
CONCLUSIONS AND RECOMMENDATIONS.	91
APPENDICES	
A: Solution to the Problem of an Overburden with Random Conductivity	93
B: Solution to the Problem of a One-Layer Anisotropic Earth with a Random Con- ductivity Distribution	102
REFERENCES	111

ILLUSTRATIONS

<u>Figure</u>	<u>Page</u>
1. The two-layer random conductivity model. . . .	5
2. Covariance functions $C(x) = \exp(-x^2/(4a^2))$ of the random function $\eta(z)$	9
3. Monopole and dipole source arrays over one-layer random conductivity model.	15
4. Normalized covariance of monopole random potential for $\alpha = 0.15$	19
5. Normalized covariance of monopole random potential for $\alpha = 1.5$	20
6. Normalized covariance of dipole random potential for $\alpha = 0.15$	21
7. Normalized covariance of dipole random potential for $\alpha = 1.5$	22
8. Distributions of sample realizations of monopole random potential at $r = 0.5$	25
9. Distributions of sample realizations of dipole random potential at $r = 0.5$	26
10. Sample realization No. 1 of potential over random conductivity model.	28
11. Sample realization No. 1 of kernel and apparent resistivity functions over random conductivity model.	29
12. Sample realization No. 2 of potential over random conductivity model.	30
13. Sample realization No. 2 of kernel and apparent resistivity functions over random conductivity model.	31
14. Sample realization No. 3 of potential over random conductivity model.	32

<u>Figure</u>	<u>Page</u>
15. Sample realization No. 3 of kernel and apparent resistivity functions over random conductivity model.	33
16. Sample realization No. 4 of potential over random conductivity model.	34
17. Sample realization No. 4 of kernel and apparent resistivity functions over random conductivity model.	35
18. Wenner and Schlumberger electrode arrays	39
19. Normalized variance of random potential for $\alpha = 0.15$	42
20. Normalized variance of random potential for $\alpha = 1.5$	43
21. Normalized covariance of anisotropic monopole random potential for $\alpha = 1.5$ at $r_1 = 0.5$	46
22. Normalized covariance of anisotropic monopole random potential for $\alpha = 1.5$ at $r_1 = 2.0$	47
23. Normalized covariance of anisotropic dipole random potential for $\alpha = 1.5$ at $r_1 = 2.0$	48
24-27. Sample realization Nos. 1-4 of kernel function for $k = \pm 0.8$	54-57
28-34. Sample realization Nos. 1-7 of percent deviation in kernel and apparent resistivity functions for $k = \pm 0.8$	59-65
35. Sample realization No. 1 of percent deviation in kernel and apparent resistivity functions for $k = \pm 0.5$	67
36. Sample realization No. 1 of percent deviation in kernel and apparent resistivity functions for $k = \pm 0.99$	68
37-43. Sample realization Nos. 1-7 of apparent resistivity function for $k = \pm 0.8$	71-77
41. Normalized covariance of two-layer random kernel function for $\alpha = 0.05$	80

<u>Figure</u>	<u>Page</u>
45. Normalized covariance of two-layer random kernel function for $\alpha = 0.1$	81
46. Distributions of sample realizations of two- layer random kernel function for $\alpha = 0.05$. . .	83
47. Distributions of sample realizations of two- layer random kernel function for $\alpha = 0.5$. . .	84

ACKNOWLEDGEMENTS

I wish to express my appreciation to my thesis advisor Professor George V. Keller for his guidance and encouragement. A special word of thanks goes to Professor Richard Barakat of Harvard University for valuable suggestions and stimulating discussions during the course of this study.

I am grateful to Professors Ralph C. Holmer, David L. Butler, Walter W. Whitman and W. Rex Bull for their helpful comments.

It is a pleasure to thank Walter L. Anderson of the U.S. Geological Survey for his assistance.

This research was supported by a grant from the Office of Naval Research under Contract No. N00014-76-C-750.

Finally, I gratefully acknowledge the financial assistance for my graduate studies provided by a Fellowship from Universiti Sains Malaysia and a travel grant from the Fulbright-Hays program.

INTRODUCTION

One of the principal objectives of electrical methods in geophysical prospecting is the study and interpretation of resistivity distributions in the earth. To facilitate the interpretation of data simple earth models are assumed. The measured potential field is compared to the theoretical field computed for the models. Interpretation of subsurface electrical structure is based on the model which provides the best fit. In order to reduce the problem to manageable proportions, it has been standard practice to consider only discrete (or deterministic) model parameters. Such assumptions have generally been adequate for data interpretation. However, it is useful and instructive to utilize models which take into consideration the inherent variability of the earth's physical properties.

As a step in this direction, this study is directed at the problem of determining the potential distribution which arises from direct current flow in a medium in which the conductivity varies randomly with depth. The noise which is consequently introduced into the system is best handled statistically.

An earth model with a random conductivity profile has been previously considered in only one paper (Naidu, 1970) in the readily available geophysical literature. In this paper only the one-layer isotropic case was treated in any

detail. This study extends the scope of the original paper by examining in considerable depth various aspects of the statistical properties of random earth potentials. An analytic solution to the more useful and practical two-layer case is also presented. The effect of anisotropy on the random conductivity model is examined. The implications of the random distribution for resistivity inversion are also considered.

The primary purpose of this dissertation is to study in some detail the direct (or forward) problem without an understanding of which all the information contained in field data cannot be effectively utilized. It is of considerable practical importance to be able to judge quantitatively the effects of the random properties of the conductivity distribution in the earth on the direct current resistivity method.

THE RANDOM CONDUCTIVITY PROBLEM

Direct current resistivity methods used in geophysical exploration consist essentially of the measurement and interpretation of electric potentials on the surface of the earth. These potentials result from the introduction of an electric current into the ground through various electrode arrays. The observed potential field is a function of the resistivity distribution in the subsurface. The interpretation of the acquired data in terms of subsurface electrical structure is an inverse (or inversion) problem. For this inversion to be possible, the solution to the direct (or forward) problem is required, that is, given a model of the earth, one needs to compute the corresponding potential distribution on the surface.

Statement of the Problem

The simplest and most widely used model assumes a half-space composed of discrete horizontal layers with sharp discontinuities in the electrical properties of the medium at the layer boundaries. Each layer is homogeneous and assumed to be either isotropic or anisotropic. Isotropy is the more common assumption however. The solution to this basic resistivity problem is well documented in the literature, for example Grant and West (1965), Keller and Frischknecht (1966), Van Nostrand and Cook (1966) and Bhattacharya and Patra (1968). Solutions have also been published for models in which the conductivity, instead of being constant over

discrete vertical intervals, is a continuous function of depth (Slichter, 1933, Langer, 1933, Meinardus, 1967 among others).

In this study the problem is generalized by assuming that the conductivity is not a deterministic function of depth z but is instead, a random function of z which is, nevertheless, closely clustered around its deterministic value. It was noted by Keller (1968) that resistivity probability density curves usually represent multimodal log-normal distributions; this is due to the presence of several lithologic types. To make the problem tractable mathematically, only unimodal normal distributions of conductivities are considered here.

Consider a model (Figure 1) in which the first layer (the overburden) of thickness h has a random conductivity profile given by

$$\sigma_1(z) = \sigma_1^0 (1 + \epsilon n(z)) \quad (2-1)$$

where σ_1^0 , a constant, is the deterministic (in this case, the mean) conductivity, ϵ is a small parameter ($\epsilon \ll 1$) and $n(z)$ is a zero-mean Gaussian random function with a prescribed covariance function C . Thus,

$$\langle n(z) \rangle = 0 \quad (2-2)$$

$$\text{and} \quad \langle n(z_1) n(z_2) \rangle = C(|z_1 - z_2|) \quad (2-3)$$

where $\langle \cdot \rangle$ denotes ensemble average or expected value.

The second layer (the basement) is assumed to have a constant conductivity σ_2^0 . Both layers are assumed to be isotropic. The first layer is isotropic only on the micro-

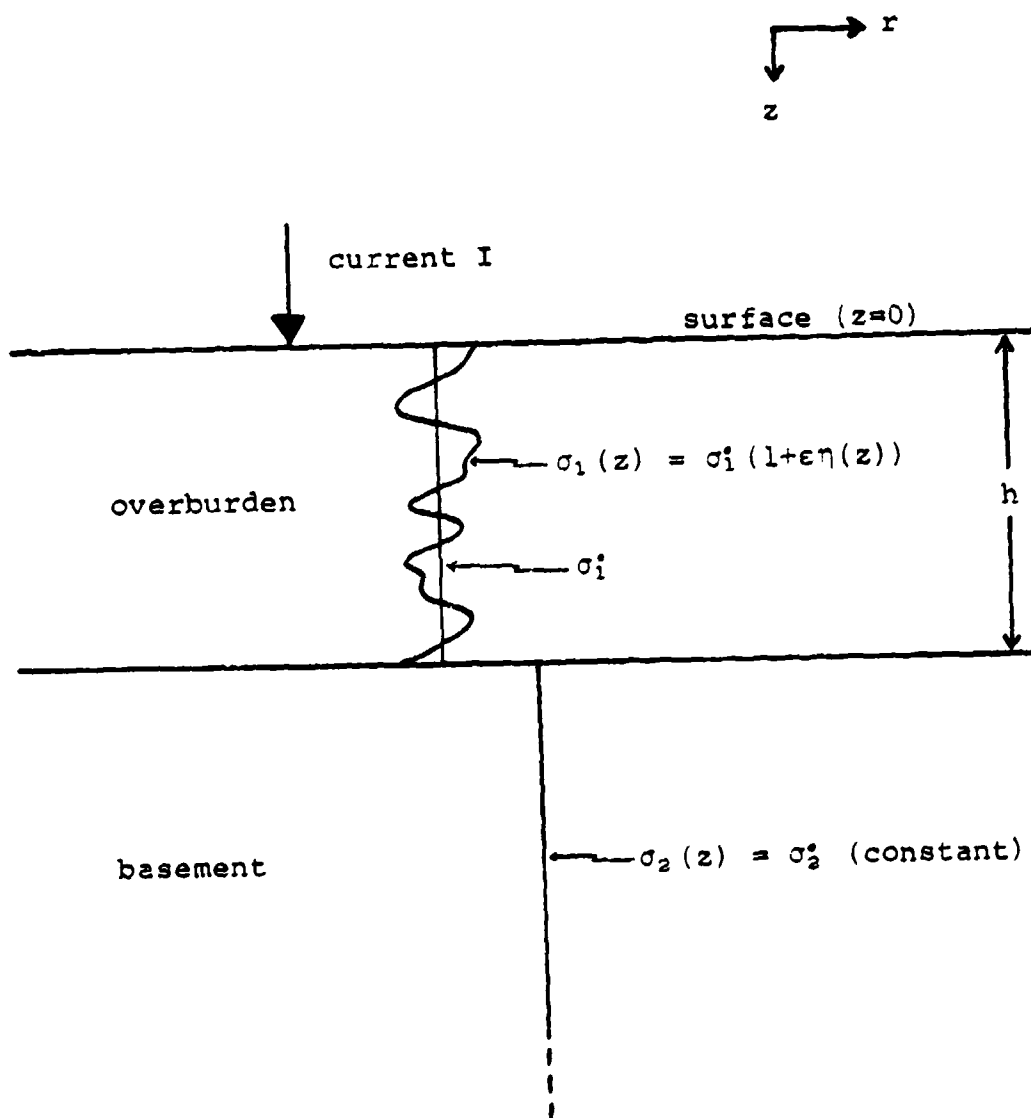


Figure 1. The two-layer random conductivity model.

scopic scale; macro-anisotropy is implicit in a random conductivity profile.

The problem is to determine the potential distribution which would result from the introduction of a direct current of strength I into the medium described above through an electrode located on the surface. The solution is derived by solving the applicable differential equation with the appropriate boundary conditions.

Boundary Conditions

Laplace's equation, in cylindrical coordinates, for inhomogeneous isotropic media is

$$\sigma(z) \frac{\partial^2 V}{\partial r^2} + \frac{1}{r} \frac{\partial V}{\partial r} + \frac{d\sigma(z)}{dz} \frac{\partial V}{\partial z} + \sigma(z) \frac{\partial^2 V}{\partial z^2} = 0 \quad (2-4)$$

This equation applies to both layers and V is the electric potential in each. Let $V_a(r, z)$ and $V_b(r, z)$ be the potentials in the first and second layers respectively.

The boundary conditions to be satisfied can be summarized as follows:

$$(a) \quad V_i(r, z) \rightarrow 0 \quad \text{as} \quad r \rightarrow \infty, \quad i = a, b \quad (2-5)$$

$$(b) \quad V_a \rightarrow \frac{I}{2\pi\sigma_1(0)r} \quad \text{as} \quad r \rightarrow 0 \quad \text{at} \quad z = 0 \quad (2-6)$$

$$(c) \quad V_b \rightarrow 0 \quad \text{as} \quad z \rightarrow \infty \quad (2-7)$$

$$(d) \quad \left. \frac{\partial V_a}{\partial z} \right|_{z=0} = \begin{cases} 0 & , \quad r \neq 0 \\ -\infty & , \quad r = 0 \end{cases} \quad (2-8)$$

$$(e) \quad V_a = V_b \quad \text{at} \quad z = h \quad (2-9)$$

$$(f) \quad \sigma_1(h) \left. \frac{\partial V_a}{\partial z} \right|_{z=h} = \sigma_2(h) \left. \frac{\partial V_b}{\partial z} \right|_{z=h} \quad (2-10)$$

Properties of the Random Function

Before proceeding with the solution, it is pertinent to review the properties of the stationary Gaussian random function $\eta(z)$ which will be useful in formulating the solution to the boundary value problem.

The integral canonical representation (Pugachev, 1965, p. 309) of $\eta(z)$ is

$$\eta(z) = \int_{-\infty}^{\infty} N(\omega) e^{i\omega z} d\omega \quad (2-11)$$

where $N(\omega)$ is white noise of the transform variable ω , the intensity of which is equal to the spectral density $S(\omega)$ of the random function $\eta(z)$. In other words, the random process $N(\omega)$ is zero-mean and uncorrelated (see also Koopmans, 1974), that is,

$$\langle N(\omega) \rangle = 0$$

and

$$\langle N(\omega_1) N(\omega_2) \rangle = S(\omega_1) \delta(\omega_1 - \omega_2) \quad (2-12)$$

where δ is the Dirac function.

It is further noted that

$$N(\omega) = \frac{1}{2\pi} \int_{-\infty}^{\infty} \eta(z) e^{-i\omega z} dz \quad (2-13)$$

If $(z_1 - z_2)$ is denoted by x , it can be shown (Pugachev, 1965) that

$$C(x) = \int_{-\infty}^{\infty} S(\omega) e^{i\omega x} d\omega \quad (2-14)$$

and

$$S(\omega) = \frac{1}{2\pi} \int_{-\infty}^{\infty} C(x) e^{-i\omega x} dx \quad (2-15)$$

where $C(x)$ is the covariance of $\eta(z)$. Thus $C(x)$ and $S(\omega)$ form a Fourier transform pair.

Boundary condition (2-8) requires that η be an even function of z . This, in turn, implies that $N(\omega)$ is an even function of ω . These symmetry relations will simplify considerably the equations above so that only real terms remain as the imaginary ones drop out.

Assume a covariance function of the form

$$C(x) = q^2 \exp(-x^2/(4\alpha^2)) \quad (2-16)$$

where q^2 is the variance of $\eta(z)$ and

α is an arbitrary constant which determines the degree of correlation. The exponential term in equation (2-16) is the correlation function of $\eta(z)$. Figure 2 shows the function $C(x)$ for various values of the parameter α .

Since the covariance function C of a real stationary random function is an even function of x , its spectral density S is also an even function. Corresponding to $C(x)$ as given above we have the spectral density function

$$S(\omega) = \frac{\alpha}{\sqrt{\pi}} q^2 e^{-\alpha^2 \omega^2} \quad (2-17)$$

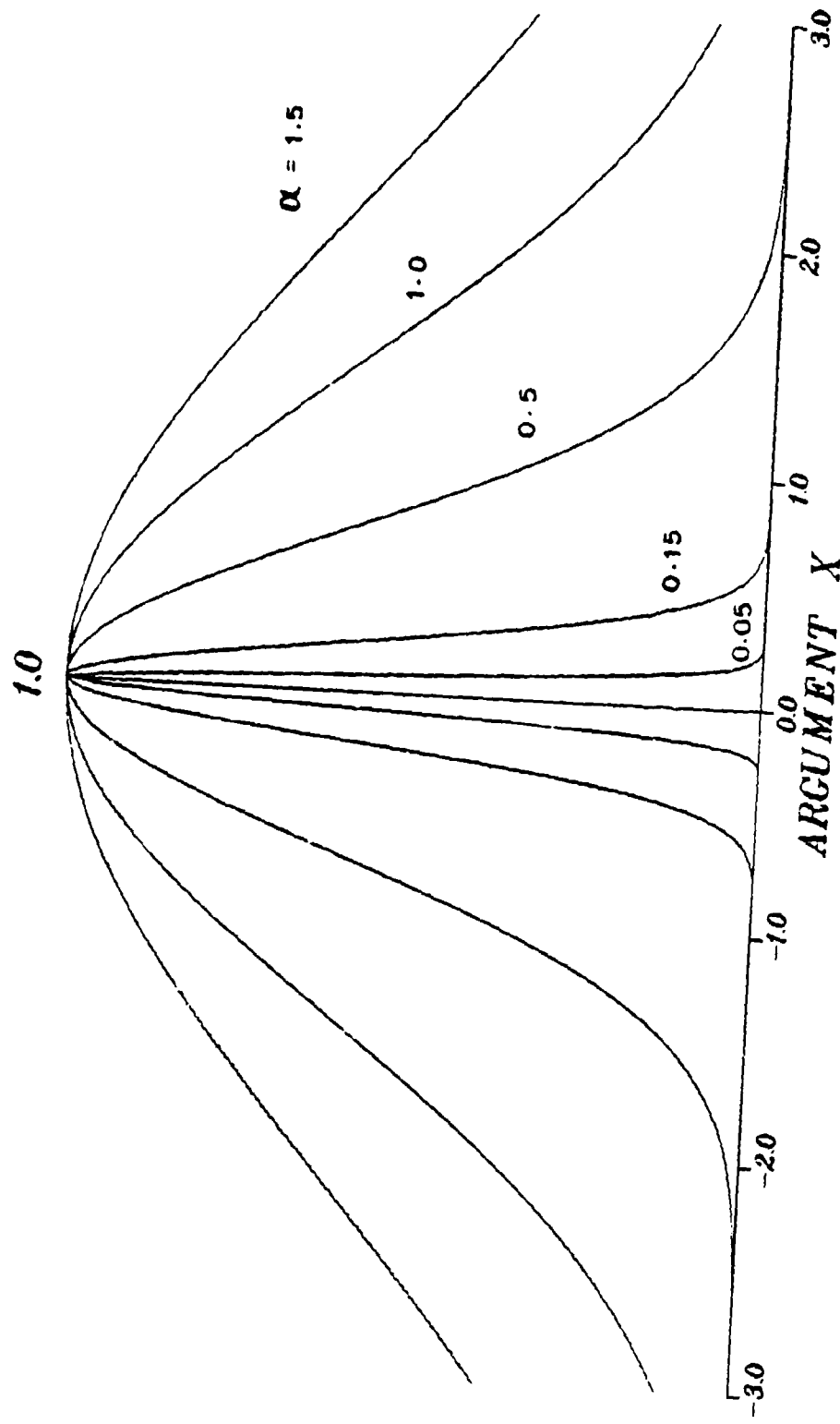


Figure 2. Covariance functions $C(x) = \exp(-x^2/(4\alpha^2))$ of the random function $\eta(z)$.

General Solution

To solve the two-layer stochastic problem, as with the deterministic, the variables are first separated:

$$V(r, z) = R(r)P(z)$$

Equation (2-4) then becomes

$$R''(r) + \frac{1}{r}R'(r) + \lambda^2 R(r) = 0 \quad (2-18)$$

and

$$(\sigma(z) P'(z))' - \lambda^2 \sigma(z) P(z) = 0 \quad (2-19)$$

where λ is the separation constant and primes denote differentiation with respect to the parameters.

The equation in r is Bessel's equation and its solution is $J_0(\lambda r)$ for both layers. The solution to equation (2-19) for the second layer is $e^{-\lambda z}$. For the stochastic first layer, however, the solution to (2-19) is more mathematically involved and the reader is referred to Appendix A for the complete development of the solution. Only the final expressions will be presented here.

The potential on the surface, to a first-order approximation, can be expressed as

$$V(r, 0) = V_0(r, 0) + \epsilon V_1(r, 0) + O(\epsilon^2) \quad (2-20)$$

where r is the distance of the point of measurement from the current source. The first term V_0 is recognized as the potential due to a "deterministic" two-layer case in which both layers have constant conductivities. Thus

$$V_0(r, 0) = \frac{A}{\sigma_1^0} \int_0^{\infty} K_0(\lambda) J_0(\lambda r) d\lambda \quad (2-21)$$

where $A \triangleq \frac{I}{2\pi}$

and

$$K_0(\lambda) = \frac{1 + ke^{-2\lambda h}}{1 - ke^{-2\lambda h}} \quad (2-22)$$

The reflection coefficient k is defined as

$$k \triangleq \frac{\sigma_1^0 - \sigma_2^0}{\sigma_1^0 + \sigma_2^0}$$

For convenience, the function K_0 will be referred to as the deterministic kernel (corresponding to the so-called Slichter kernel in deterministic models) and V_0 will be called the deterministic potential.

The term V_1 can be viewed as a first-order perturbation of V_0 due to the fact that the conductivity of the first layer is not a constant, but is a random function of depth.

In Appendix A, the following solution is derived:

$$V_1(r, 0) = \frac{A}{\sigma_1^0} \int_0^{\infty} K_1(\lambda) J_0(\lambda r) d\lambda \quad (2-23)$$

$$\begin{aligned} \text{where } K_1(\lambda) = & - \frac{8\lambda^2 v}{\phi} \int_0^{\infty} \frac{N}{\mu} d\omega \\ & + \frac{8\lambda^2(1-k^2)e^{-2\lambda h}}{\phi^2} \int_0^{\infty} \frac{N \cos \omega h}{\mu} d\omega \\ & - \frac{4\lambda(1+k^2)e^{-2\lambda h}}{\phi^2} \int_0^{\infty} \frac{N \omega \sin \omega h}{\mu} d\omega \quad (2-24) \end{aligned}$$

For brevity in notation the following symbols have been used:

$$\phi = 1 - ke^{-2\lambda h}$$

$$\psi = 1 + ke^{-2\lambda h}$$

$$\mu = \omega^2 + 4\lambda^2$$

It is convenient to refer to V_1 and K_1 as the stochastic (or random) potential and the stochastic (or random) kernel respectively.

Equations (2-21) through (2-24) together represent the general solution to the two-layer stochastic boundary value problem.

Reduction to the One-Layer Case

Let the stochastic first layer extend to infinity in the z direction. The model then becomes a half-space whose conductivity varies randomly about its mean (or equivalently, a randomly layered semi-infinite medium).

The solution to this boundary value problem is readily obtained from the general solution above by letting the overburden thickness h tend to infinity. Thus

$$K_0(\lambda) = 1 \quad (2-25)$$

$$V_0(r, 0) = \frac{A}{r\sigma_1^0} \quad (2-26)$$

$$K_1(\lambda) = -8\lambda^2 \int_0^\infty \frac{N}{u} d\omega \quad (2-27)$$

In this special case K_0 and V_0 are, respectively, the kernel and potential functions of a homogeneous isotropic half-space. V_1 is the perturbation potential which arises from the random nature of the conductivity profile.

The equations above are in agreement with those derived by Naidu (1970) for the one-layer case. The anisotropic one-layer stochastic problem is solved directly in Appendix B using a procedure different from Naidu's. In addition, the concept of anisotropy is carried further here than in the original paper.

THE ONE-LAYER CASE

Considerable insight into the random conductivity problem may be gained by examining first the statistical properties of the single layer case. To simplify the discussion, it will be confined mainly to the isotropic case. Anisotropy is dealt with separately at the end of the chapter.

Monopole and Dipole Potentials

All the expressions for the potentials which were presented in the previous chapter apply to a monopole source. If, instead, the source is a dipole (Figure 3), it can be shown that we merely have to replace A by B and $J_0(\lambda r)$ by $\lambda J_1(\lambda r)$ in all previous equations. The kernel functions, being independent of electrode configurations, remain unchanged. Thus, denoting dipole potentials by U , to distinguish them from monopole potentials V , we have

$$U_0(r, \phi) = \frac{B}{r^2 \sigma_1^0} \quad (3-1)$$

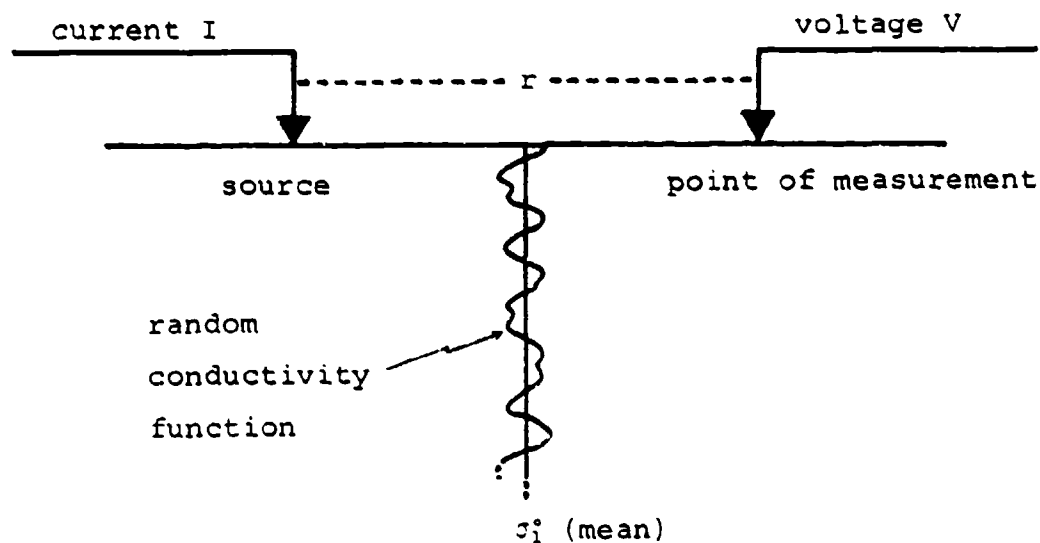
$$U_1(r, \phi) = \frac{B}{\sigma_1^0} \int_0^\infty K_1(\lambda) \lambda J_1(\lambda r) d\lambda \quad (3-2)$$

where K_1 is given in equation (2-27) and

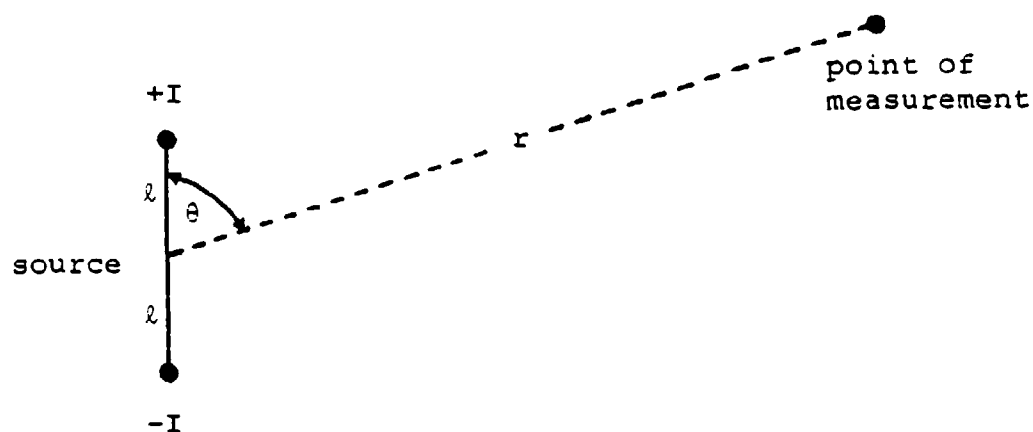
$$B \triangleq \frac{I l \cos \theta}{\pi}$$

l = half-length of dipole source

θ = azimuth of the point of measurement from the dipole.



(a) Monopole source (cross-sectional view)



(b) Dipole source (plan view)

Figure 3. Monopole and dipole source arrays over one-layer random conductivity model.

For the sake of brevity in notation all explicit references to the parameters of the potentials will be suppressed; unless otherwise stated, they are understood to be $(r, 0)$.

After normalizing the stochastic potentials by their respective deterministic potentials, reversing the order of integration and integrating once we obtain

$$\begin{aligned}\tilde{V}_1 &= \frac{V_1}{V_0} = 2 \int_0^\infty \left\{ \frac{\pi}{2} \frac{\omega r}{2} Q_0\left(\frac{\omega r}{2}\right) - 1 \right\} N(\omega) d\omega \\ &= 2 \int_0^\infty g_1(\omega r) N(\omega) d\omega\end{aligned}\quad (3-3)$$

and

$$\begin{aligned}\tilde{U}_1 &= \frac{U_1}{U_0} = 2 \int_0^\infty \left[\left(\frac{\omega r}{2}\right)^2 \left\{ 1 - \frac{\pi}{2} Q_1\left(\frac{\omega r}{2}\right) \right\} - 1 \right] N(\omega) d\omega \\ &= 2 \int_0^\infty g_2(\omega r) N(\omega) d\omega\end{aligned}\quad (3-4)$$

where $Q_1(x) \triangleq I_1(x) - L_1(x)$

$I_1(x)$ = modified Bessel function of order 1.

$L_1(x)$ = modified Struve function of order 1.

For details of the derivation of the equations above the reader is referred to Appendix B.

Ensemble Statistics

Evidently the normalized random potentials \tilde{V}_1 and \tilde{U}_1 are non-Gaussian random functions. It is instructive to examine their ensemble statistics.

Their means are obviously zero because the random function $N(\omega)$ is zero-mean. The covariance of \tilde{V}_1 is

$$\begin{aligned} \langle \tilde{V}_1(r_1) \tilde{V}_1(r_2) \rangle &= 4 \int_0^\infty \int_0^\infty g_1(\omega r_1) g_1(\omega r_2) \langle N(\omega_1) N(\omega_2) \rangle d\omega_1 d\omega_2 \\ &= 4 \int_0^\infty g_1(\omega r_1) g_1(\omega r_2) S(\omega) d\omega \\ &= \frac{4\alpha q^2}{\sqrt{\pi}} \int_0^\infty g_1(\omega r_1) g_1(\omega r_2) e^{-\alpha^2 \omega^2} d\omega \quad (3-5) \end{aligned}$$

It is to be noted that equations (2-12) and (2-17) have been used in the derivation above.

The normalized covariance is defined as

$$R_1(r_1, r_2) = \frac{\langle \tilde{V}_1(r_1) \tilde{V}_1(r_2) \rangle}{\{ \langle \tilde{V}_1(r_1) \tilde{V}_1(r_1) \rangle \langle \tilde{V}_1(r_2) \tilde{V}_1(r_2) \rangle \}^{\frac{1}{2}}} \quad (3-6)$$

For dipole excitation the corresponding expressions

$$\text{are } \langle \tilde{U}_1(r_1) \tilde{U}_1(r_2) \rangle = \frac{4\alpha q^2}{\sqrt{\pi}} \int_0^\infty g_2(\omega r_1) g_2(\omega r_2) e^{-\alpha^2 \omega^2} d\omega \quad (3-7)$$

and

$$R_2(r_1, r_2) = \frac{\langle \tilde{U}_1(r_1) \tilde{U}_1(r_2) \rangle}{\{ \langle \tilde{U}_1(r_1) \tilde{U}_1(r_1) \rangle \langle \tilde{U}_1(r_2) \tilde{U}_1(r_2) \rangle \}^{\frac{1}{2}}} \quad (3-8)$$

The Q_1 functions were evaluated by means of polynomial approximations and power series expansions (Abramowitz and Stegun, 1965, p. 378 and p. 498). As the argument increases from zero Q_0 decreases monotonically from 1.0 to zero while Q_1 increases monotonically from zero to its asymptotic value of $2/\pi$. The exponential term in equations (3-5) and (3-7) ensure rapid convergence of the integrals. Using numerical integration techniques the normalized covariance functions R_1

and R_2 were computed for five representative values of α and for various distances r from the source.

Some typical results are shown in Figures 4 through 7. From equation (2-16) and Figure 2, it is obvious that a smaller value of the parameter α implies that the random function $\eta(z)$ is less correlated and vice versa. Figures 4 and 5 show that as α decreases the covariance curves become narrower, that is, the normalized random potentials become less correlated. Hence, it can be concluded that as the correlation of the random conductivity function decreases, the correlation of the normalized random monopole potential decreases too.

Similar conclusions can be drawn for the normalized random potentials which result from dipole excitation (Figures 6 and 7).

Sample Statistics

The study of the sample statistics of the random potentials requires the generation of a large number of sample realizations of the random potentials for both the monopole and dipole cases. (A sample realization is an observation on a random process.) In order to do this the random potentials have to be expressed in terms of the function $\eta(z)$ explicitly.

For the monopole case, it is recalled from equations (2-23) and (2-27) that

$$V_1 = A^* \int_0^\infty -8\lambda^2 J_0(\lambda r) \int_0^\infty \frac{N(\omega)}{\mu} d\omega d\lambda \quad (3-9)$$

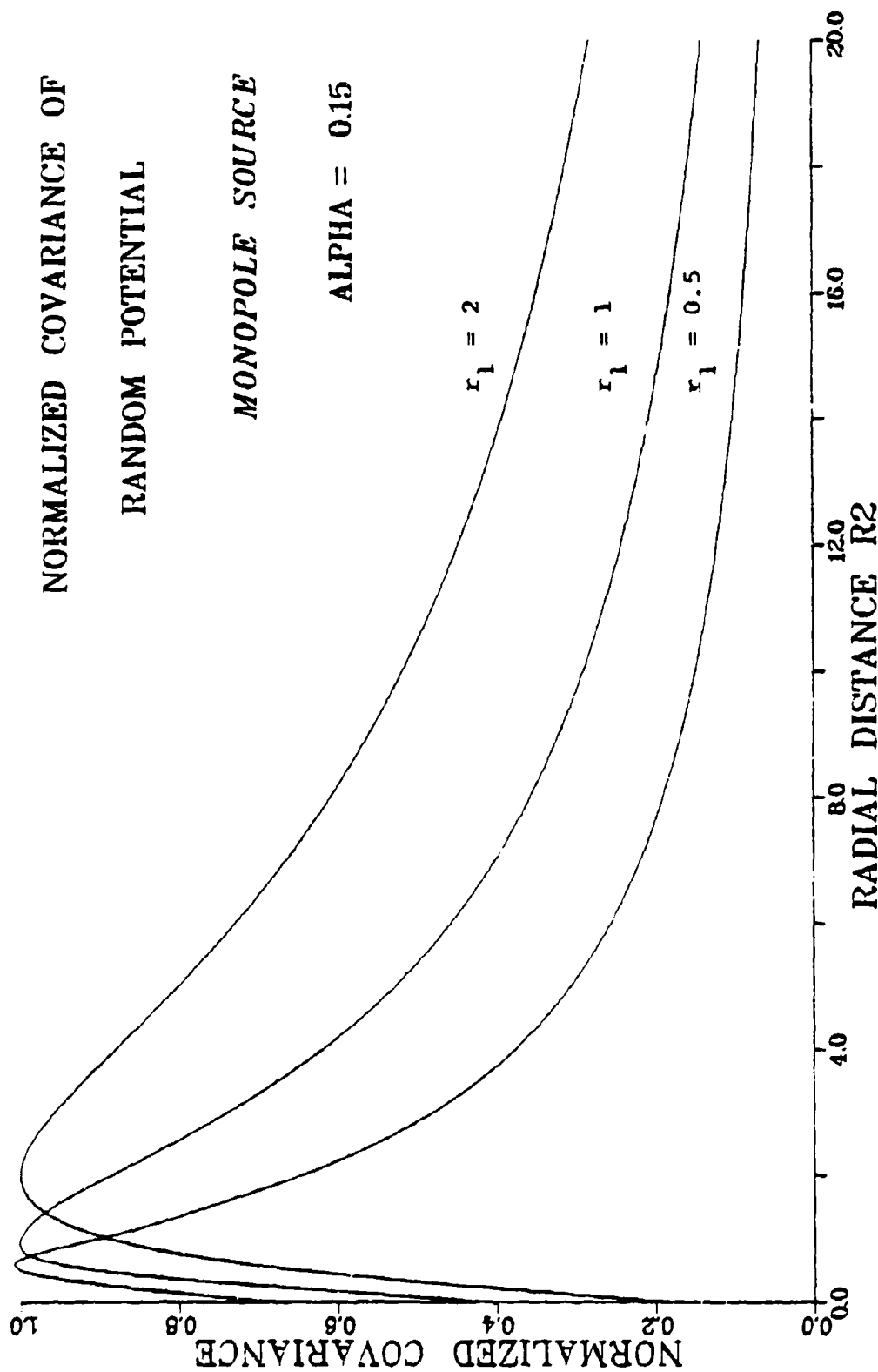


Figure 4. Normalized covariance of monopole random potential for $\alpha = 0.15$.

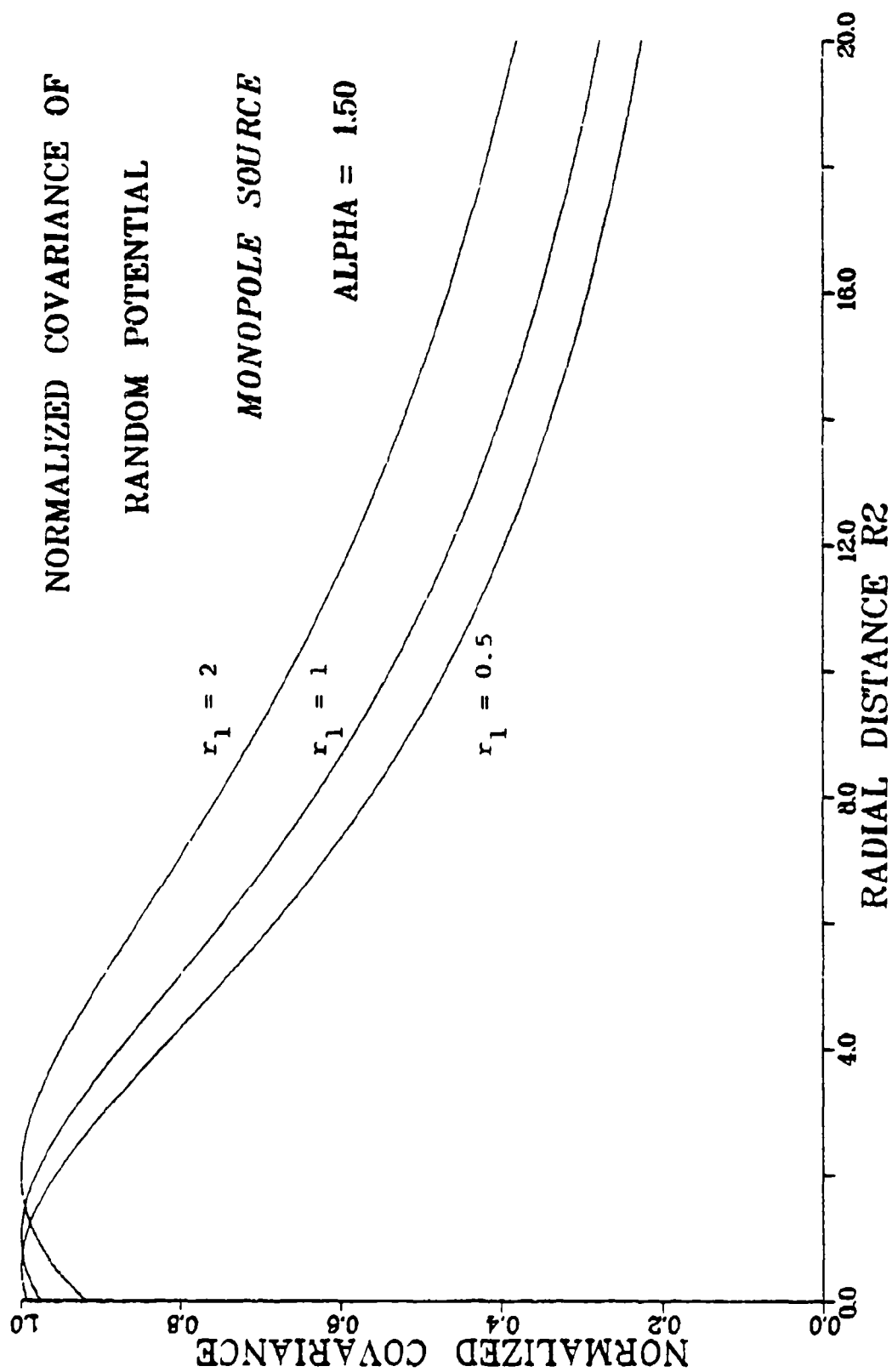


Figure 5. Normalized covariance of monopole random potential for $\alpha = 1.5$.

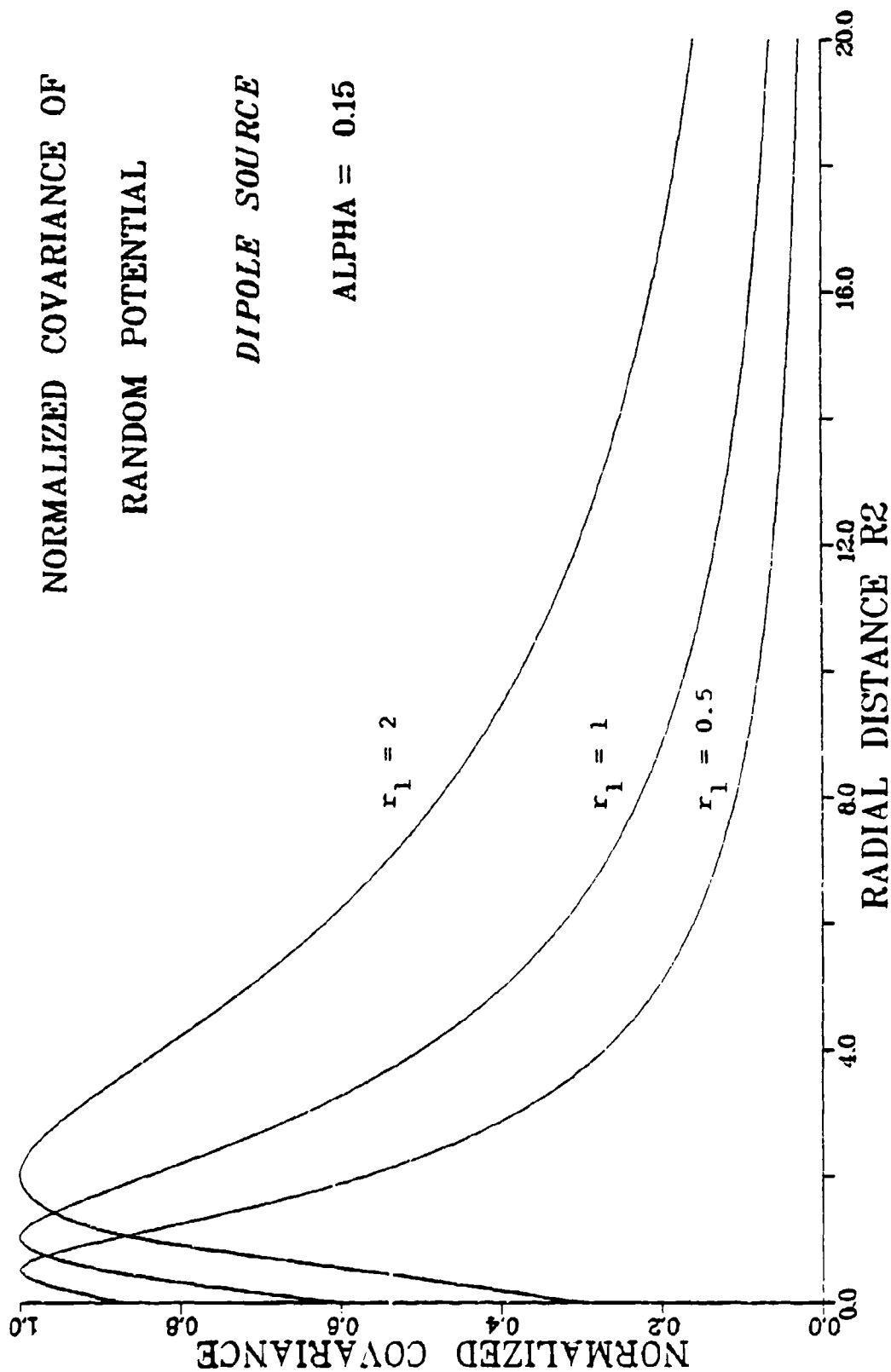


Figure 6. Normalized covariance of dipole random potential for $\alpha = 0.15$.

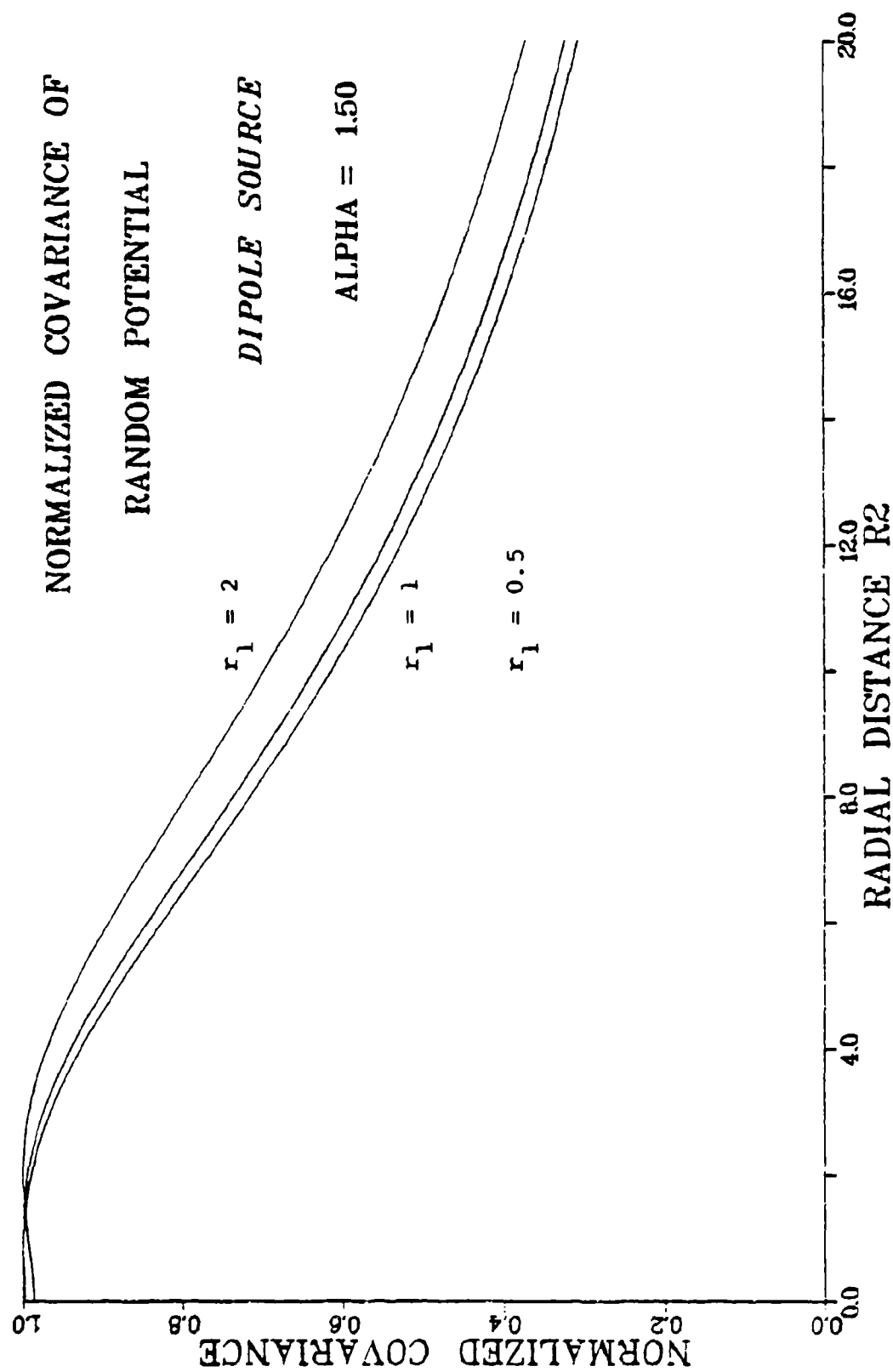


Figure 7. Normalized covariance of dipole random potential for $\alpha = 1.5$.

where $A^* = A/\sigma_1^0$

and $\mu = \omega^2 + 4\lambda^2$

Substituting for $N(\omega)$ with equation (2-13) and changing the order of integration we have

$$V_1 = -\frac{8A^*}{\pi} \int_0^\infty \lambda^2 J_0(\lambda r) \int_0^\infty \eta(z) \int_0^\infty \frac{\cos \omega z}{\mu} d\omega dz d\lambda \quad (3-10)$$

Evaluating the third integral analytically (Dwight, 1961)

we obtain

$$V_1 = -2A^* \int_0^\infty \eta(z) \int_0^\infty \lambda e^{-2\lambda z} J_0(\lambda r) d\lambda dz \quad (3-11)$$

Differentiating the Lipschitz integral (Watson, 1966)

$$\int_0^\infty e^{-2\lambda z} J_0(\lambda r) d\lambda = (r^2 + 4z^2)^{-\frac{1}{2}}$$

with respect to z the second integral in equation (3-11)

can also be evaluated analytically. Thus,

$$\begin{aligned} V_1 &= -4A^* \int_0^\infty \frac{\eta(z) z dz}{(r^2 + 4z^2)^{3/2}} \\ &= -4A^* M(r) \end{aligned} \quad (3-12)$$

When the dipole case is similarly handled we have

$$\begin{aligned} U_1 &= -12B^* r \int_0^\infty \frac{\eta(z) z dz}{(r^2 + 4z^2)^{5/2}} \\ &= -12B^* D(r) \end{aligned} \quad (3-13)$$

where

$$B^* = B/\sigma_1^0$$

The stationary Gaussian random function $\eta(z)$ was generated by standard procedures (see, for example, Newman and Odell, 1971 and Hemmerle, 1967). Essentially, Gaussian weights were applied to unit normal random variables obtained via central limit convergence from uniform random variables. The latter were supplied by a random number generator. The subroutine for generating $\eta(z)$ was modified from a version prepared by Barakat (personal communication, 1976).

It is evident that the denominators in the integrals $M(r)$ and $D(r)$ will ensure rapid convergence. Two hundred sample realizations for each of several selected values of r and α were computed for both functions $M(r)$ and $D(r)$. The results were tabulated in the form of histograms, examples of which are presented in Figures 8 and 9 for the monopole and dipole cases respectively.

The computed means are generally less than 0.01. These are close enough to the theoretical value of zero within the limits of sampling error. The standard deviations are of the order of 0.1 and the coefficients of skewness (normalized third product moments) are not greater than about 0.1 in magnitude.

All distributions of the random monopole and dipole potentials generated for various values of r and α were subjected to the chi-square goodness of fit test (Walpole and Meyers, 1972, for example). It was found that at the 5% level of significance the Gaussian distribution provides a

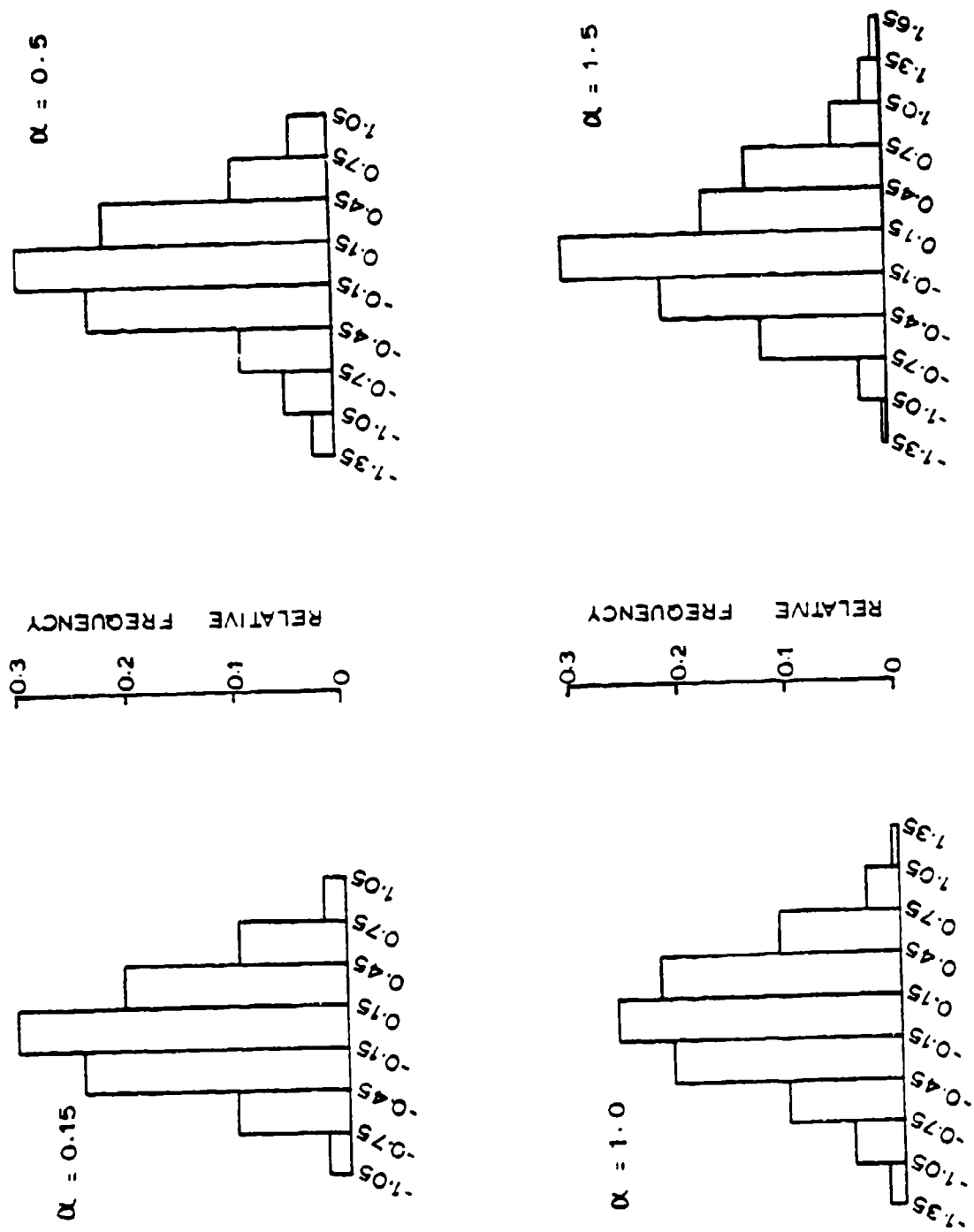


Figure 8. Distributions of sample realizations of monopole random potential at $r = 0.5$.

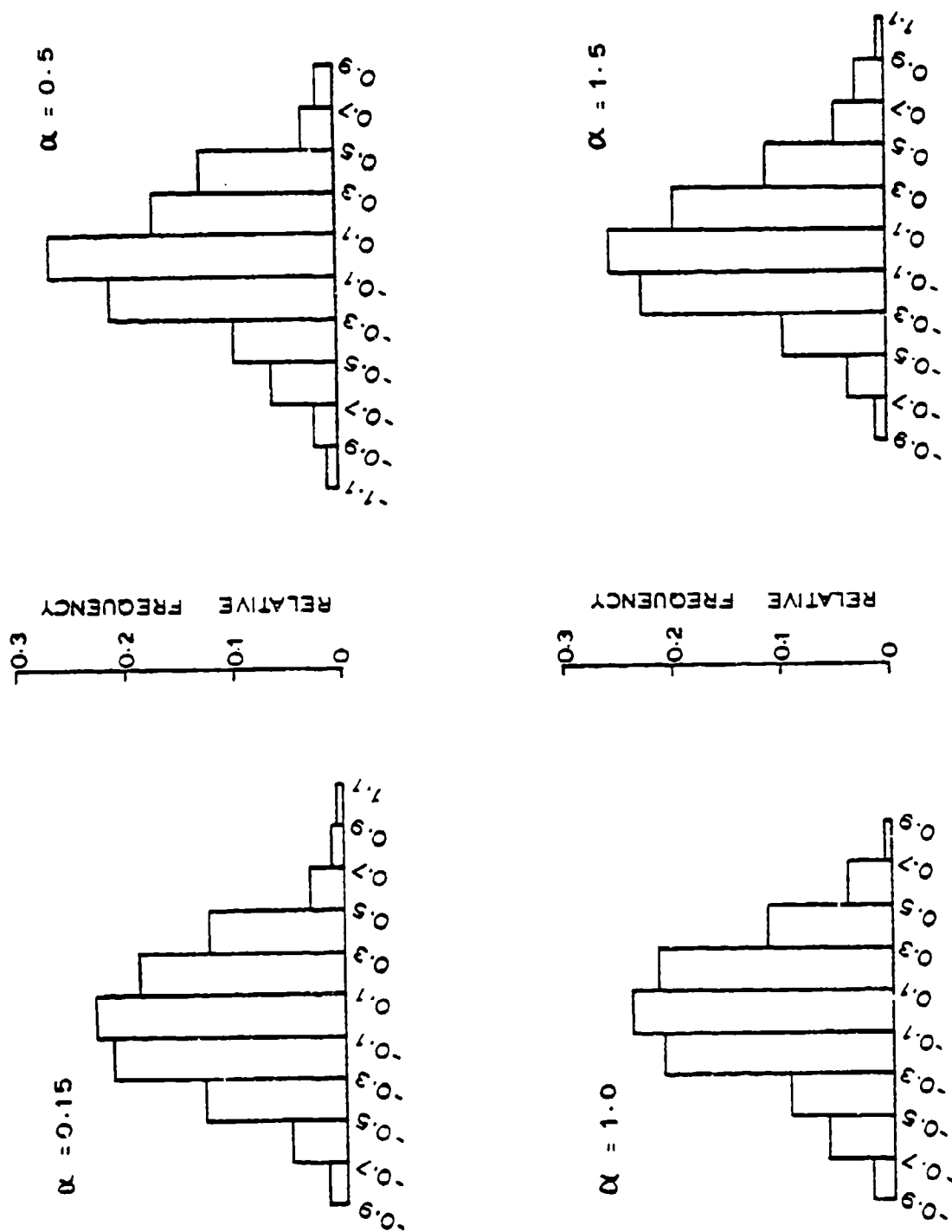


Figure 9. Distributions of sample realizations of dipole random potential at $r = 0.5$.

good fit for all the distributions of random potentials that were generated. The sample statistics therefore indicate that the normalized random potentials \tilde{V}_1 and \tilde{U}_1 are normally distributed, at the 5% level of significance, about their mean (deterministic) values.

Sample Realizations

It is informative to see how the random function $\eta(z)$ affects the measured voltage, the kernel function and the apparent resistivity. Some examples are shown here.

As noted earlier, the total potential for monopole excitation, to a first-order approximation, is

$$\begin{aligned} V(r) &= V_0(r) + \epsilon V_1(r) \\ &= \frac{A^*}{r} - \epsilon 4A^* M(r) \end{aligned}$$

Normalizing by A^* the expression above becomes

$$V^*(r) = \frac{1}{r} - 4\epsilon M(r) \quad (3-14)$$

Similarly, for the dipole case, after normalizing by B^* the equation is

$$U^*(r) = \frac{1}{r^2} - 12\epsilon D(r) \quad (3-15)$$

Four representative sample realizations of the total potential measured over a random medium for both source arrays are shown in Figures 10, 12, 14 and 16. In the figures, the solid lines represent the "normal" potential measured over a homogeneous half-space. The curves with circles superimposed show what the measured voltages will be if the random con-

T-1950

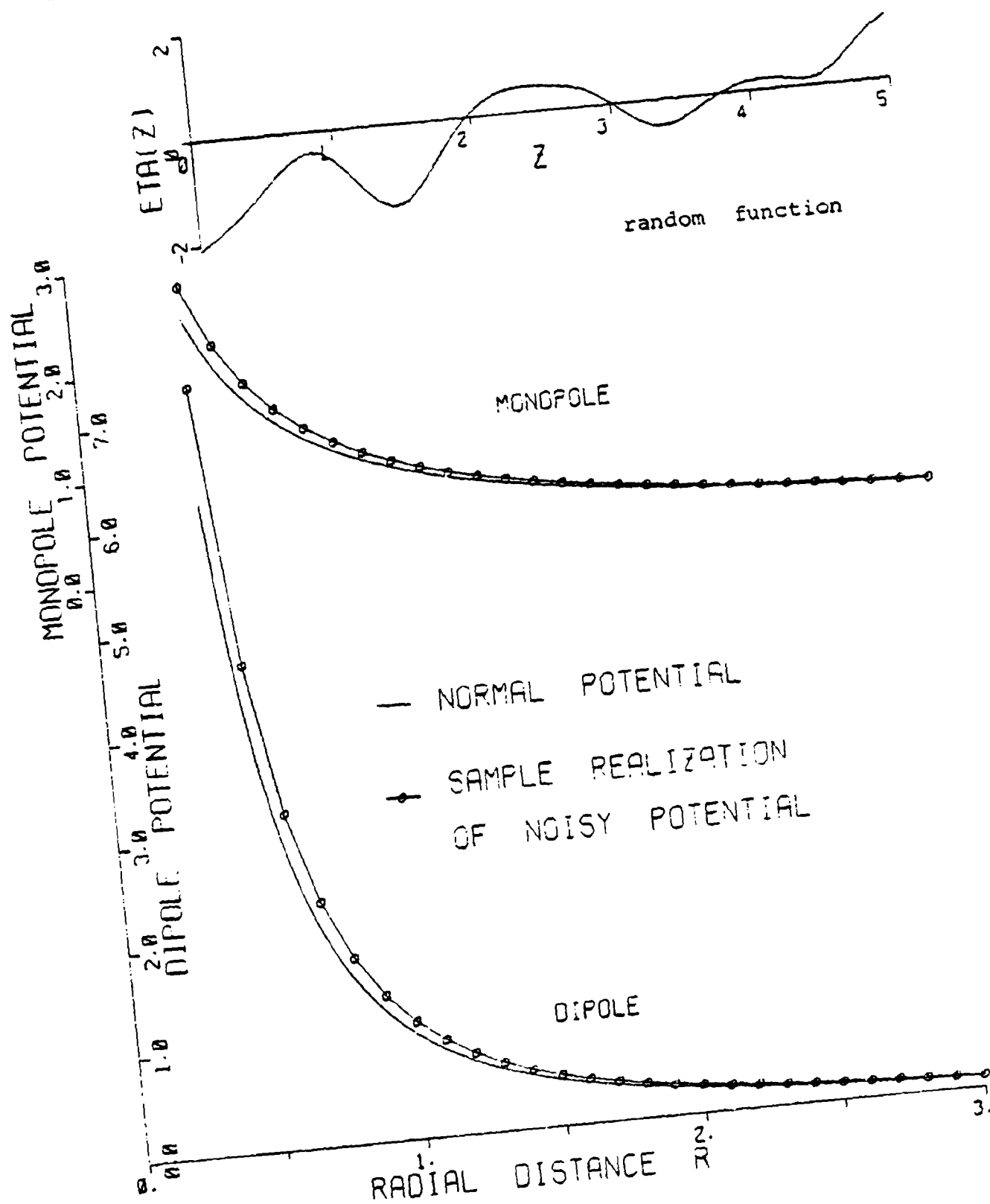


Figure 10. Sample realization No. 1 of potential over random conductivity model.

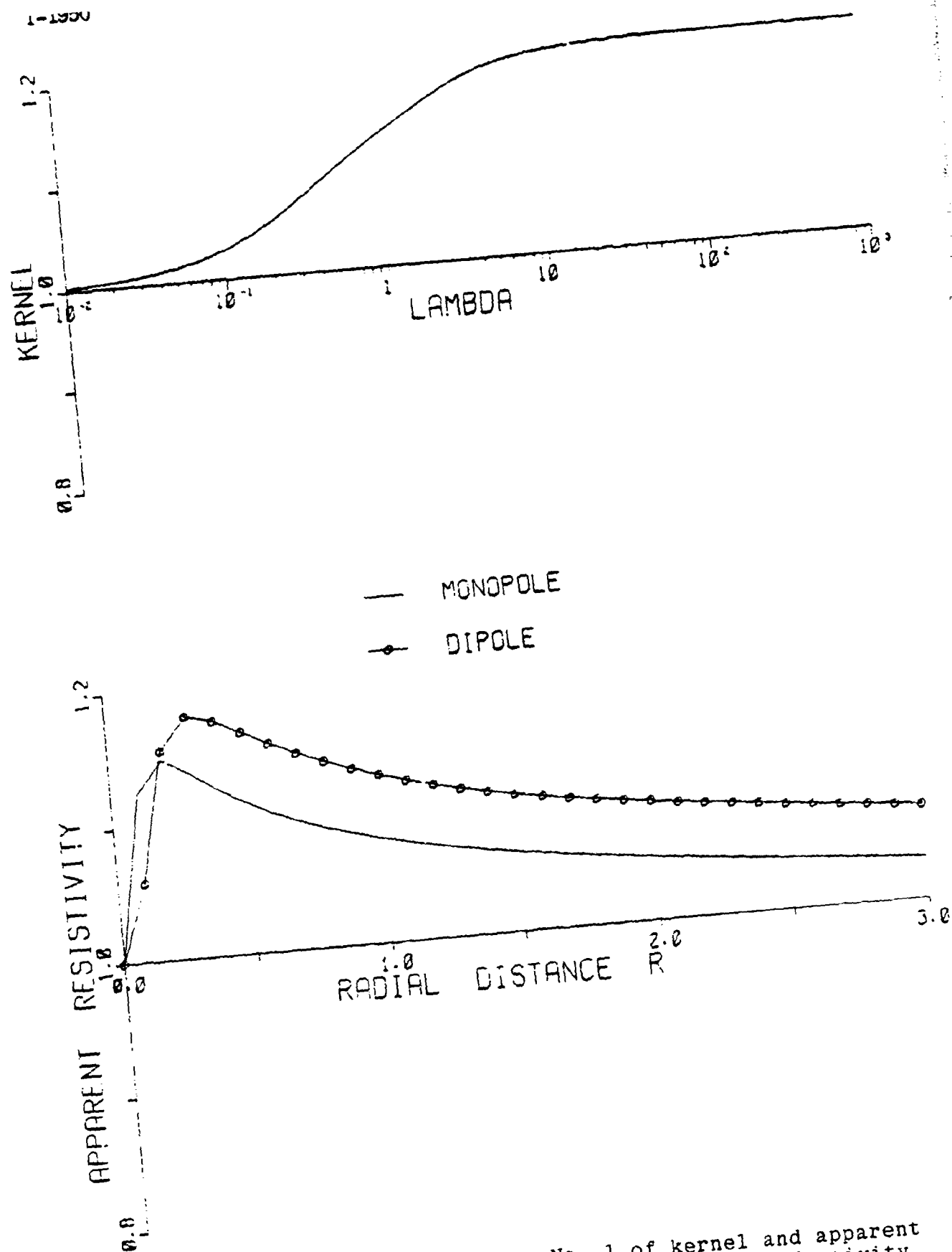


Figure 11. Sample realization No. 1 of kernel and apparent resistivity functions over random conductivity model.

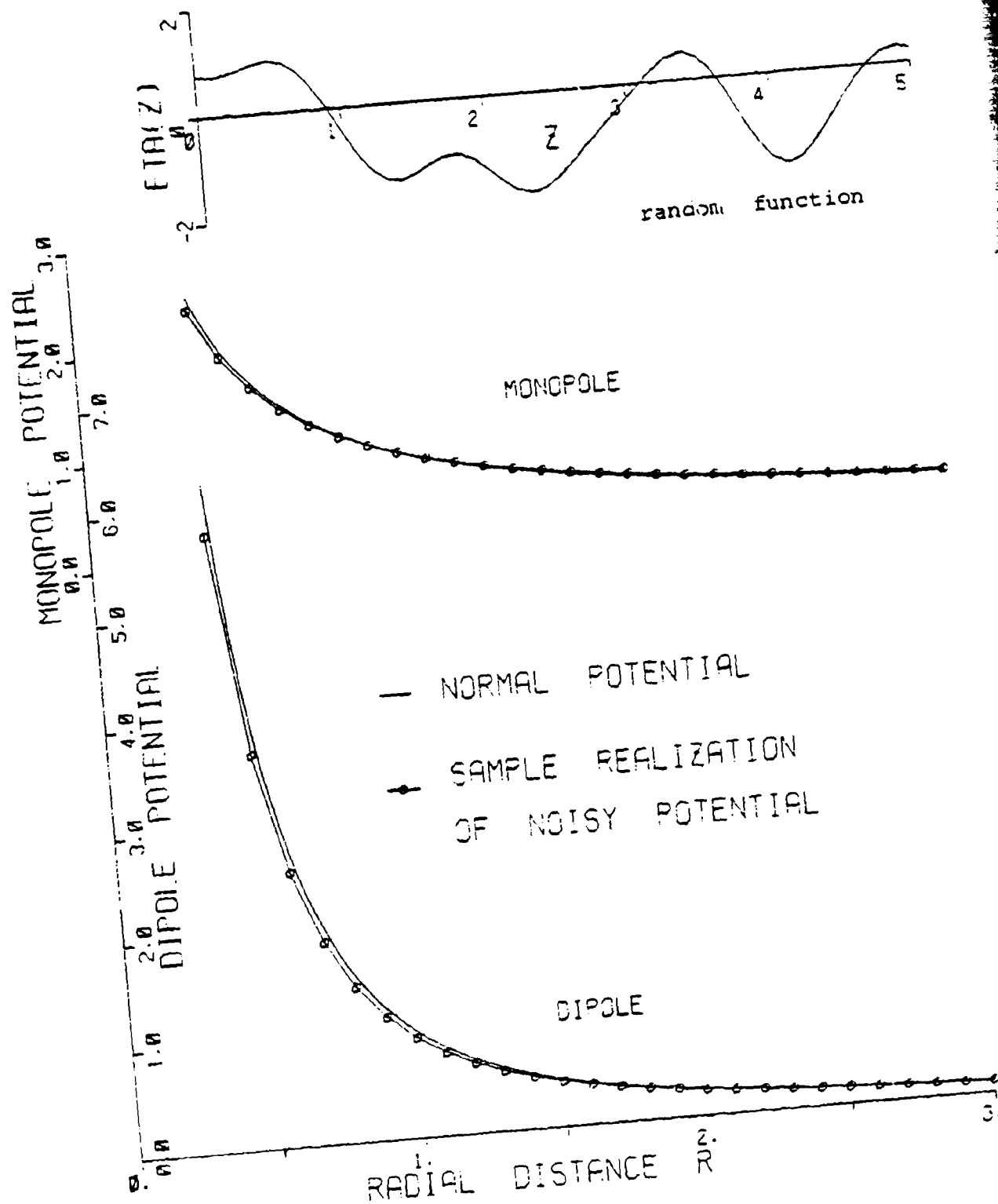


Figure 12. Sample realization No. 2 of potential over random conductivity model.

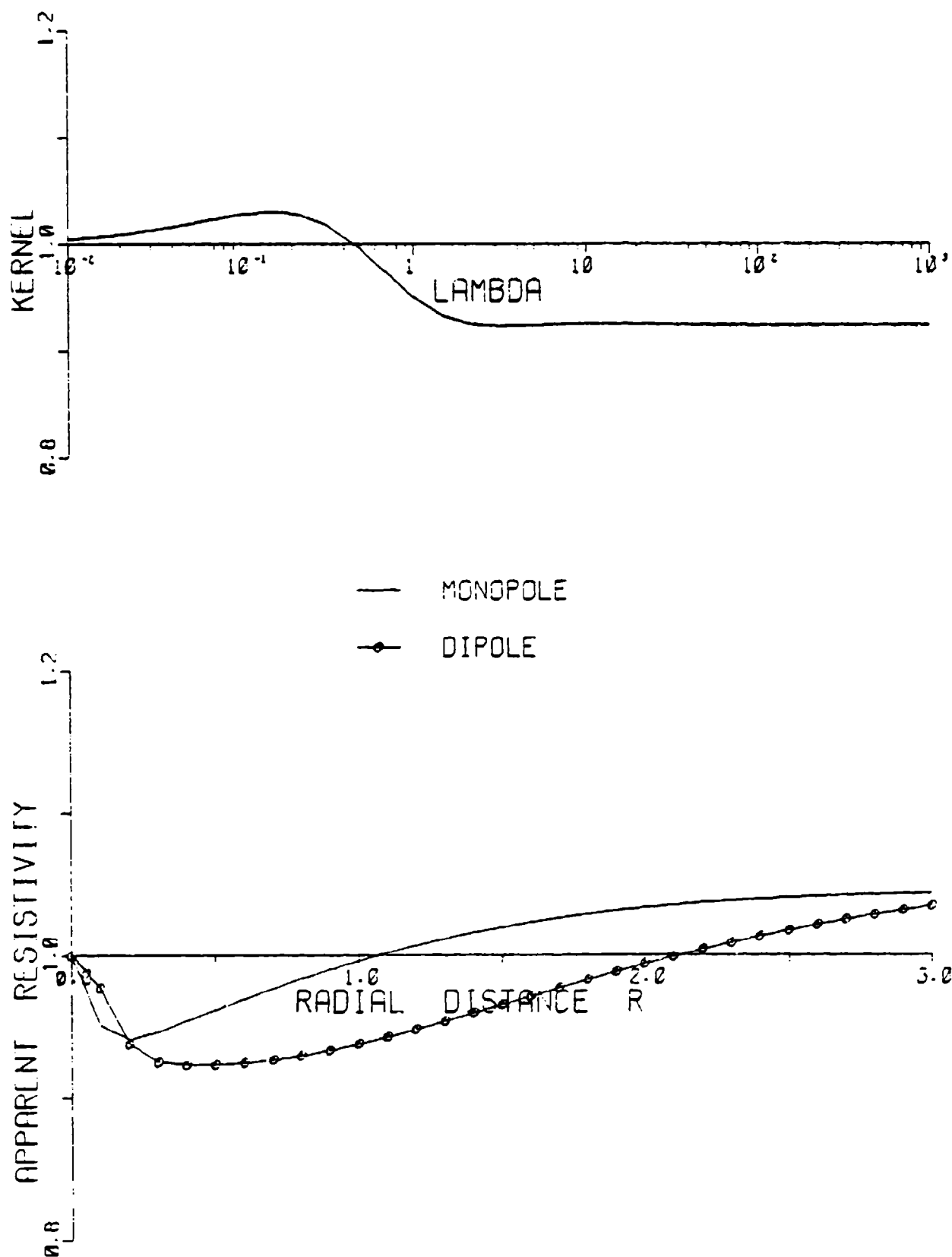


Figure 13. Sample realization No. 2 of kernel and apparent resistivity functions over random conductivity model.

T-1950

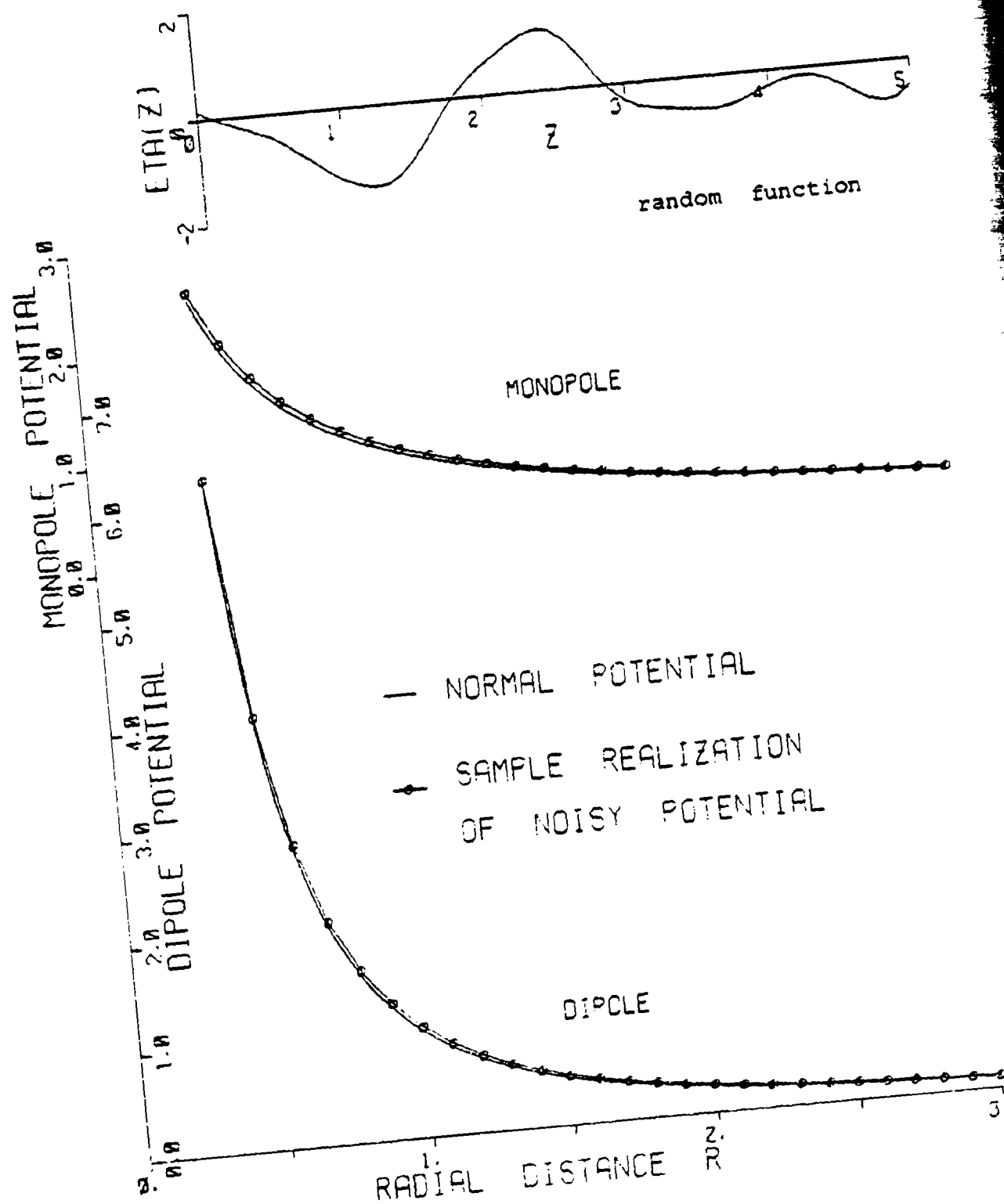


Figure 14. Sample realization No. 3 of potential over random conductivity model.

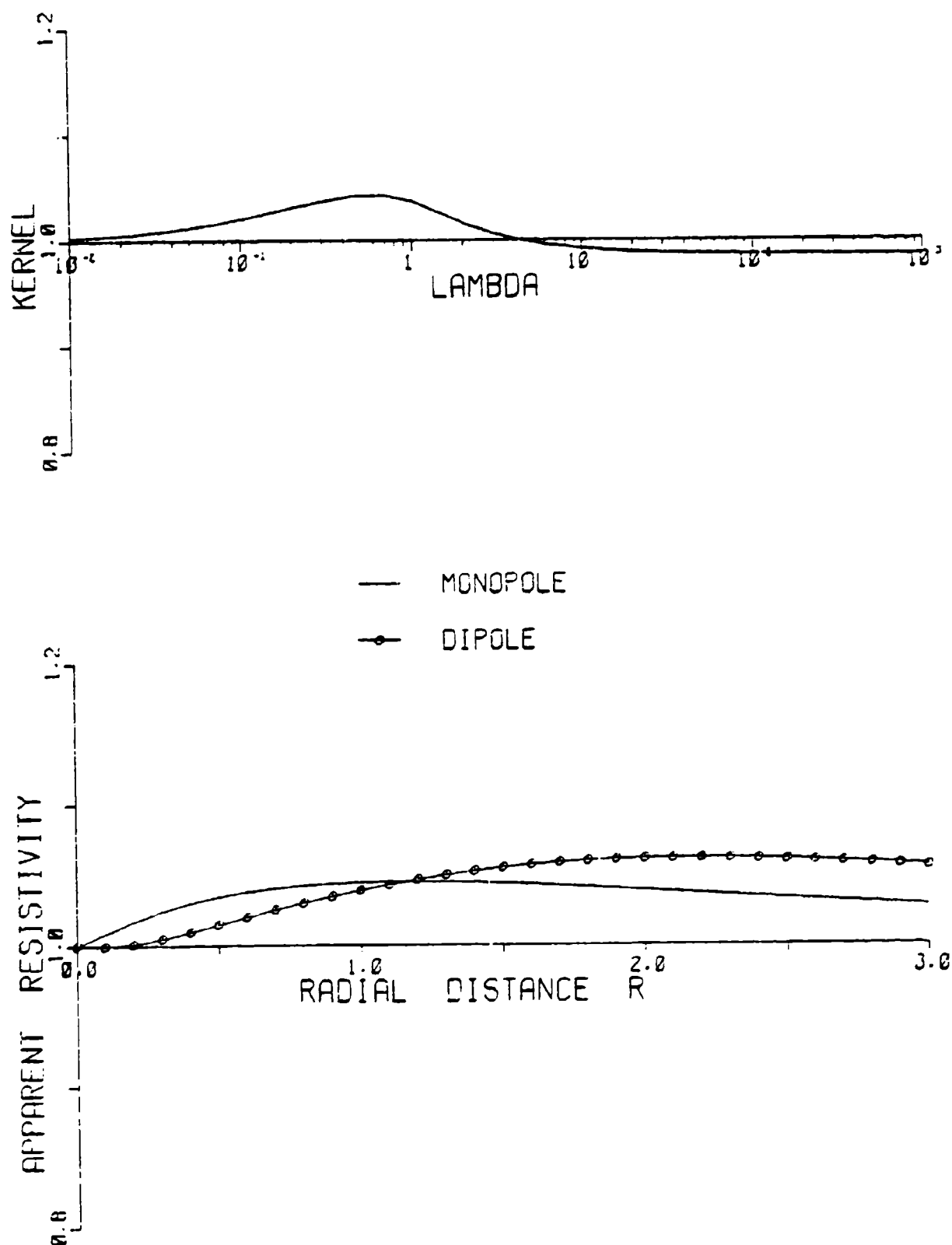


Figure 15. Sample realization No. 3 of kernel and apparent resistivity functions over random conductivity model.

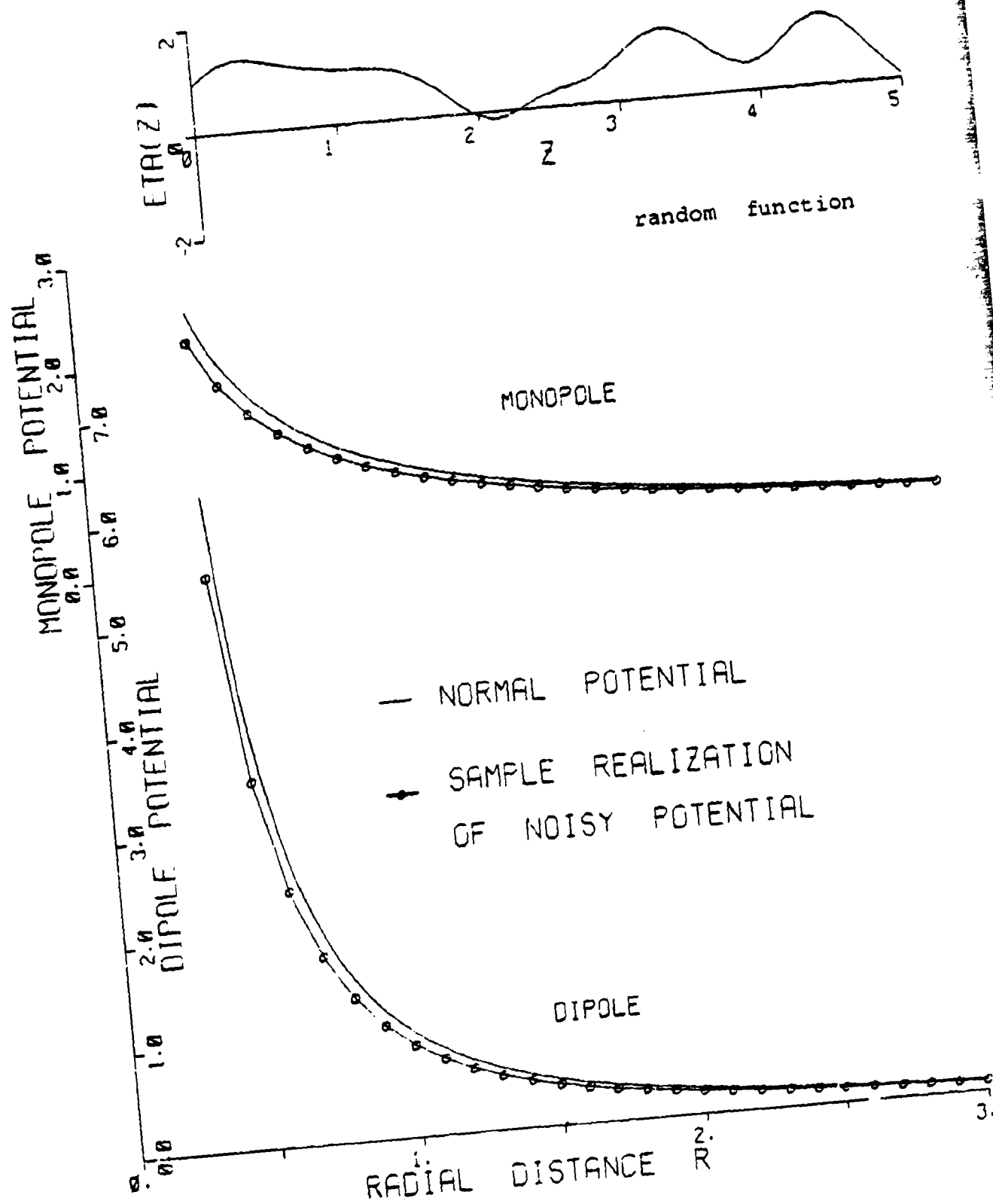


Figure 16. Sample realization No. 4 of potential over random conductivity model.

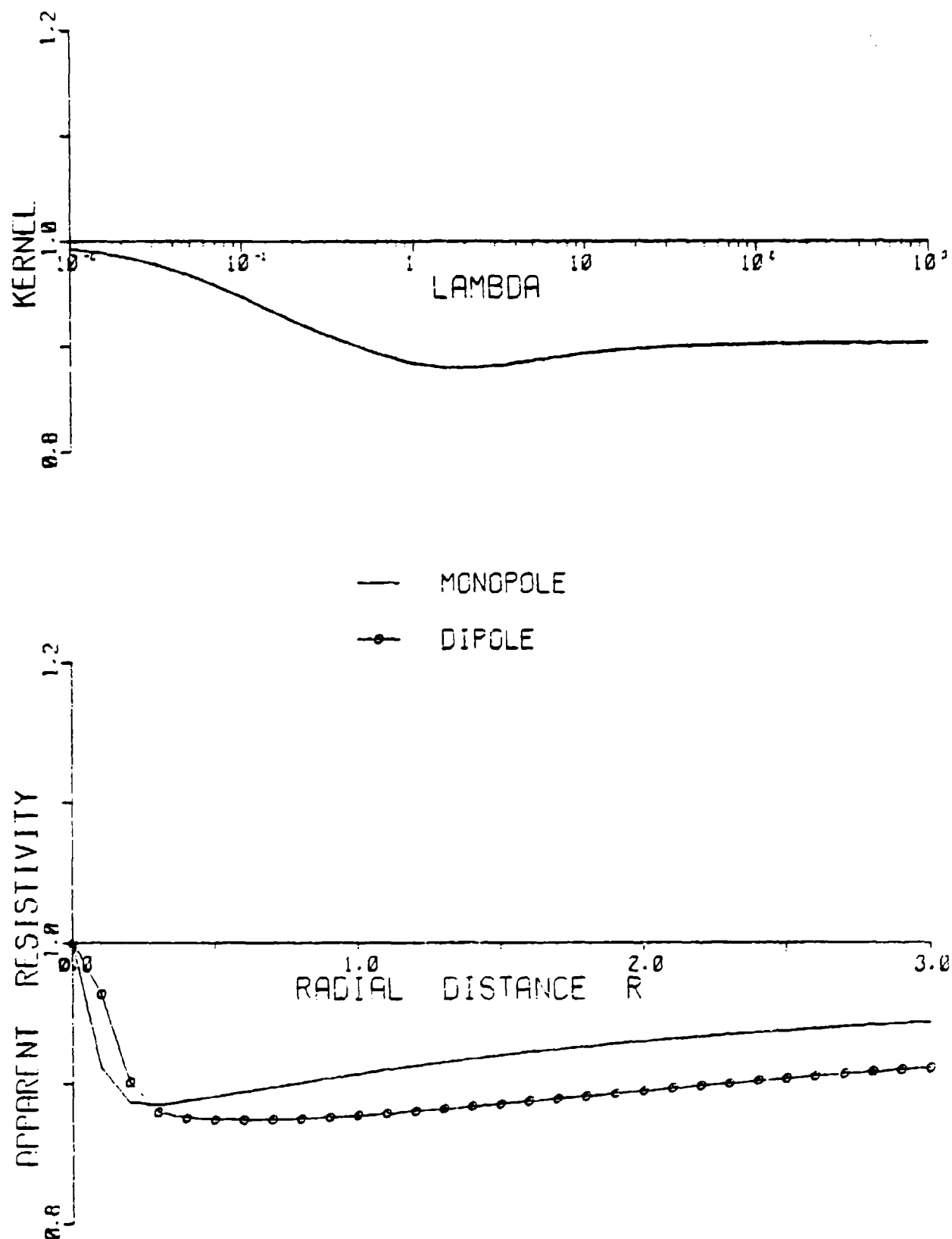


Figure 17. Sample realization No. 4 of kernel and apparent resistivity functions over random conductivity model.

ductivity functions are as shown at the top of the figures. The parameter α is arbitrarily set at 0.15 (corresponding to a weakly correlated $\eta(z)$). To make the variations in the random voltage large enough to be discerned on the graphs, the parameter ϵ has been set at a relatively large value of 0.1. It is apparent that in the transformation from a random conductivity distribution to the measured potential, high frequency information has been lost. The random potentials corresponding to each conductivity distribution are smooth functions of r . Herein lies the difficulty of distinguishing noise in the system from the signal itself.

It is more useful to examine the kernel and apparent resistivity functions. The stochastic kernel given in equation (2-27) can be expressed in terms of $\eta(z)$ explicitly as

$$K_1(\lambda) = - 2\lambda \int_0^{\infty} \eta(z) e^{-2\lambda z} dz \quad (3-16)$$

The "total" kernel is

$$\begin{aligned} K(\lambda) &= K_0(\lambda) + \epsilon K_1(\lambda) \\ &= 1 - 2\epsilon\lambda \int_0^{\infty} \eta(z) e^{-2\lambda z} dz \end{aligned} \quad (3-17)$$

Let us examine the asymptotes of the kernel function. Clearly,

$$K_1(0) = 0$$

It is less obvious, but nevertheless readily proved, that

$$K_1(\lambda) \rightarrow -\eta(0) \quad \text{as} \quad \lambda \rightarrow \infty$$

It should be noted that in computing $K_1(\lambda)$, by numerical integration, we need a mesh size Δz that becomes progressively smaller as λ gets correspondingly larger. This is necessary for a reliable approximation to the value of the integral.

The total kernel functions $K(\lambda)$ for the same four sample realizations that were used in the previous figures are shown in Figures 11, 13, 15 and 17. The deviations from the normal kernel, $K_0(\lambda) = 1$, depend on the nature of the random conductivity function. However, the most important factor is its value at the surface $\eta(0)$. For all practical purposes this asymptote is reached for λ values of about 100.

The normalized apparent resistivity measured with a pole-pole (or single pole) array may be expressed as

$$\rho^*(r) = \frac{\rho_a(r)}{\rho^0} = 1 - 4\epsilon r M(r) \quad (3-18)$$

where $\rho_a(r)$ is the apparent resistivity and ρ^0 is the reciprocal of σ_1^0 .

The corresponding expression for the pole-dipole array is

$$\rho^*(r) = \frac{\rho_a(r)}{\rho^0} = 1 - 12\epsilon r^2 D(r) \quad (3-19)$$

These normalized apparent resistivities are shown in Figures 11, 13, 15 and 17 in which they are referred to as "monopole" and "dipole" apparent resistivity curves. For a homogeneous half-space these normalized apparent resistivities have constant values of one. The deviations from this mean value reflect the random nature of the conductivity profile.

Clearly, these deviations approach zero as distance r from the source increases.

The corresponding Wenner and Schlumberger apparent resistivities will now be briefly examined. The normalized Wenner apparent resistivity is

$$\begin{aligned}\rho_w^*(a) &= \frac{\rho_{a,w}(a)}{\rho^0} = 2a \int_0^\infty K(\lambda) [J_0(\lambda a) - J_0(2\lambda a)] d\lambda \\ &= 1 - 8\epsilon a (M(a) - M(2a))\end{aligned}\quad (3-20)$$

where a is the electrode spacing (Figure 18). It can be shown that

$$\rho_w^* \rightarrow 1 - \epsilon\eta(0) \quad \text{as} \quad a \rightarrow 0$$

and

$$\rho_w^* \rightarrow 1 \quad \text{as} \quad a \rightarrow \infty$$

The normalized Schlumberger apparent resistivity is

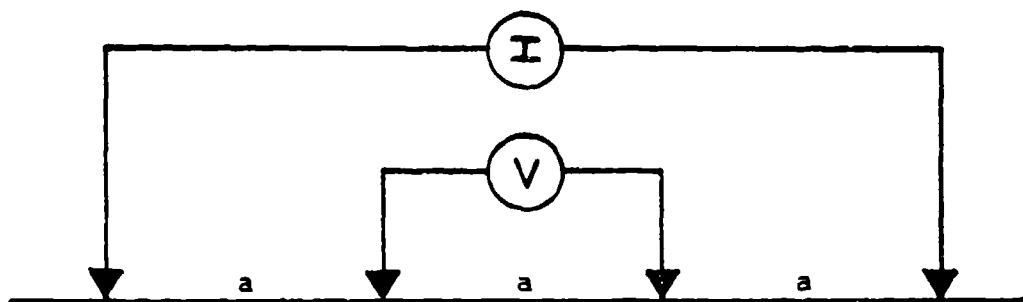
$$\begin{aligned}\rho_s^*(a) &= \frac{\rho_{a,s}(a)}{\rho^0} = a^2 \int_0^\infty K(\lambda) \lambda J_1(\lambda a) d\lambda \\ &= 1 - 12\epsilon a^2 D(a)\end{aligned}\quad (3-21)$$

where the electrode spacing a is as shown in Figure 18. It is obvious that

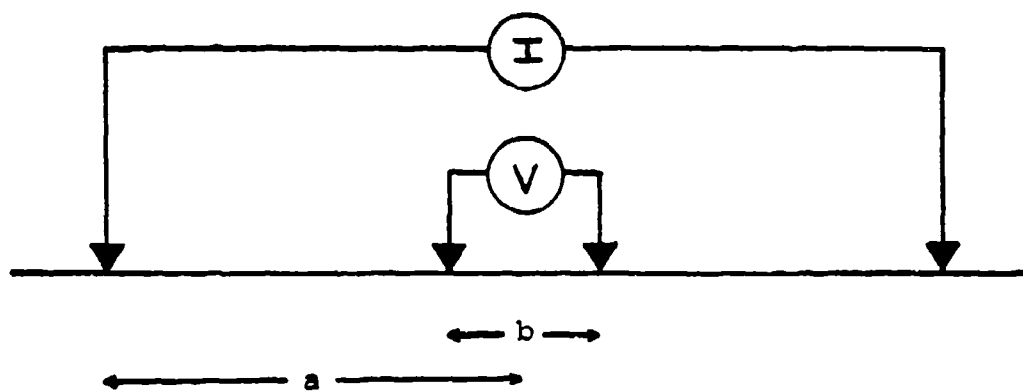
$$\rho_s^* \rightarrow 1 - \epsilon\eta(0) \quad \text{as} \quad a \rightarrow 0$$

and

$$\rho_s^* \rightarrow 1 \quad \text{as} \quad a \rightarrow \infty$$



Wenner Array



Schlumberger Array

Figure 18. Wenner and Schlumberger electrode arrays.

Thus, for small electrode spacings the resistivity measured with either array will be equal to the resistivity of the near-surface zone and for large electrode spacings the effect of the random profile will be negligible since all the variations tend to be averaged out when a greater depth of the section is probed. These apparent resistivity curves would be similar in shape to the kernel curves shown if the independent variable on the latter is regarded as $1/a$ instead of λ . These resistivity curves resemble the standard two- or three-layer curves for deterministic models. Although the deviations from the corresponding curves for a homogeneous earth are relatively small, these shifts in the curves for small values of a are significant enough to affect the accuracy of data interpretation. It is more convenient to examine this in the next chapter when the two-layer model is considered.

Sensitivity to Resistivity Variations

An indication of the relative sensitivity of direct current methods to variations in the conductivity profile may be obtained by studying the variance of the random potentials. For monopole excitation the variance is

$$\langle \tilde{V}_1(r) \tilde{V}_1(r) \rangle = \frac{4\alpha q^2}{\sqrt{\pi}} \int_0^{\infty} \{g_1(\omega r)\}^2 e^{-\alpha^2 \omega^2} d\omega \quad (3-22)$$

For dipole excitation, we have

$$\langle \tilde{U}_1(r) \tilde{U}_1(r) \rangle = \frac{4\alpha q^2}{\sqrt{\pi}} \int_0^{\infty} \{g_2(\omega r)\}^2 e^{-\alpha^2 \omega^2} d\omega \quad (3-23)$$

The variance at $r=0$ for both source configurations is equal to $2q^2$ as can be readily verified. Hence, the variance of the normalized random potential for both cases is twice the variance of the random conductivity function η . This is also the maximum value of the variance.

The variances of the monopole and dipole random potentials, after normalizing by $2q^2$, are shown in Figures 19 and 20 for $\alpha = 0.15$ and $\alpha = 1.5$ respectively. It is apparent that the variances of the random potentials decrease as measurements are taken farther from the source. This indicates, not unexpectedly, that the sensitivity of the measurements to variations in the conductivity profile decreases markedly with distance from the source. The variance is larger for a more correlated random conductivity function (that is, when α is large). For a completely uncorrelated function $\eta(z)$ the variance is zero except in the vicinity of the source. In such a case, the conductivity variations cannot, theoretically, be detected.

It is interesting to note that the variance of the normalized random dipole potential is always greater than that due to a monopole. This leads to the conclusion that measurements made with a dipole source are more sensitive to conductivity variations in the subsurface than those made with a monopole

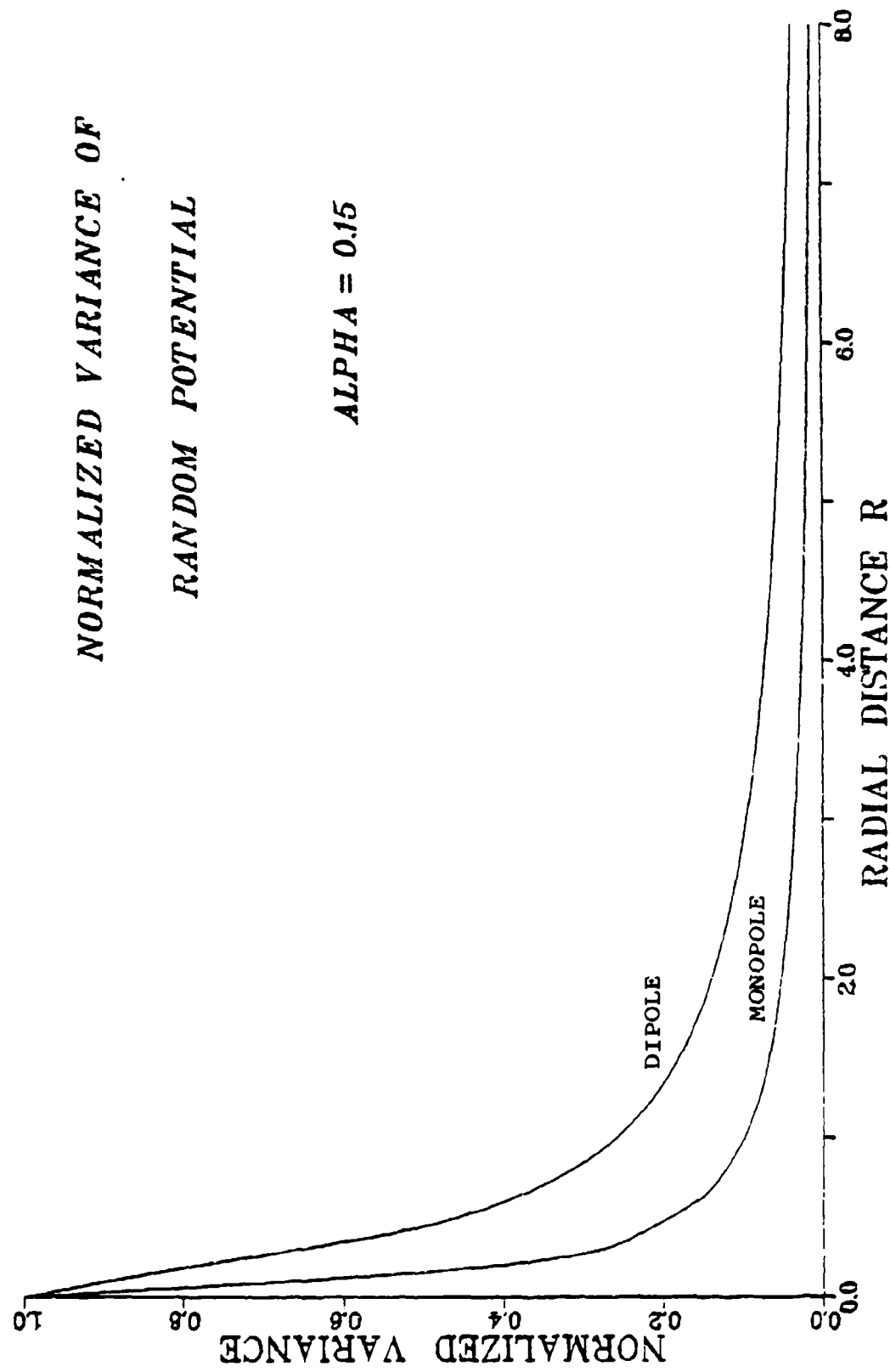


Figure 19. Normalized variance of random potential for $\alpha = 0.15$.

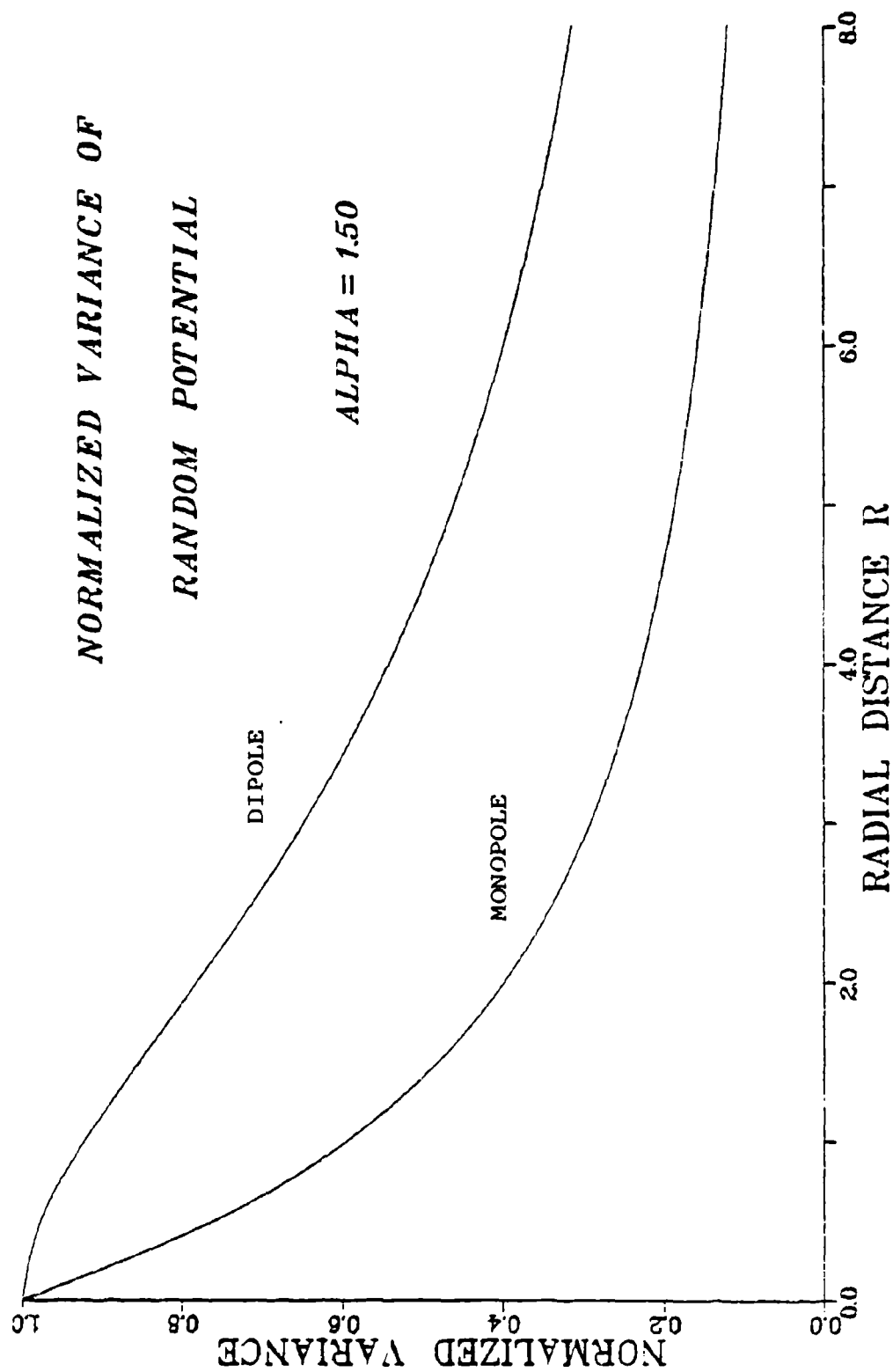


Figure 20. Normalized variance of random potential for $\alpha = 1.5$.

source. Consequently, the signal to noise ratio for dipole excitation decreases more rapidly with distance from the source than that for monopole excitation.

Anisotropy

The resistivity of a rock may depend on the direction in which a current flows through it. One cause of this is the microscopic structure of the rock; the alignment of mineral grains may permit current to flow more readily along the direction of the bedding plane or schistosity than perpendicular to it. This is referred to as micro-anisotropy. A sequence of parallel layers each with its own thickness and resistivity will also give rise to a preferred direction of current flow. In this case, we refer to structural anisotropy or macro-anisotropy. For excellent discussions on the nature and effects of anisotropy the reader is referred to Schlumberger et al., 1934, Kunetz, 1966 and Keller, 1968.

Let us first examine the effects of micro-anisotropy. Consider a one-layer medium in which the radial and vertical conductivity functions are given by

$$\sigma_r(z) = \sigma_r^0 (1 + \epsilon \eta_r(z)) \quad (3-24)$$

$$\sigma_z(z) = \sigma_z^0 (1 + \epsilon \eta_z(z)) \quad (3-25)$$

in which the constants σ_r^0 and σ_z^0 are the mean conductivities in the r and z directions respectively and η_r and η_z are zero-mean stationary Gaussian random functions of z with prescribed covariance functions.

The coefficient of anisotropy β is defined as

$$\beta = \frac{\sqrt{\sigma_r^0}}{\sqrt{\sigma_z^0}} \quad (3-26)$$

Case I: If it is assumed that $\sigma_r(z)/\sigma_z(z)$ is constant for all z , then

$$\eta_r(z) = \eta_z(z)$$

In the interest of brevity in notation the subscripts (which are now superfluous) for the function η and its transform N will be dropped. As shown in Appendix B, the normalized random potentials for monopole and dipole sources are

$$\tilde{V}_1(r, 0) = 2 \int_0^\infty \left\{ \frac{\pi}{2} \frac{\omega r}{2\beta} Q_0\left(\frac{\omega r}{2\beta}\right) - 1 \right\} N(\omega) d\omega \quad (3-27)$$

$$\tilde{U}_1(r, 0) = 2 \int_0^\infty \left[\left(\frac{\omega r}{2\beta}\right)^2 \left\{ 1 - \frac{\pi}{2} Q_1\left(\frac{\omega r}{2\beta}\right) \right\} - 1 \right] N(\omega) d\omega \quad (3-28)$$

These equations differ from (3-3) and (3-4) for the isotropic case only in the fact that there is now an additional factor β .

The normalized covariances for various β and r_1 values are shown in Figures 21 through 23. Inspection of these curves leads to the following conclusion. The larger the coefficient of anisotropy the more correlated is the random potential. It can also be shown that the variances of the random potentials for a fixed distance r increases with β .

It is apparent that the term β in the equations above are, essentially, no more than a scaling factor on the distance r . Hence, not much additional information is gained by con-

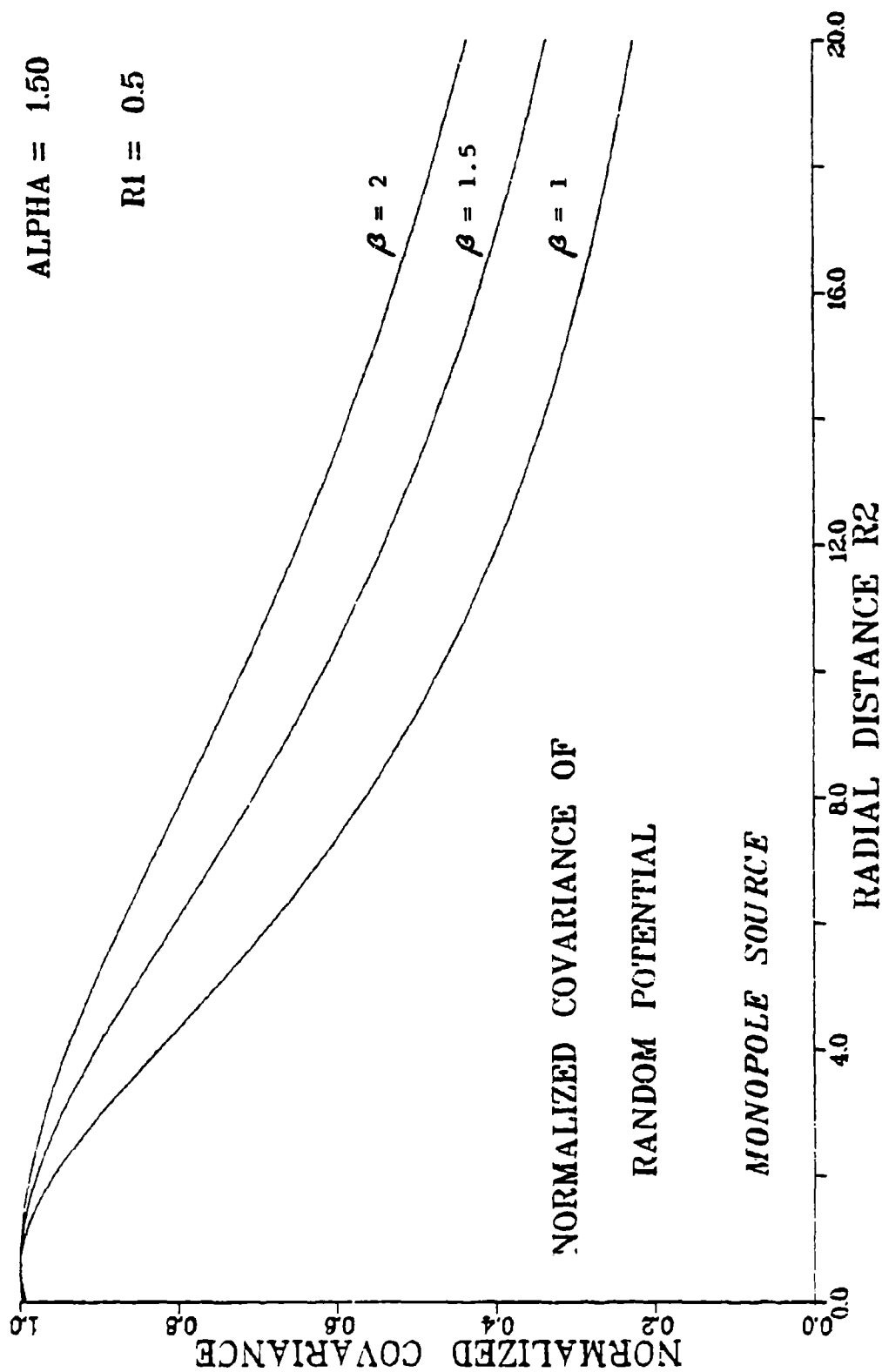


Figure 21. Normalized covariance of anisotropic monopole random potential for $\alpha = 1.5$ at $r_1 = 0.5$.

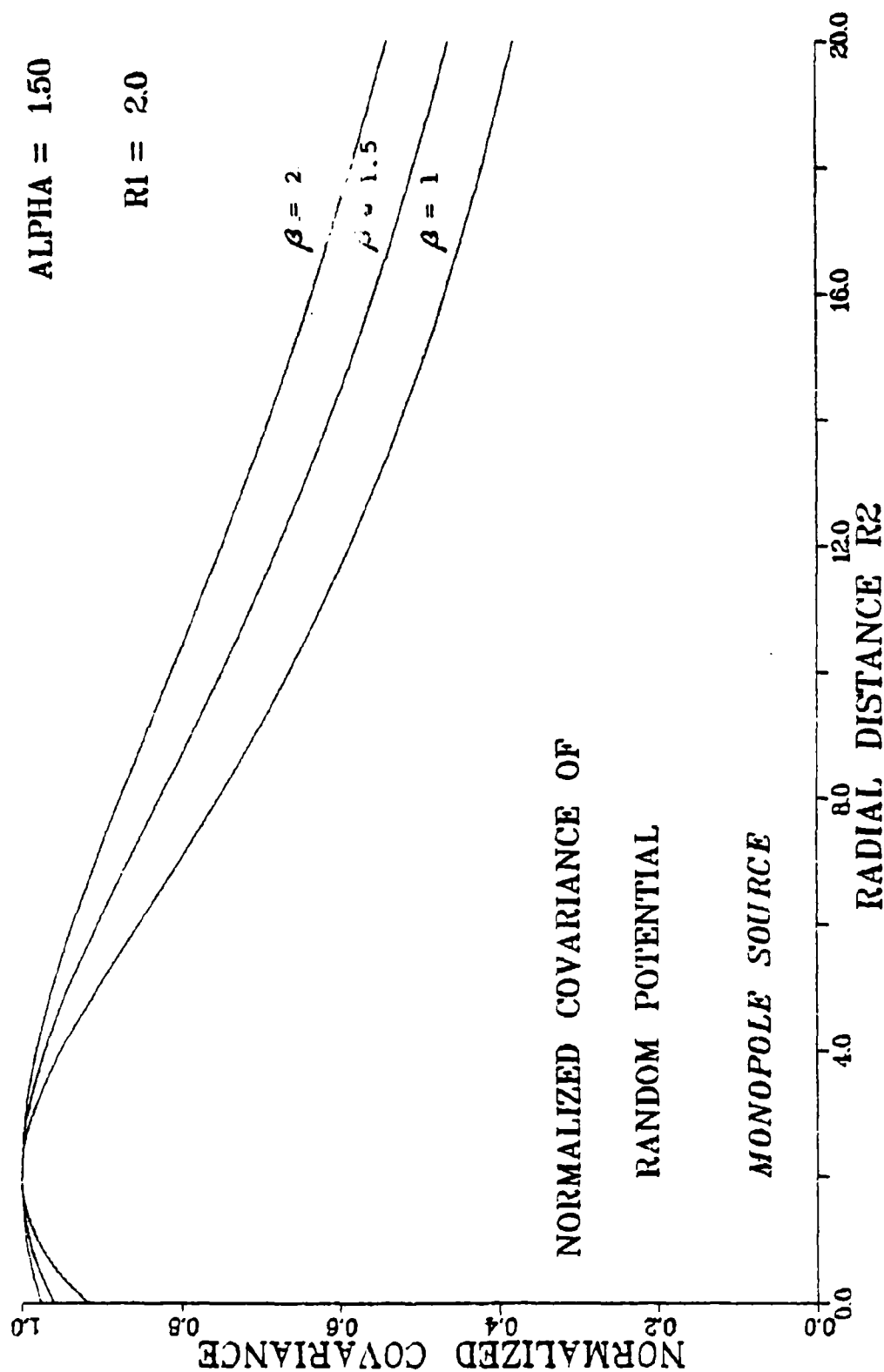


Figure 22. Normalized covariance of anisotropic monopole random potential for $\alpha = 1.5$ at $r_1 = 2.0$.

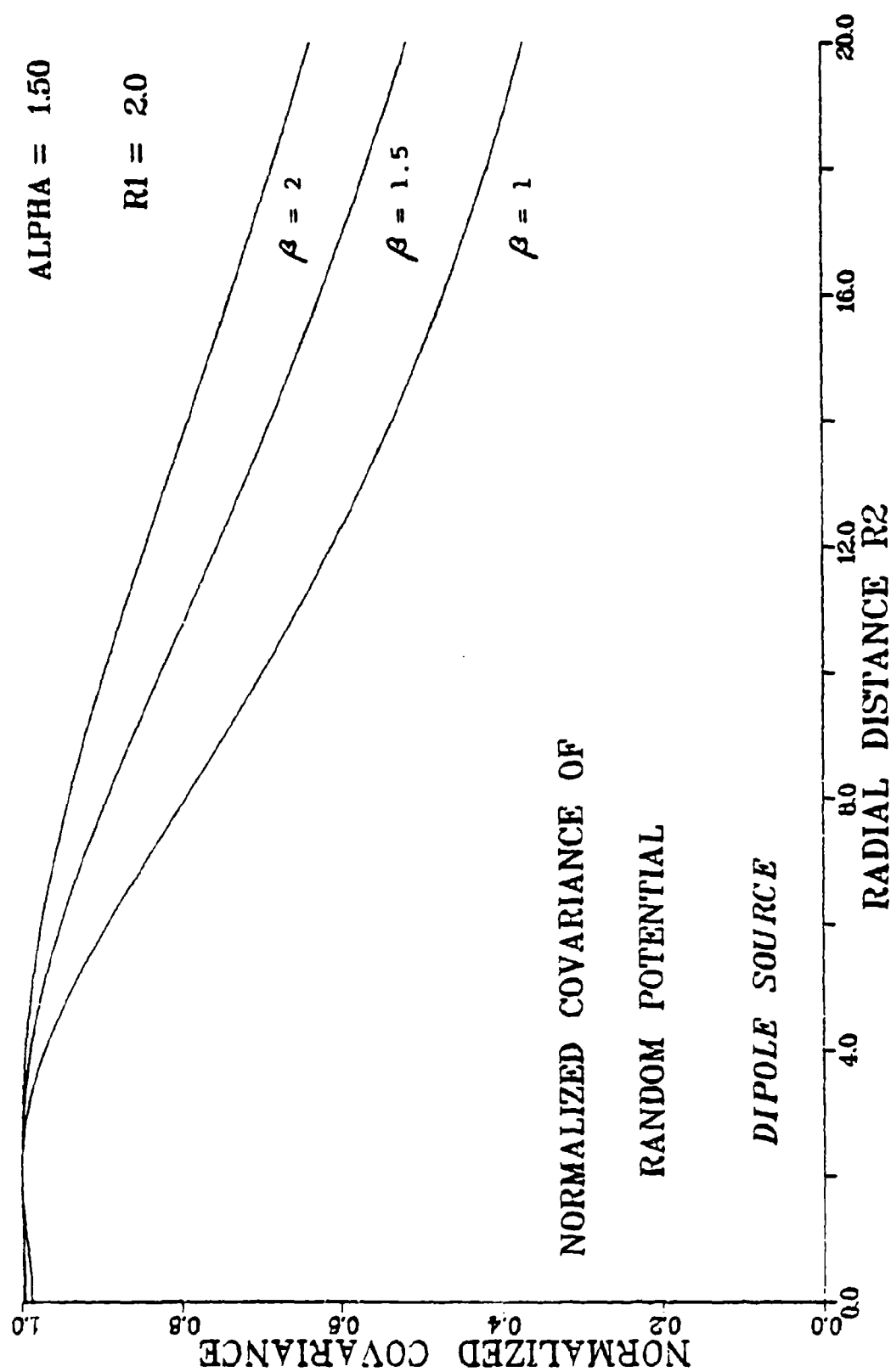


Figure 23. Normalized covariance of anisotropic dipole random potential for $\alpha = 1.5$ at $r_1 = 2.0$.

sidering anisotropy separately, as is well known.

Case II: Instead of letting σ_r be random, let us assume it is constant,

$$\sigma_r = \sigma_r^0.$$

This implies $\eta_r(z) = 0$. The monopole and dipole potentials, as shown in Appendix B, are half the corresponding values for Case I. It is therefore unnecessary to pursue this case any further.

Macro-anisotropy: Before leaving the subject of anisotropy, it is pertinent to note that even in the so-called "isotropic" case, macro-anisotropy is implicitly present when a random conductivity profile is assumed. This is illustrated in the following manner. The average transverse resistivity of a succession of beds, in the limit, as bed thicknesses tend to zero, can be expressed in the form

$$\rho_t = \frac{\int \rho(z) dz}{H}$$

where $\rho(z)$ is the resistivity as a function of depth and H is the total thickness of the sequence.

On the other hand, the average longitudinal conductivity of the sequence is given by

$$\sigma_l = \frac{\int \sigma(z) dz}{H}$$

where $\sigma(z)$ is the conductivity as a function of depth.

The coefficient of macro-anisotropy is

$$\beta = \sqrt{\rho_t \sigma_l} .$$

This value is extremely close to 1.0 for the conductivity distributions that have been used here. Even for the relatively large value of 0.1 for the parameter ϵ , this coefficient of anisotropy is only about 1.005 on the average.

THE TWO-LAYER CASE

The randomly conductive overburden problem proposed in this study arises in nature when a sedimentary basin is underlain by a basement. One can conceive of a sequence of thinly layered sediments with slightly different electrical characteristics for each layer. The conductivities, however, deviate only marginally from the mean of the sedimentary section as a whole. Frequently the "electrical" basement will have a much higher resistivity than the overburden (that is, the reflection coefficient k is positive). For all practical purposes the basement resistivity is constant relative to the variability in the more conductive overburden. However, one can conceivably have a situation in the field in which the basement is more conductive. The question then naturally arises as to whether the model, as it is assumed, is applicable. It would seem to be more appropriate in this case to have the variability in the more conductive basement. It should be pointed out, however, that shallower layers have a greater effect on the surface measurements than deeper layers.

In any case, the statistical properties of the random overburden model for both positive and negative reflection coefficients will be examined, bearing in mind that the case of a more resistive basement is generally of greater interest from a practical viewpoint. It is appropriate to stress here that although this is referred to as a "two-layer" model, one

is in fact dealing with infinitely many layers in the overburden. Equivalently, one may refer to this as a randomly layered model.

Sample Realizations

It is of considerable interest to the interpreter of field data to know the extent to which the variability in the conductivity profile affects the apparent resistivity and kernel function curves. With this in mind, some representative sample realizations of the random conductivity function and the corresponding kernel and apparent resistivity curves will be examined.

Kernel function: The equation for the stochastic kernel in equation (2-24) can be rewritten explicitly in terms of z as follows:

$$K_1(\lambda) = - \frac{2\lambda v}{\phi} \int_0^h \eta(z) e^{-2\lambda z} dz - \frac{4k^2 \lambda e^{-4\lambda h}}{\phi^2} \int_0^h \eta(z) \cosh 2\lambda z dz \quad (4-1)$$

It is recalled from equation (2-22) that the deterministic two-layer kernel is

$$K_0(\lambda) = \frac{v}{\phi} .$$

The total kernel is

$$K(\lambda) = K_0(\lambda) + \epsilon K_1(\lambda) .$$

The asymptotes of the kernel functions are worth examining.

As $\lambda \rightarrow 0$, $K_0 \rightarrow \frac{1+k}{1-k}$

and

as $\lambda \rightarrow \infty$, $K_0 \rightarrow 1$.

Obviously, $K_1 \rightarrow 0$ as $\lambda \rightarrow 0$ except when the basement is infinitely resistive ($k = 1$) in which case the expression increases without limit and the solution is not applicable. To derive the other asymptote the equation for K_1 needs to be rewritten as

$$K_1(\lambda) = - \frac{2(1+ke^{-2\lambda h})\lambda}{(1-ke^{-2\lambda h})} \int_0^h \eta(z)e^{-2\lambda z} dz$$

$$- \frac{2k^2\lambda}{(1-ke^{-2\lambda h})} \frac{1}{2} \int_0^h \{e^{-2\lambda(2h-z)} + e^{-2\lambda(2h+z)}\} \eta(z) dz \quad (4-2)$$

For large λ (> 5) the second integral is negligible compared to the first. (For $\lambda = 4$ the first integral is 3 orders of magnitude larger than the second; for $\lambda = 5$ it is 4 orders of magnitude larger. The ratio of the first to the second is approximately $e^{2\lambda}$ for large λ .) In addition, for large λ , the first term in equation (4-2) approaches $-\eta(0)$. Hence, $K(\lambda) \rightarrow \frac{1+k}{1-k}$ as $\lambda \rightarrow 0$ and $K(\lambda) \rightarrow 1 - \epsilon\eta(0)$ as $\lambda \rightarrow \infty$. The second asymptote is independent of k .

Some examples of the sample realizations of the kernel function $K(\lambda)$ for $k = \pm 0.8$ and $\alpha = 0.05$ are presented in Figures 24 through 27. Superimposed on these are the deter-

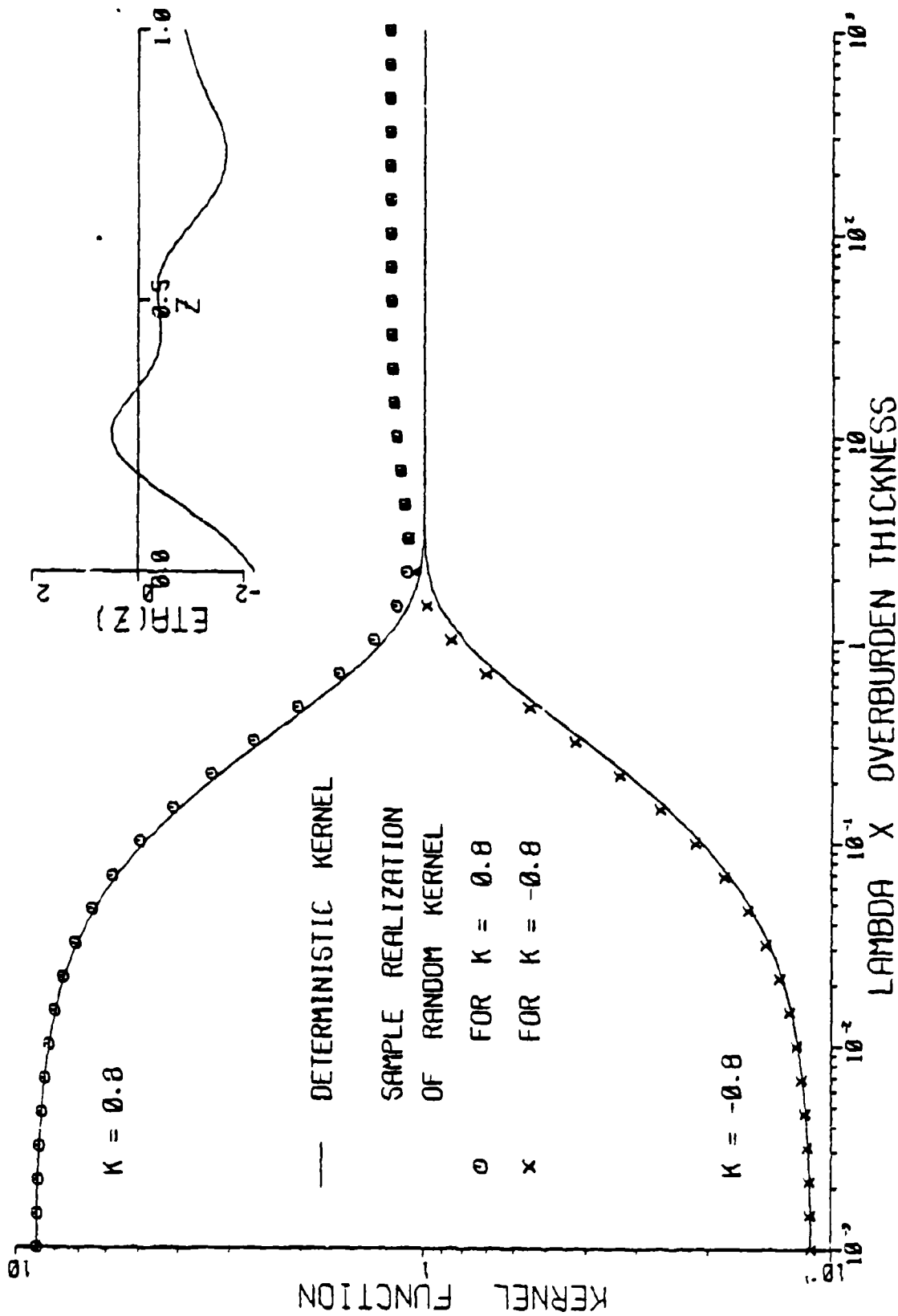


Figure 24. Sample realization No. 1 of kernel function for $k = \pm 0.8$.

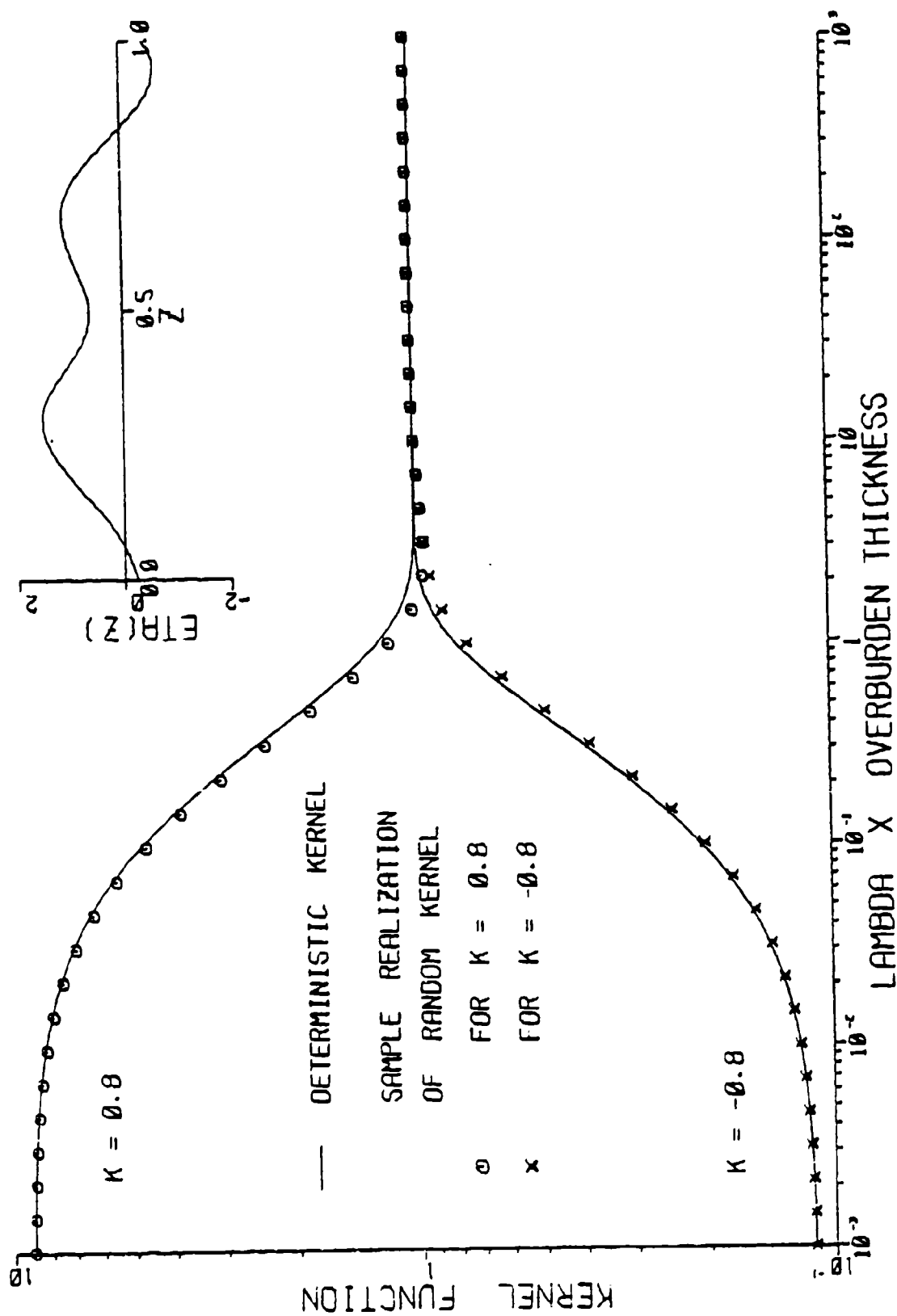


Figure 25. Sample realization No. 2 of kernel function for $k = \pm 0.8$.

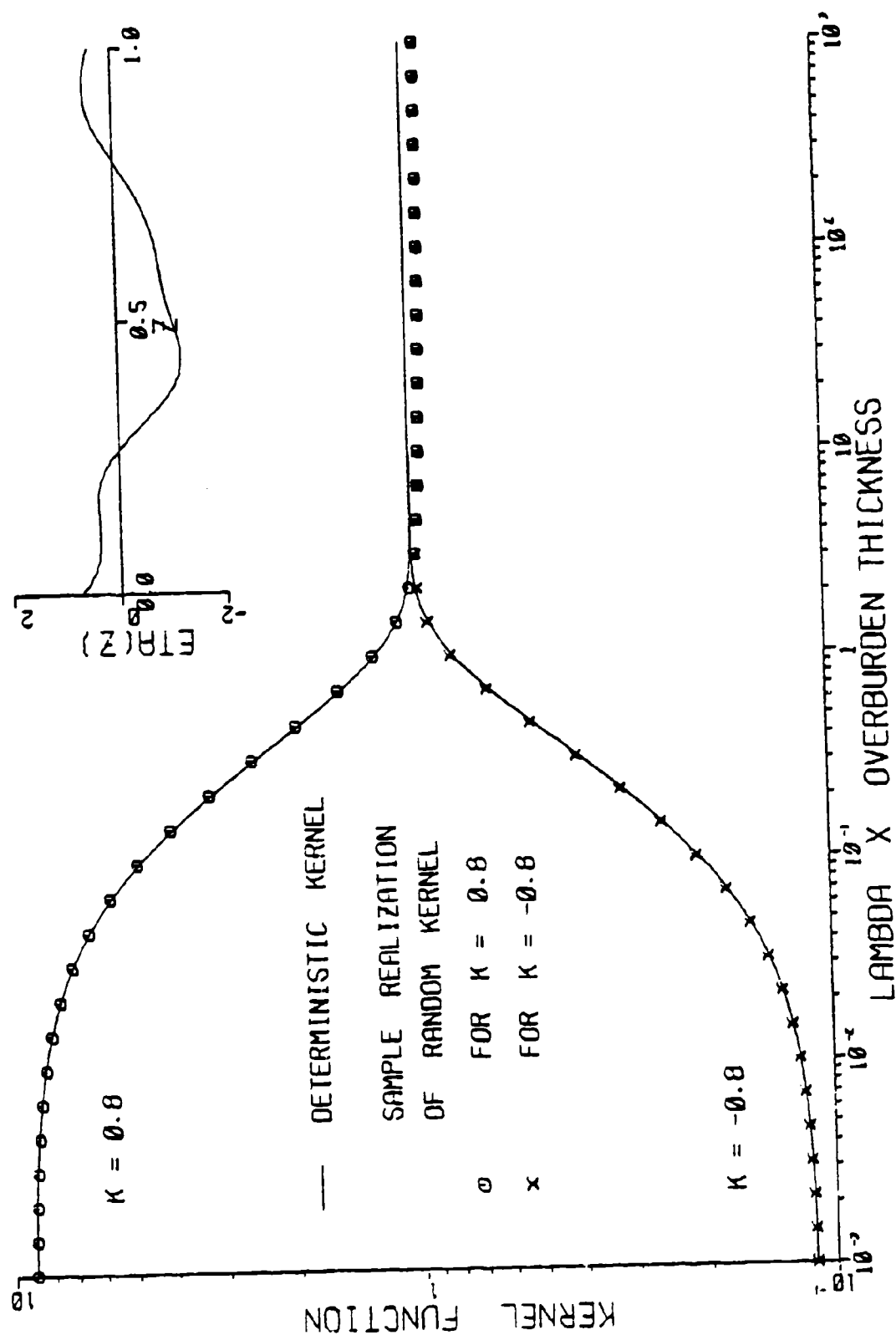


Figure 26. Sample realization No. 3 of kernel function for $k = \pm 0.8$.

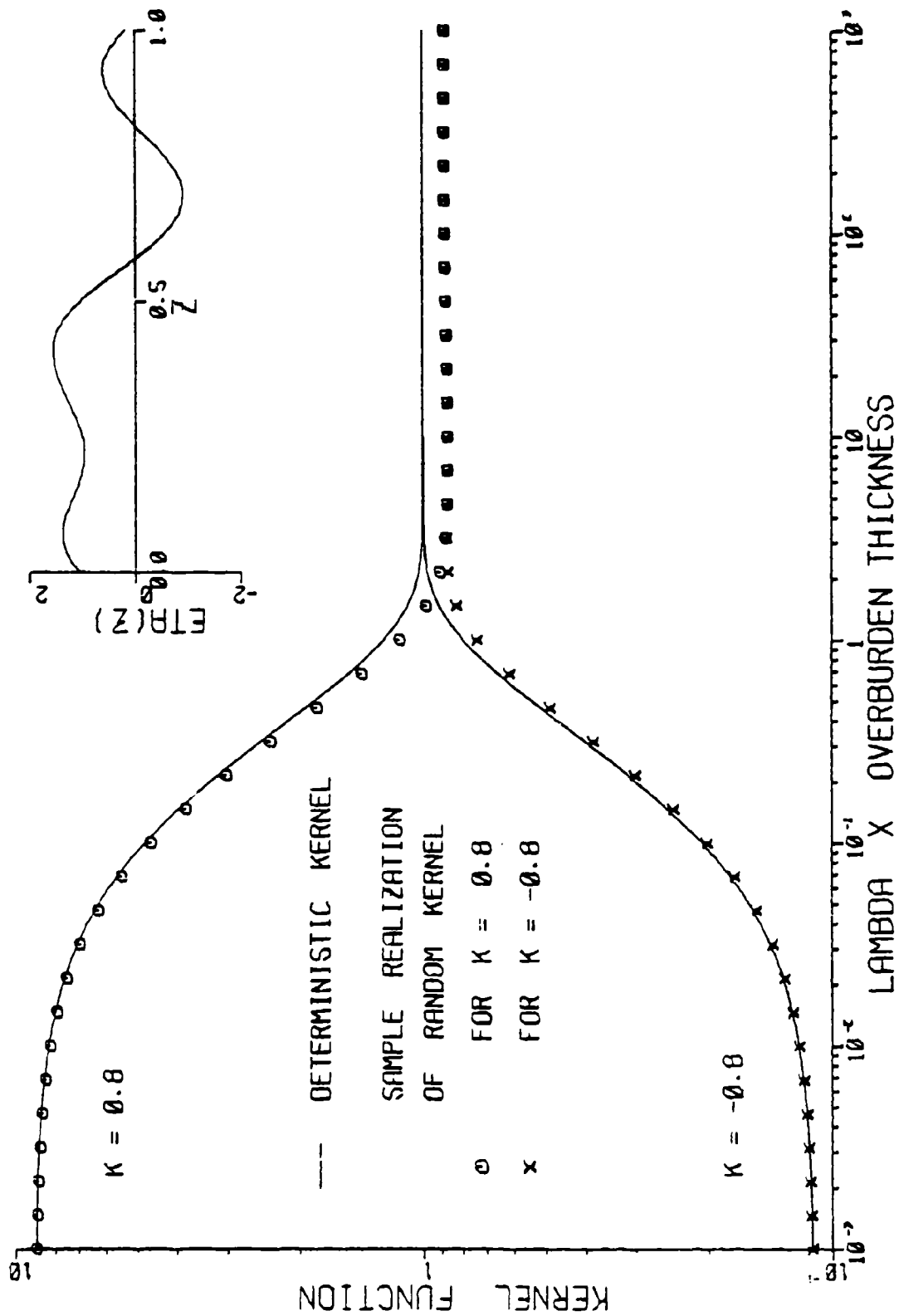


Figure 27. Sample realization No. 4 of kernel function for $k = \pm 0.8$.

ministic kernel functions $K_0(\lambda)$ plotted as solid lines in the figures. The random conductivity functions $\eta(z)$ are shown in the upper right-hand corners of the graphs. The parameter ϵ has been set at the relatively large value of 0.1 to accentuate the deviations from the mean. The abscissa in each graph is in dimensionless units of λh .

These representative curves show the range and nature of deviations from the mean. The most important factor evidently is the value $\eta(0)$. Depending on the actual nature of $\eta(z)$ the kernel functions may look like those of a deterministic two-layer case (with appropriate shifts in the axes) or, in extreme cases, for example in Figure 24, they may resemble those of three-layer models.

The deviations in the kernel function are more clearly illustrated if graphs of the changes relative to the corresponding deterministic values are plotted. The relative change is defined as

$$\frac{\epsilon K_1(\lambda)}{K_0(\lambda)} \times 100\%$$

Curves showing these relative deviations comprise the upper halves of Figures 28 to 34, the first four of which correspond to the same four random functions used in Figures 24 to 27. The asymptotic values are zero (as $\lambda \rightarrow 0$) and $-\epsilon\eta(0) \times 100\%$ (as λ approaches infinity). These deviations are either positive or negative depending on the actual form of the random function and on the particular λ values.

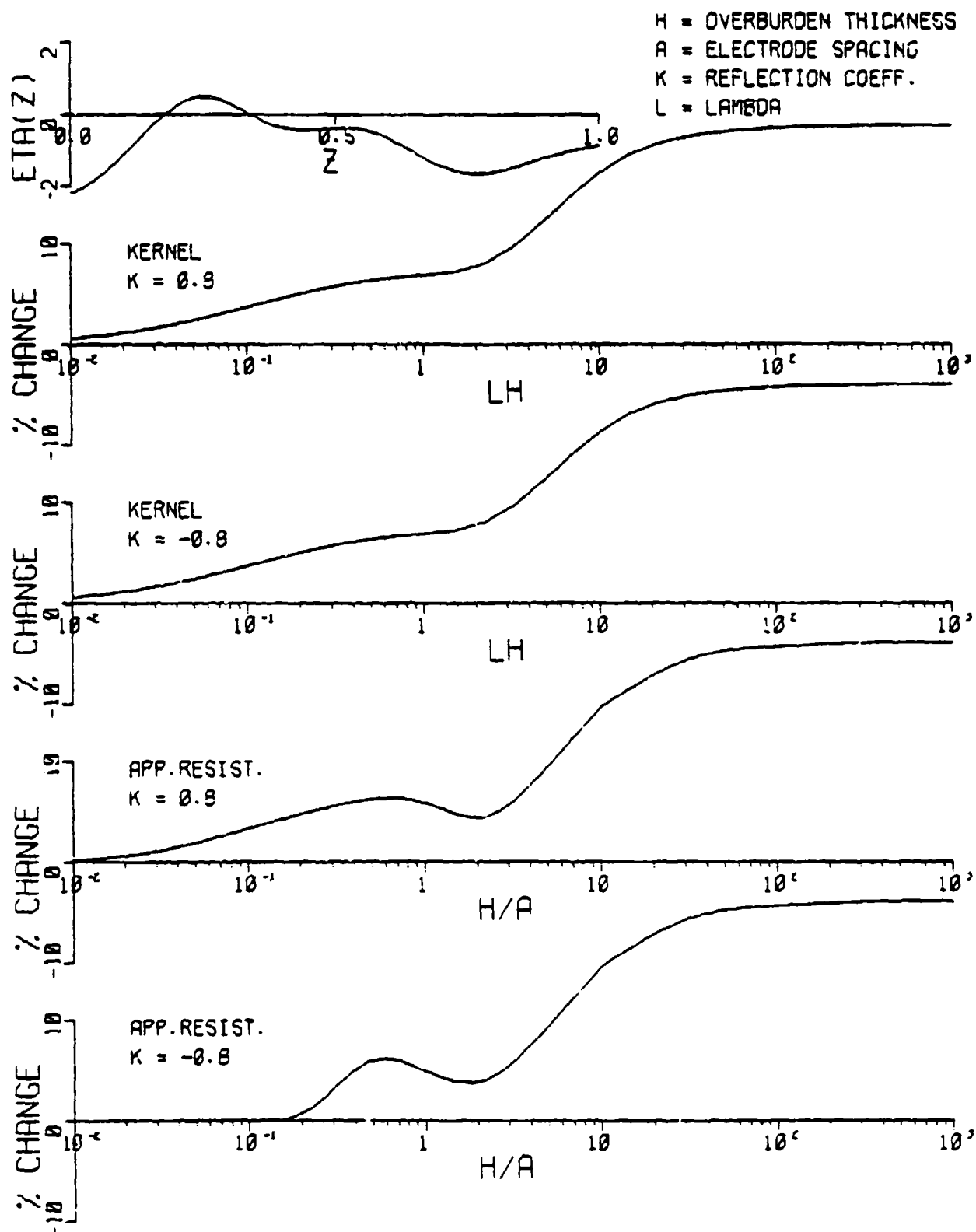


Figure 28. Sample realization No. 1 of percent deviation in kernel and apparent resistivity functions for $k = \pm 0.8$.

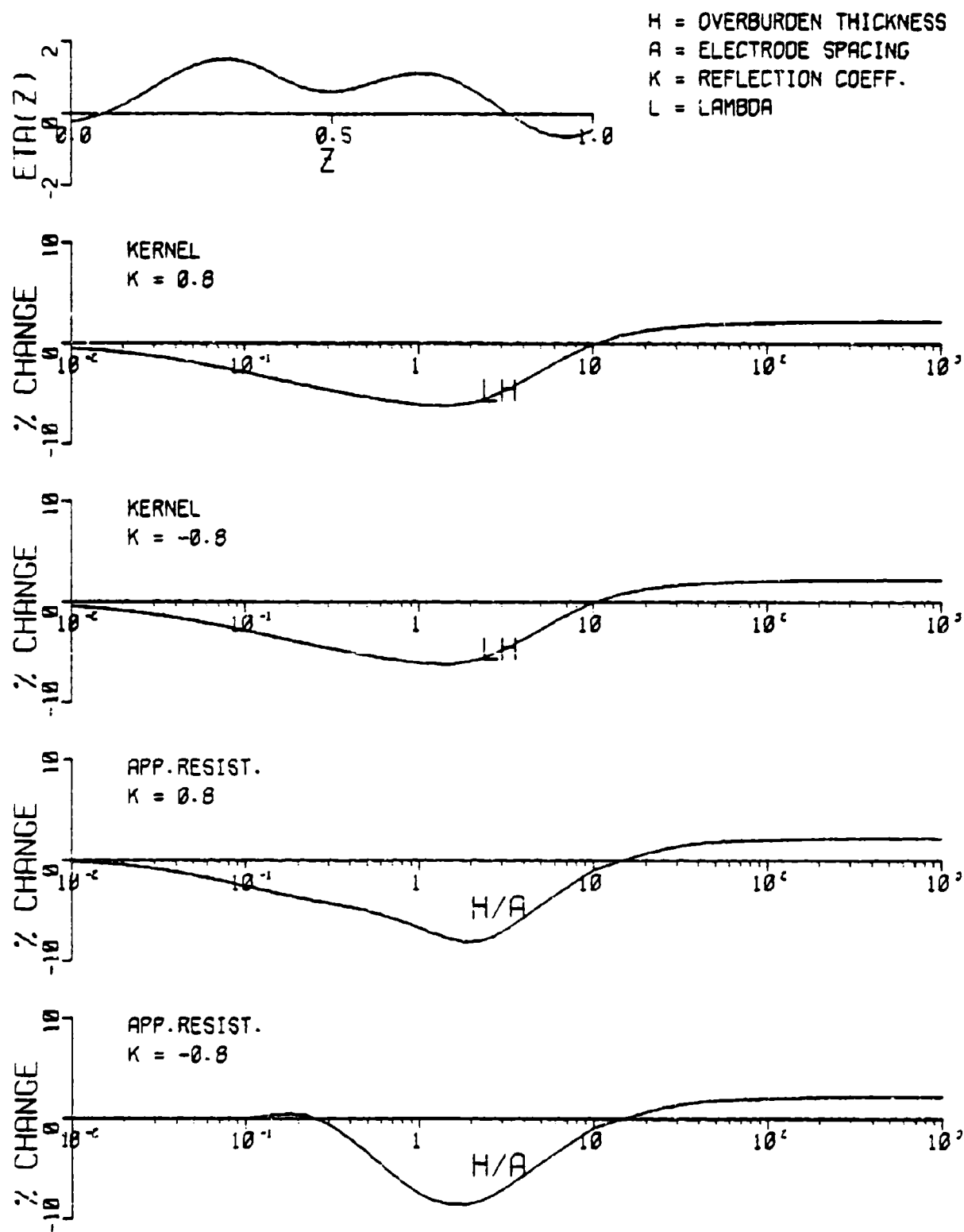


Figure 29. Sample realization No. 2 of percent deviation in kernel and apparent resistivity functions for $k = \pm 0.8$.

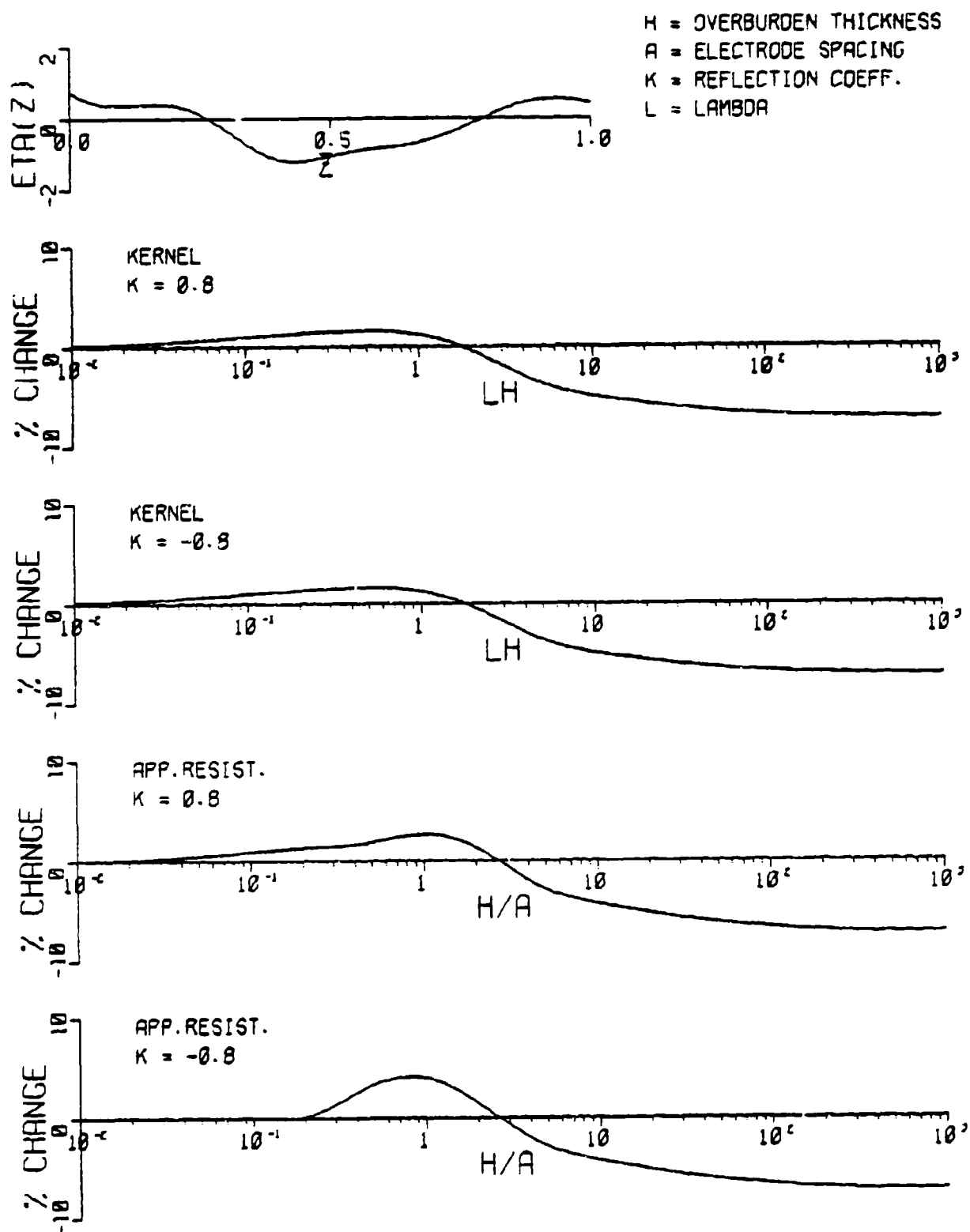


Figure 30. Sample realization No. 3 of percent deviation in kernel and apparent resistivity functions for $k = \pm 0.8$.

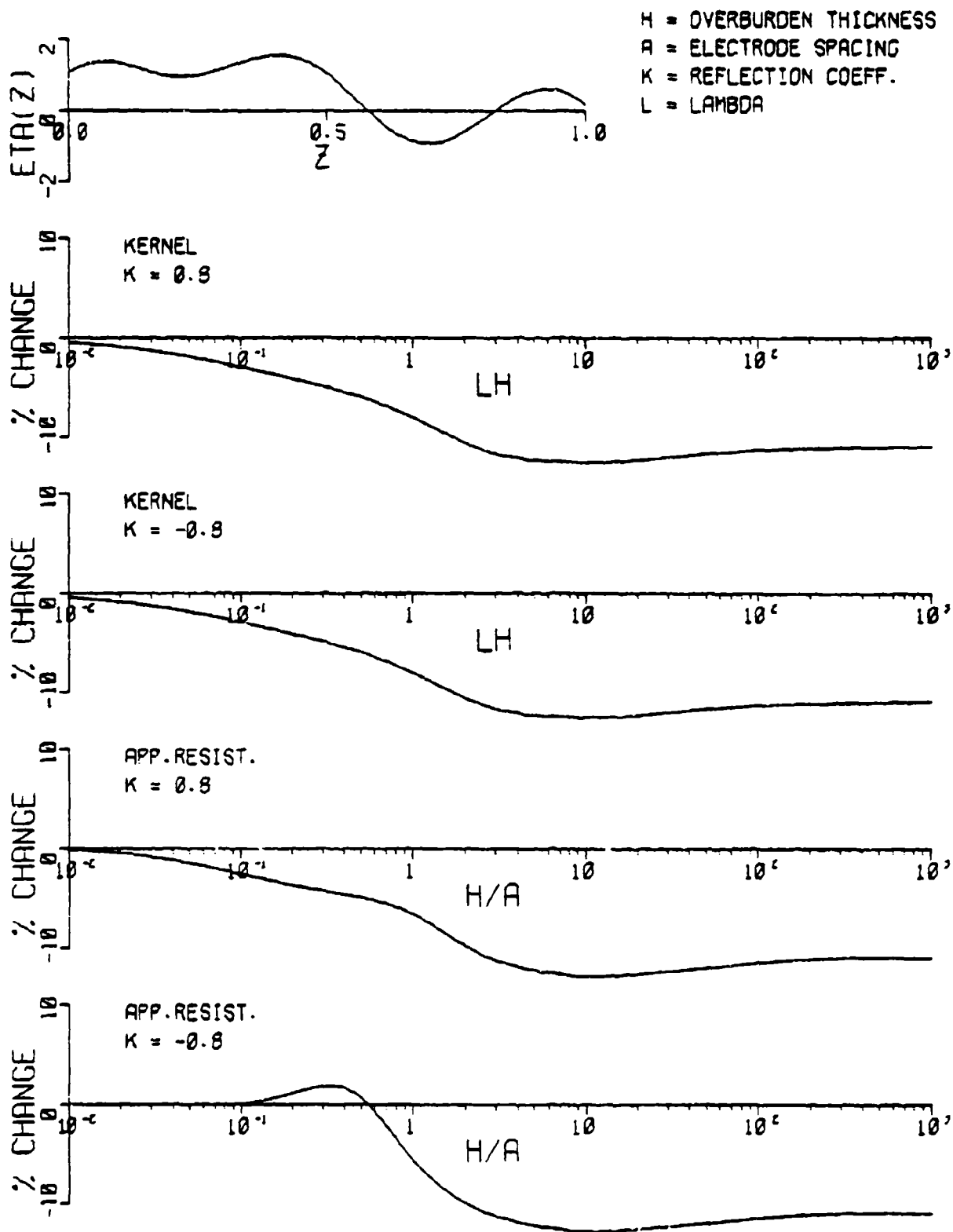


Figure 31. Sample realization No. 4 of percent deviation in kernel and apparent resistivity functions for $k = \pm 0.8$.

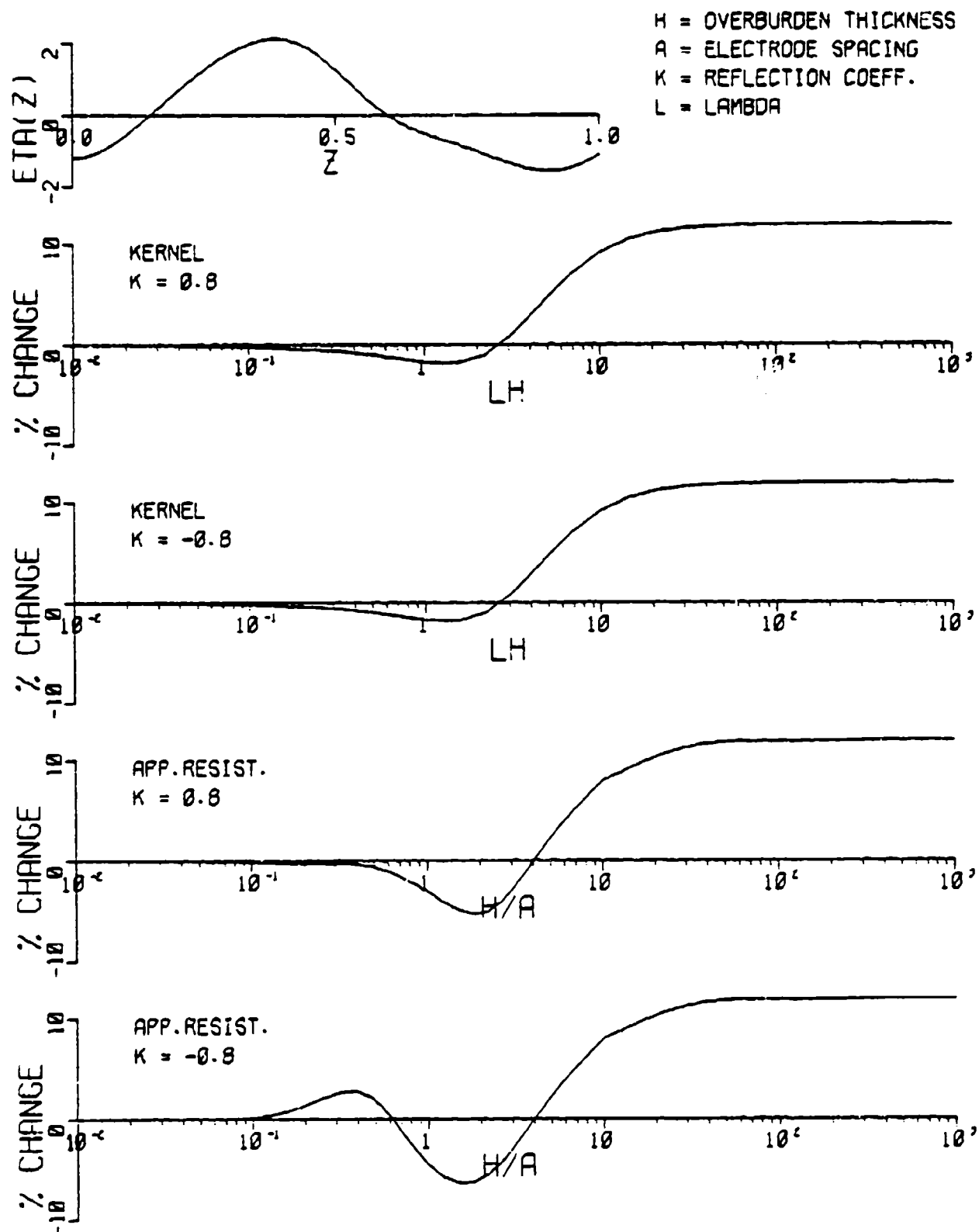


Figure 32. Sample realization No. 5 of percent deviation in kernel and apparent resistivity functions for $k = \pm 0.8$.

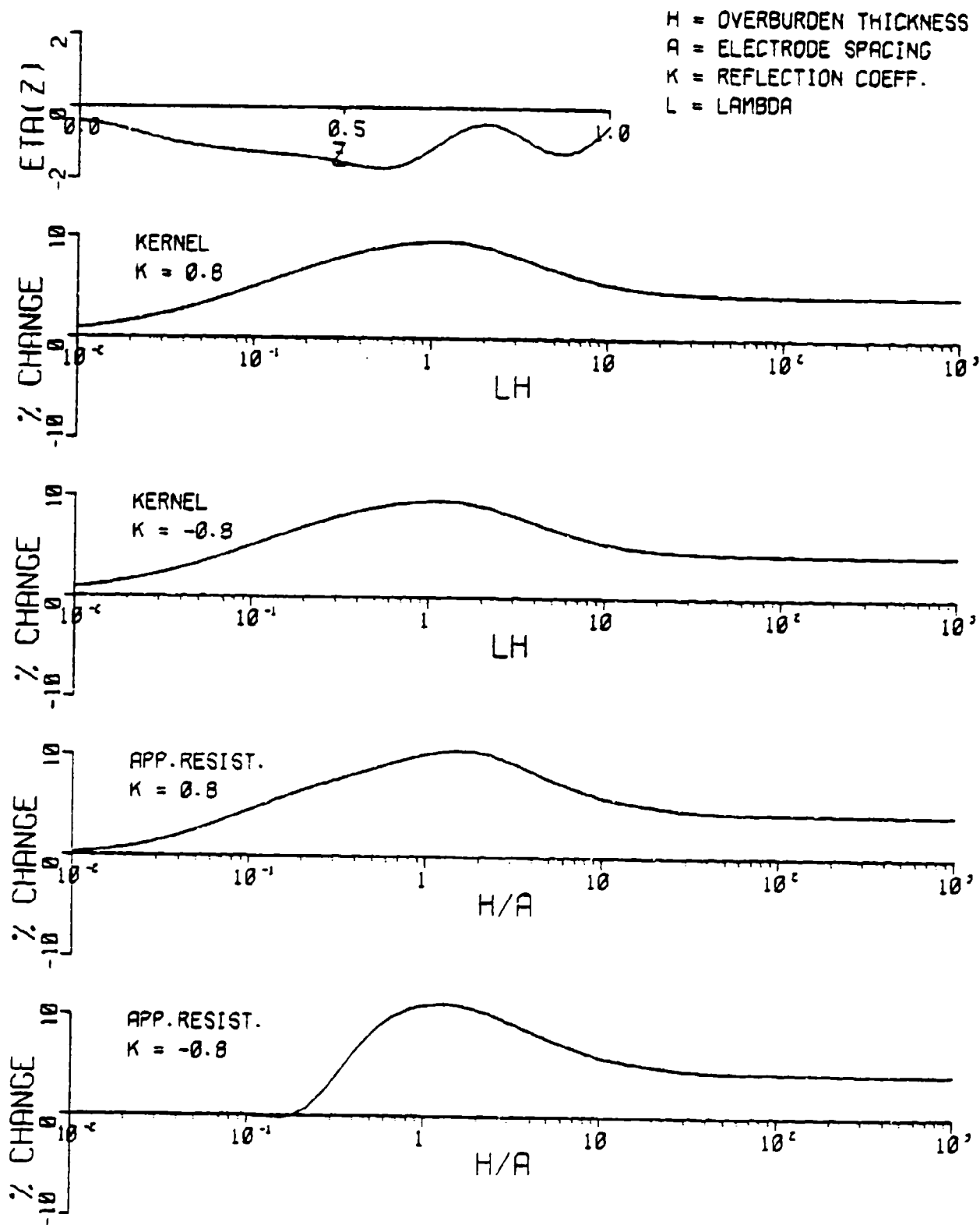


Figure 33. Sample realization No. 6 of percent deviation in kernel and apparent resistivity functions for $k = \pm 0.8$.

H = OVERBURDEN THICKNESS
 A = ELECTRODE SPACING
 K = REFLECTION COEFF.
 L = LAMBDA

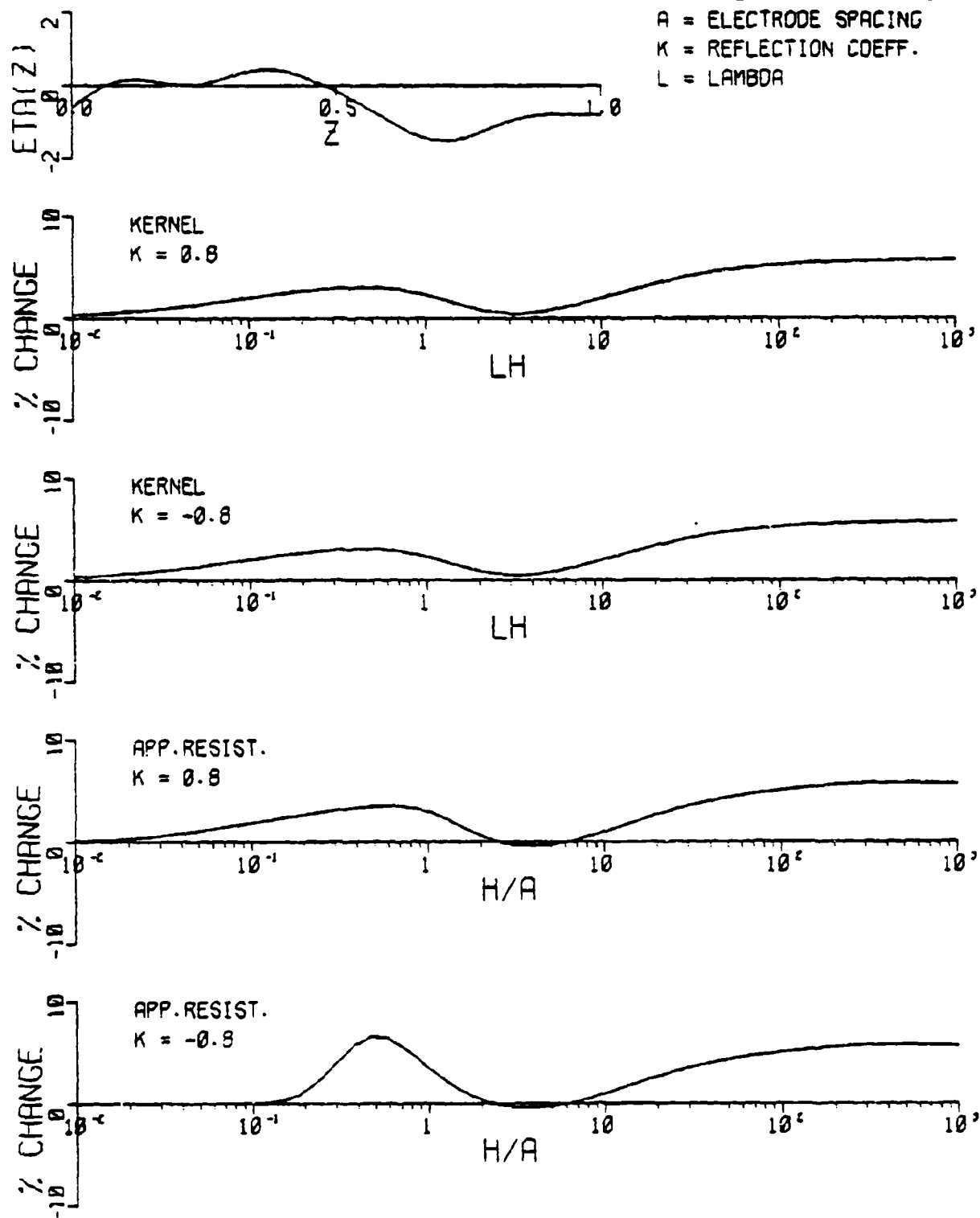


Figure 34. Sample realization No. 7 of percent deviation in kernel and apparent resistivity functions for $k = \pm 0.8$.

It is interesting to note that the curves for $k = + 0.8$ and $k = - 0.8$ are identical. To see the theoretical basis for this let us write

$$\frac{|K_1(\lambda)|}{K_0(\lambda)} = 2\lambda \int_0^h \eta(z) e^{-2\lambda z} dz + \frac{4k^2\lambda}{(1-k^2 e^{-4\lambda h})} \int_0^h \eta(z) e^{-4\lambda h} \cosh 2\lambda z dz. \quad (4-3)$$

Evidently, this ratio is independent of the sign of k . The magnitude of k , however, does affect the ratio. Inasmuch as the ratio, for large λ , depends only on the first term in the equation above, it is independent of the magnitude of k . For small λ values however, the second term becomes significant; its value increases as $|k|$ increases. In any case, this ratio tends to zero as λ approaches zero. This discussion is supported by Figures 35 and 36 for $k = \pm 0.5$ and $k = \pm 0.99$ respectively. They are to be compared to Figure 28 which uses the same realization of the random function.

Apparent resistivity: As noted previously, the normalized apparent resistivities for the Wenner and Schlumberger arrays are, respectively,

$$\rho_w^*(a) = 2a \int_0^\infty K(\lambda) \{J_0(\lambda a) - J_0(2\lambda a)\} d\lambda \quad (4-4)$$

and

$$\rho_s^*(a) = a^2 \int_0^\infty K(\lambda) \lambda J_1(\lambda a) d\lambda. \quad (4-5)$$

Only the Wenner array will be used for the following discussion.

Since $K(\lambda) = K_0(\lambda) + \epsilon K_1(\lambda)$ equation (4-4) can be decomposed into deterministic and stochastic parts:

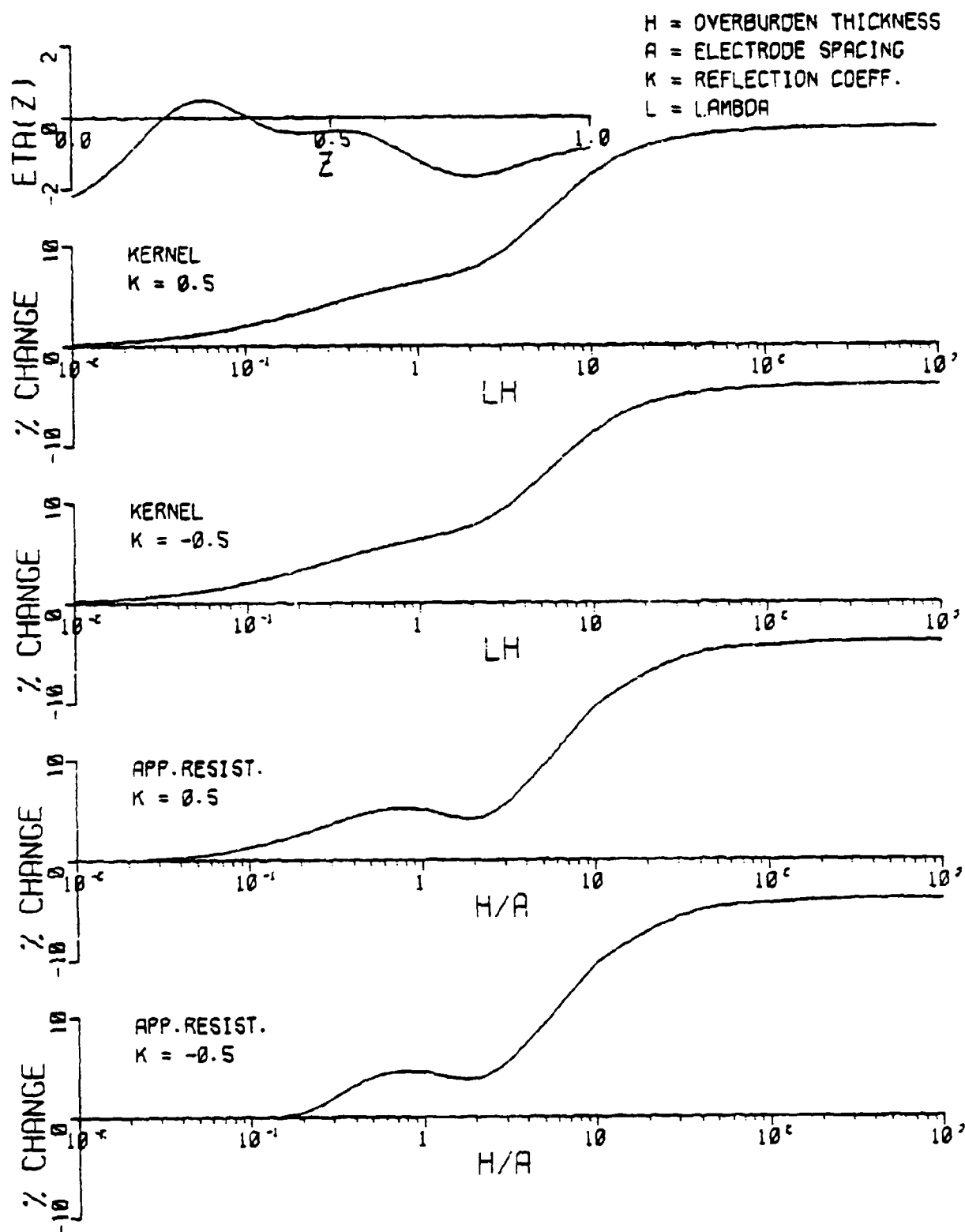


Figure 35. Sample realization No. 1 of percent deviation in kernel and apparent resistivity functions for $k = \pm 0.5$.

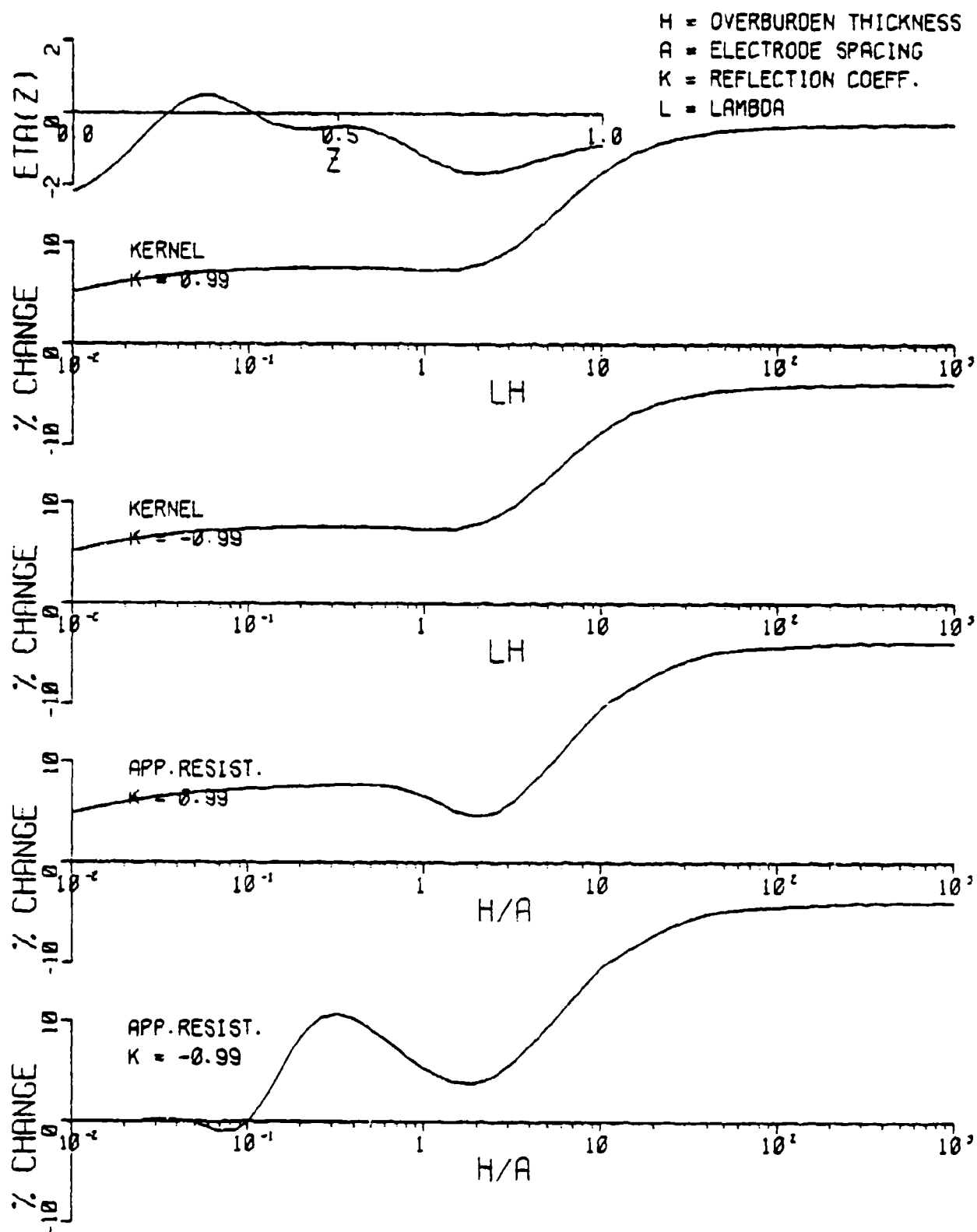


Figure 36. Sample realization No. 1 of percent deviation in kernel and apparent resistivity functions for $k = \pm 0.99$.

$$\rho_{w,0}^* = 2a \int_0^\infty K_0(\lambda) \{J_0(\lambda a) - J_0(2\lambda a)\} d\lambda \quad (4-6)$$

$$\begin{aligned} \rho_{w,1}^* = & -4a \int_0^h n(z) \int_0^\infty f_1 \{J_0(\lambda a) - J_0(2\lambda a)\} d\lambda dz \\ & -8ak^2 \int_0^h n(z) \int_0^\infty f_2 \{J_0(\lambda a) - J_0(2\lambda a)\} d\lambda dz \quad (4-7) \end{aligned}$$

$$\text{where } f_1(\lambda, z) = \frac{\lambda(1+ke^{-2\lambda h})e^{-2\lambda z}}{(1-ke^{-2\lambda h})} \quad (4-8)$$

$$f_2(\lambda, z) = \frac{\lambda e^{-4\lambda h} \cosh 2\lambda z}{(1-ke^{-2\lambda h})^2} \quad (4-9)$$

A rapid and reasonably accurate procedure for evaluating Hankel transform integrals is the use of digital linear filters. This method is already well established (for example Ghosh, 1971 and Anderson, 1975). In general, this approach is about five times faster than numerical integration by Gaussian quadrature and provides acceptable accuracy of about four significant figures (Anderson, 1974).

In order for this method to be applicable however, the functions to be transformed (f_1 and f_2 in this case) must be monotonic decreasing as $\lambda \rightarrow \infty$. Inspection of equation (4-8) reveals that f_1 satisfies this requirement except when $z = 0$. In this special case one can expand f_1 as an infinite series, find the Hankel transform analytically term by term (Erdélyi, 1954) and finally obtain a power series expression as follows:

$$\int_0^{\infty} f_1(\lambda, 0) J_0(\lambda r) = 4h \sum_{n=1}^{\infty} \frac{nk^n}{((2nh)^2 + r^2)^{3/2}} \quad (4-10)$$

It is interesting to note that even when $z = 0$ the digital filter approach yields results of acceptable accuracy when compared with the exact value as given in equation (4-10).

Similarly, it can be shown that f_2 approaches zero as $\lambda \rightarrow \infty$ for all values of z . Hence, we can apply Hankel transform filters for the evaluation of part of equation (4-7).

Equation (4-6) for the deterministic term can also be evaluated by the digital filter approach if it is rewritten in the form

$$\rho_{w,0}^* = 1 + 4a \int_0^{\infty} \frac{ke^{-2\lambda h}}{1 - ke^{-2\lambda h}} \{J_0(\lambda a) - J_0(2\lambda a)\} d\lambda \quad (4-11)$$

Seven representative sample realizations of normalized Wenner apparent resistivity curves for $\alpha = 0.05$, $\epsilon = 0.1$ and $k = \pm 0.8$ are shown in Figures 37 through 43. The abscissae are in dimensionless units of a/h . These curves are similar to those for the kernel functions (if the abscissae are reversed) except for the well known fact that apparent resistivity curves are not symmetrical about the line $\rho_w^* = 1$ for positive and negative values of k ; the kernel function, on the other hand, is symmetrical about the line $K(\lambda) = 1$ for positive and negative values of k .

It is intuitively obvious that as the electrode spacing a approaches zero, the normalized apparent resistivity approaches $1 - \epsilon n(0)$. As the spacing a becomes large ρ_w^*

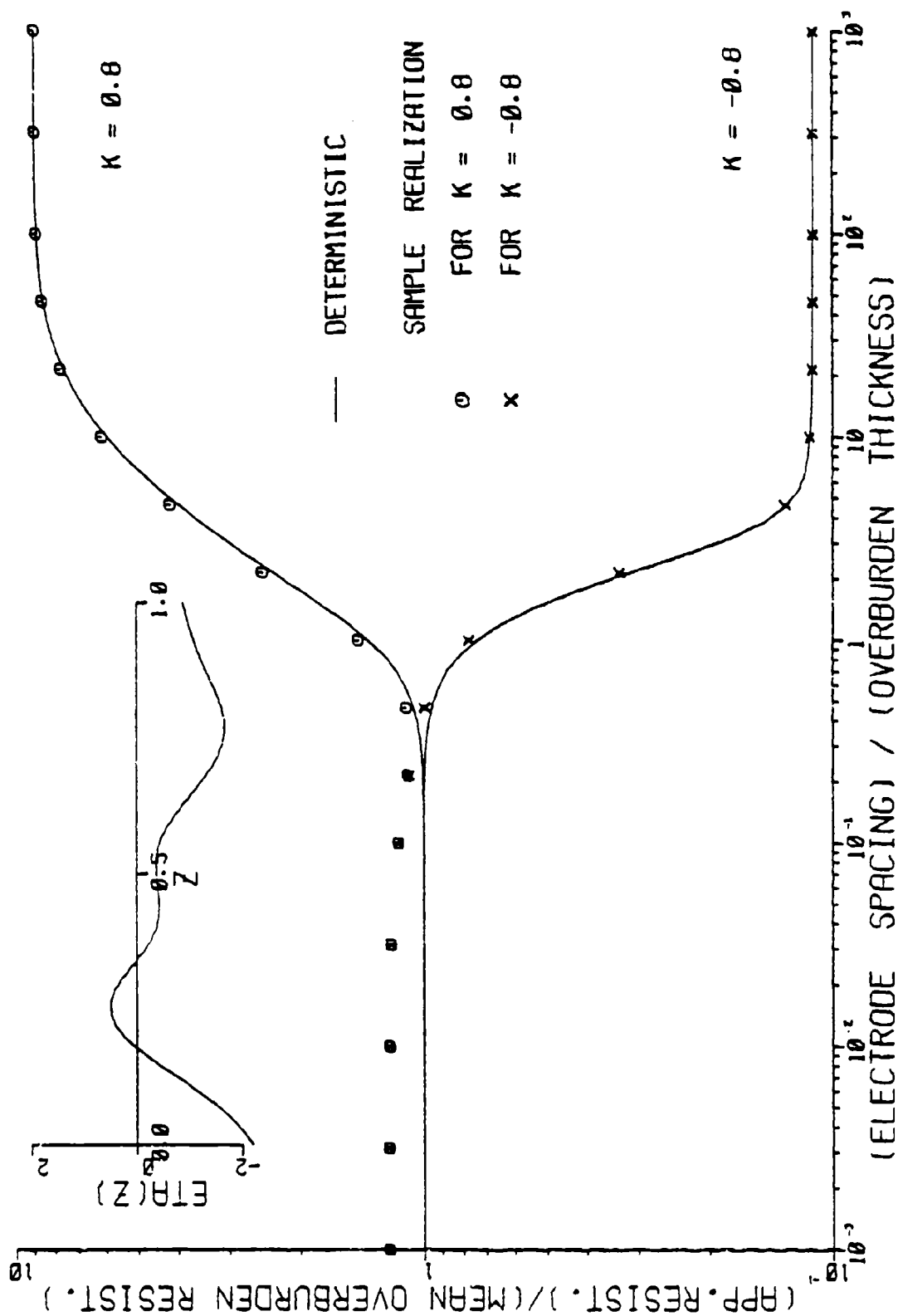


Figure 37. Sample realization No. 1 of apparent resistivity function for $k = \pm 0.8$.

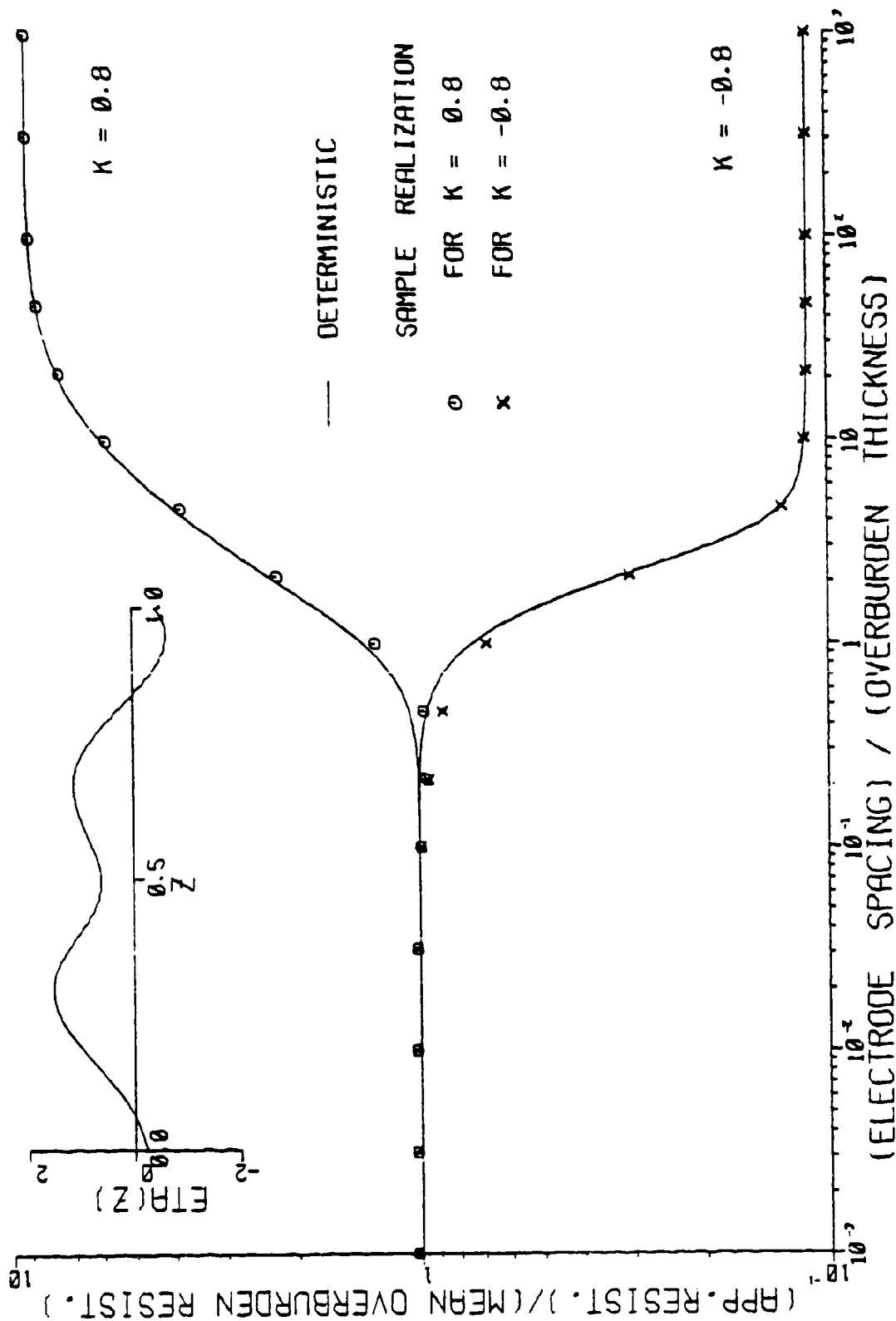
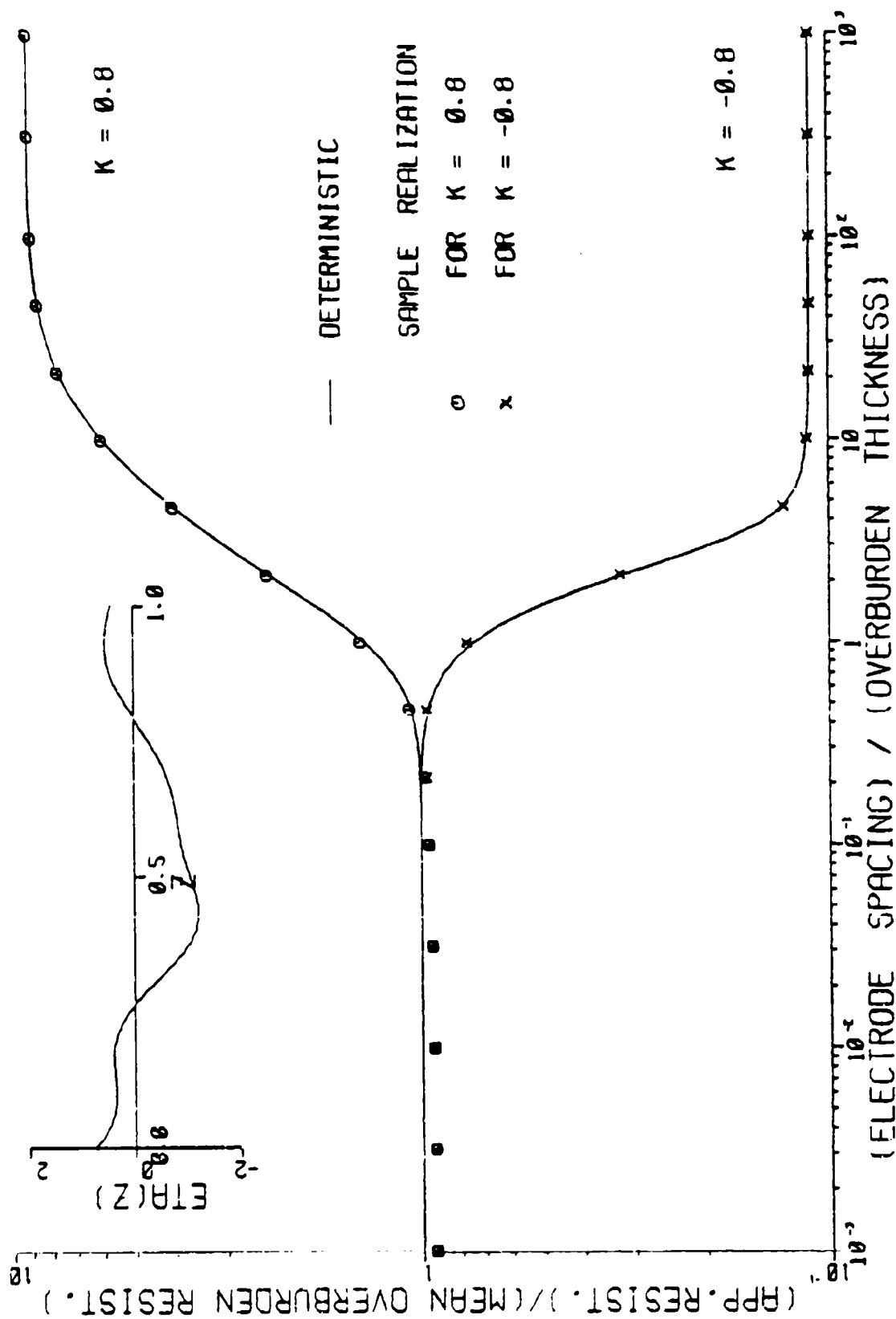


Figure 38. Sample realization No. 2 of apparent resistivity function for $k = \pm 0.8$.

Figure 39. Sample realization No. 3 of apparent resistivity function for $k = \pm 0.8$.

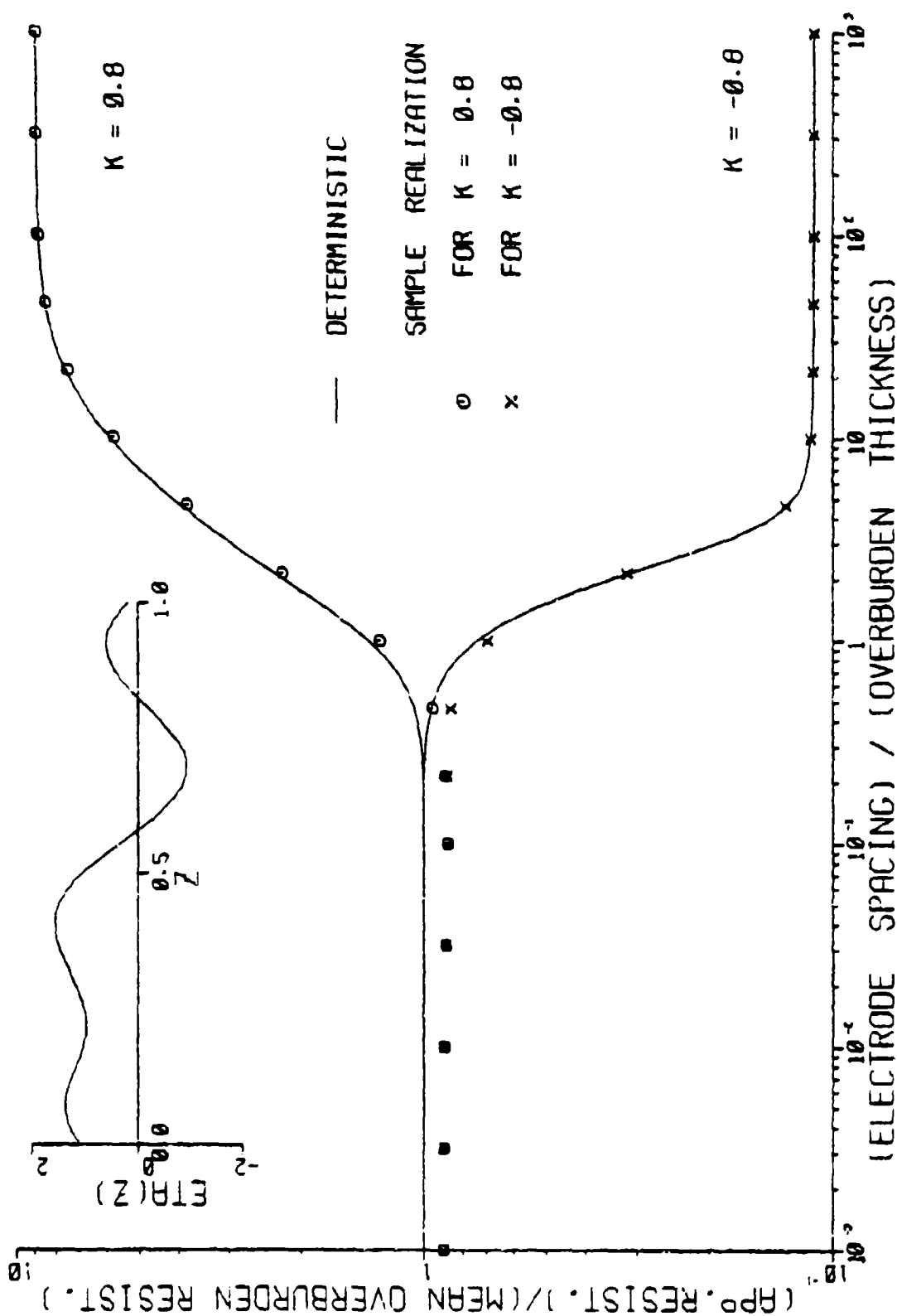


Figure 40. Sample realization No. 4 of apparent resistivity function for $k = \pm 0.8$.

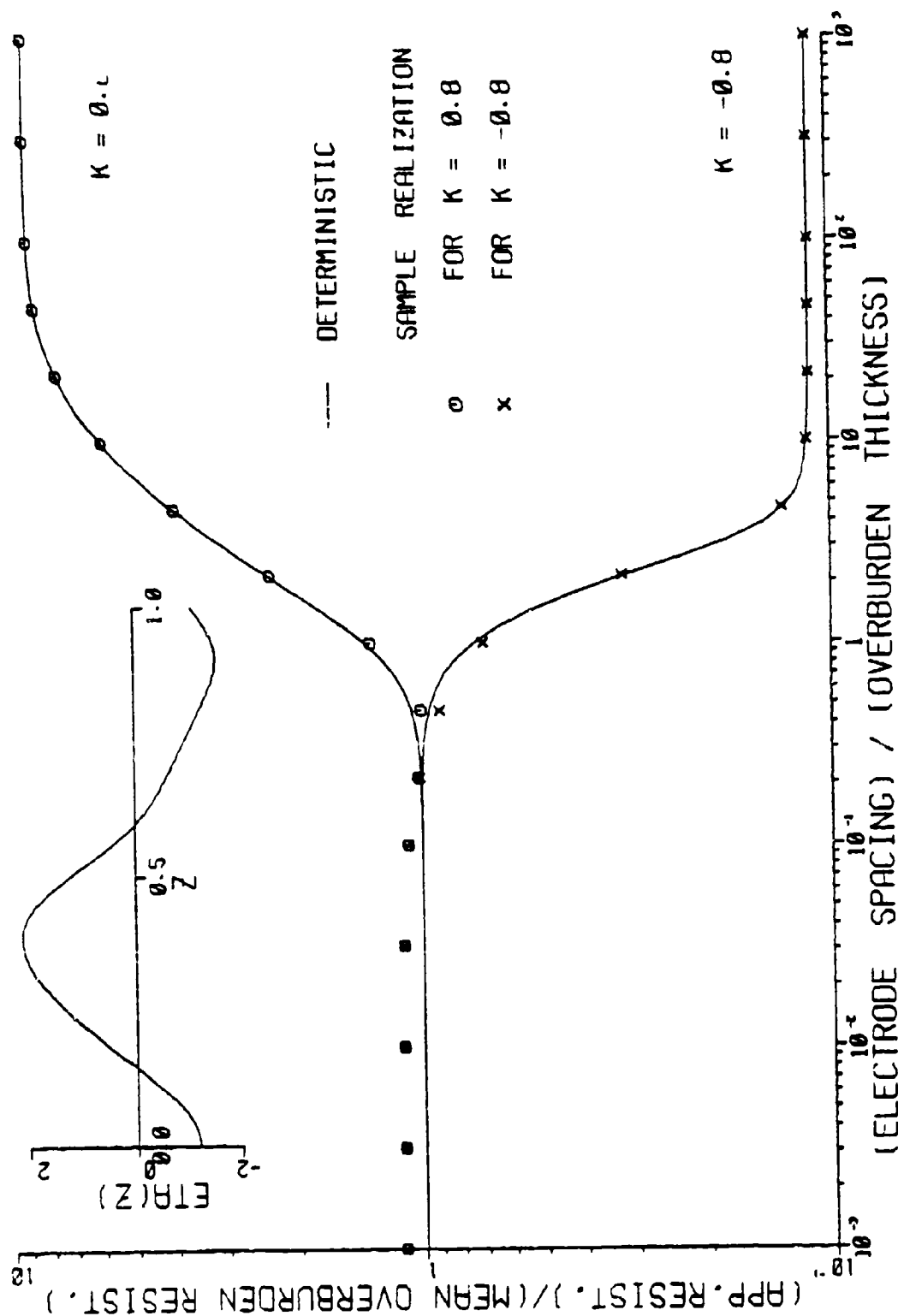


Figure 41. Sample realization No. 5 of apparent resistivity function for $k = \pm 0.8$.

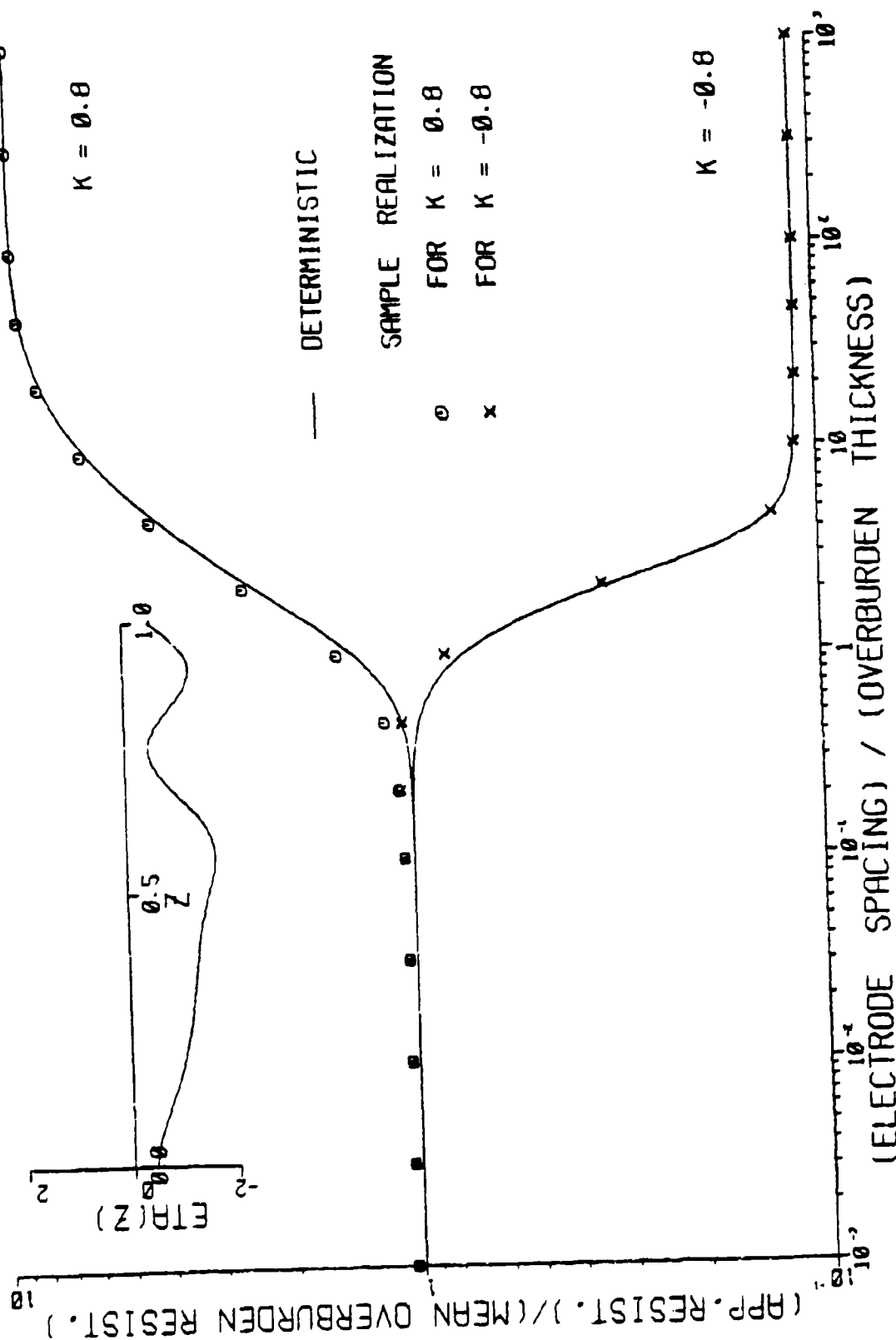


Figure 42. Sample realization No. 6 of apparent resistivity function for $k = \pm 0.8$.

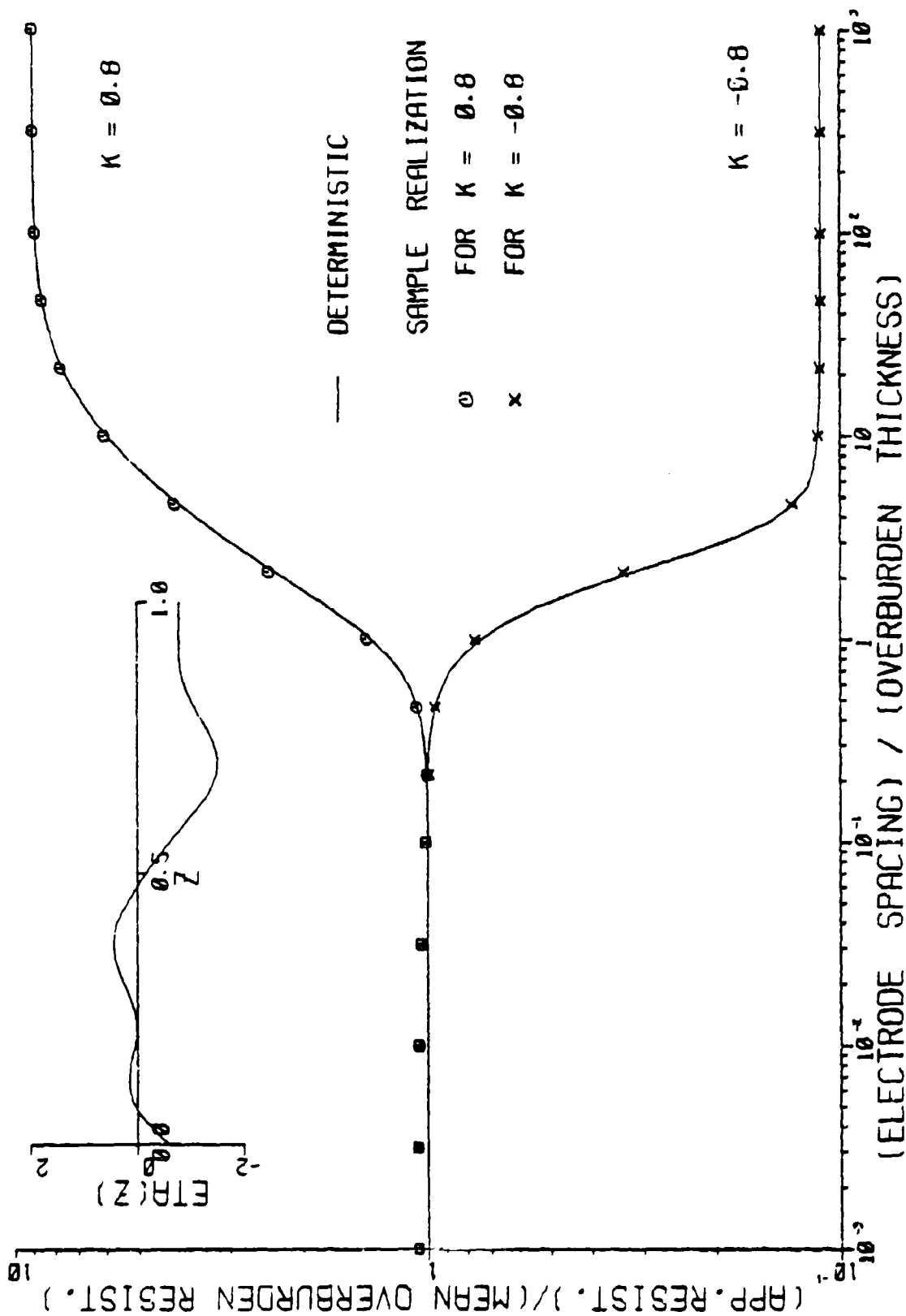


Figure 43. Sample realization No. 7 of apparent resistivity function for $k = \pm 0.8$.

approaches the deterministic value of $(1 + k)/(1 - k)$ as the effect of the random nature of the overburden becomes negligible. Most of the information in this part of the sounding curve is returned from the basement.

The relative deviations from the mean apparent resistivity curves are shown in the lower halves of Figures 28 to 36. The asymmetric nature of the apparent resistivity curves with respect to the sign of k is quite apparent. It is interesting to note that the curves for positive k are remarkably similar to those for the kernel function.

As in the case of the kernel function an increase in the magnitude of k increases the relative change in the apparent resistivity curves for large electrode spacings, but has no effect for small spacings. The difference between the curves for positive and negative values of k is accentuated if k has a greater magnitude.

Ensemble Statistics

It has been well established in the literature that the kernel function embodies all the information about layer parameters which are contained in the apparent resistivity curve itself. In the interest of economy in computation time the study of ensemble statistics is confined to the kernel function instead of the apparent resistivity function to which it is related via a Hankel transformation.

Equation (2-24) rewritten in a more convenient form becomes

$$K_1(\lambda) = W \int_0^{\infty} (q_1 + q_2 + q_3) N(\omega) d\omega \quad (4-12)$$

where

$$W(\lambda) = - \frac{4\lambda}{\phi}$$

$$q_1(\omega, \lambda) = \frac{2\lambda\nu}{\mu}$$

$$q_2(\omega, \lambda) = - \frac{2\lambda e^{-2\lambda h}(1-k^2)\cos \omega h}{\phi \mu}$$

$$q_3(\omega, \lambda) = \frac{e^{-2\lambda h}(1+k^2) \omega \sin \omega h}{\phi \mu}$$

The mean $\langle K_1(\lambda) \rangle$ is obviously zero since $\langle N(\omega) \rangle$ is zero. The covariance is

$$\langle K_1(\lambda_1) K_1(\lambda_2) \rangle = \frac{\alpha q^2}{\sqrt{\pi}} W(\lambda_1) W(\lambda_2) \int_0^{\infty} T(\omega, \lambda_1) T(\omega, \lambda_2) e^{-\alpha^2 \omega^2} d\omega \quad (4-13)$$

where $T = q_1 + q_2 + q_3$.

Convergence of the integral is assured by the presence of the exponential term. The covariance, normalized by the standard deviations, is

$$R(\lambda_1, \lambda_2) = \frac{\langle K_1(\lambda_1) K_1(\lambda_2) \rangle}{\{\langle K_1(\lambda_1) K_1(\lambda_1) \rangle \langle K_1(\lambda_2) K_1(\lambda_2) \rangle\}^{1/2}} \quad (4-14)$$

The normalized covariance, computed for representative values of λ and α are shown in Figures 44 and 45. It is clear that as α increases the stochastic kernel function becomes more correlated. In addition, the larger the λ value the more correlated is the random kernel. Thus, a more correlated

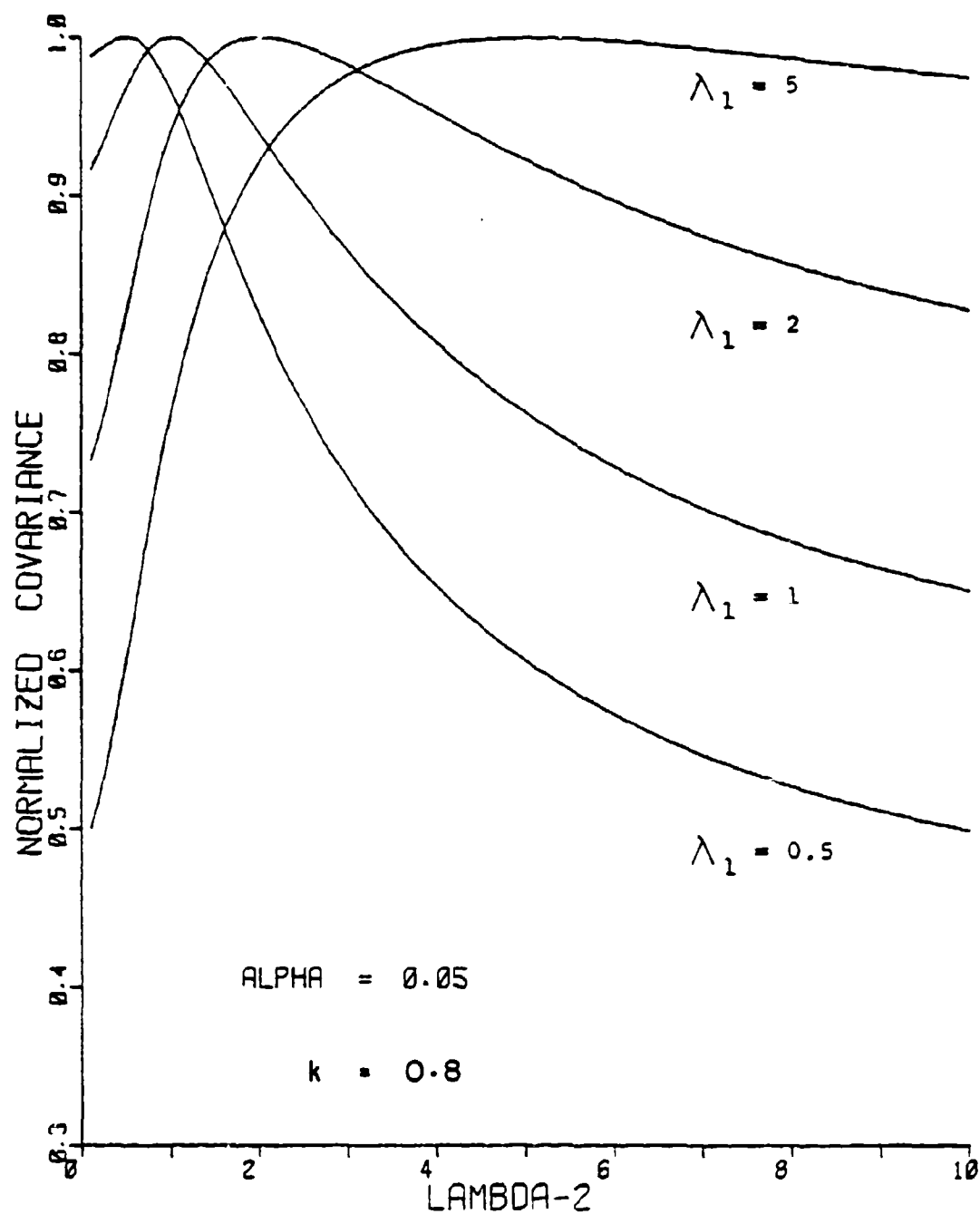


Figure 44. Normalized covariance of two-layer random kernel function for $\alpha = 0.05$.

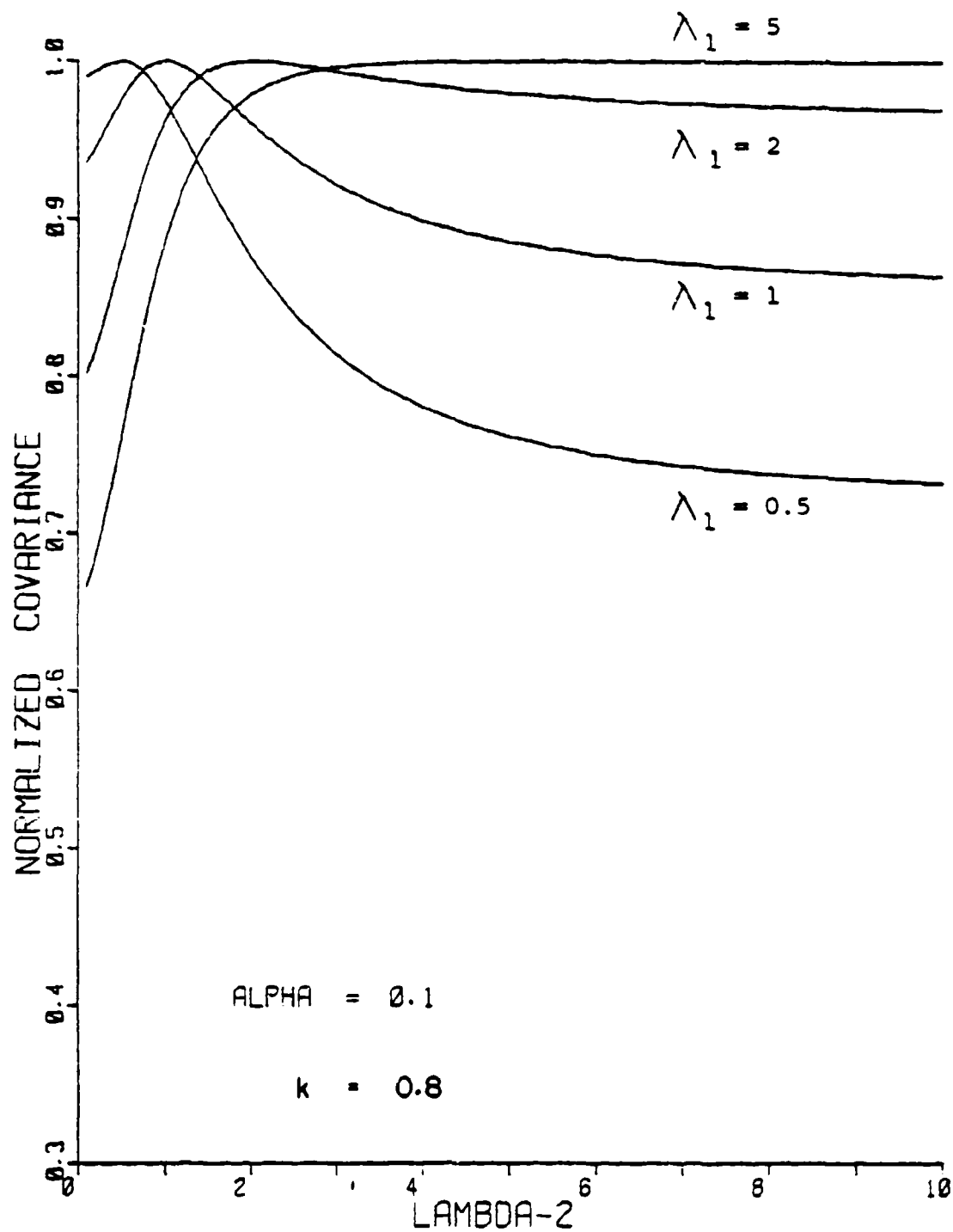


Figure 45. Normalized covariance of two-layer random kernel function for $\alpha = 0.1$.

random function $\eta(z)$ will be reflected in a more correlated random kernel function.

Sample Statistics

Two hundred sample realizations of the random kernel as given in equation (4-1) were computed and the distributions tabulated in the form of histograms. Some of these are shown in Figures 46 and 47. Using the chi-square goodness of fit test all the distributions generated for various α and λ values were found to be Gaussian at the 5% level of significance.

The computed means are generally much less than 0.05 while the standard deviations are approximately in the range 0.5 to 1.0. The coefficients of skewness are in general less than 0.2 in magnitude, being about evenly distributed between positive and negative values.

It is known that a Gaussian process preserves its Gaussian form after a linear transformation (Freeman, 1958). Inasmuch as the Hankel transformation of the kernel function to the apparent resistivity function is a linear process (Ghosh, 1971) one may conclude that the random apparent resistivities are, at the 5% level of significance, normally distributed about their mean values.

Effect on Interpretation of Data

It is appropriate at this point to pose the following questions. What effect does a random distribution of earth conductivities have on resistivity sounding curves? To what

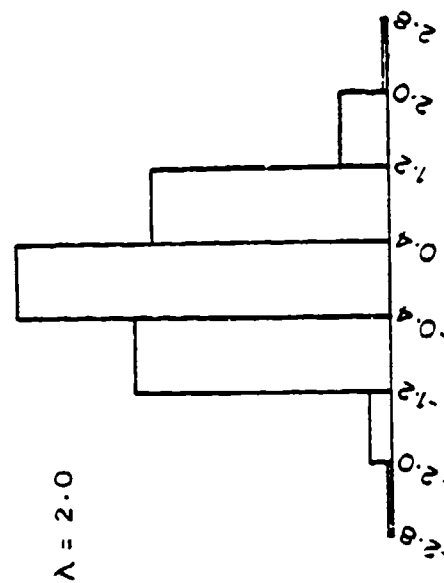
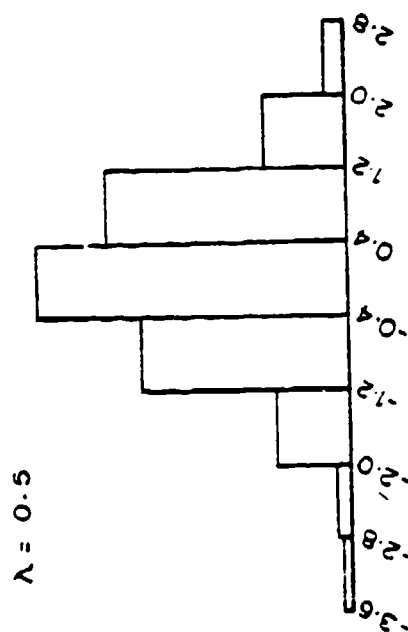
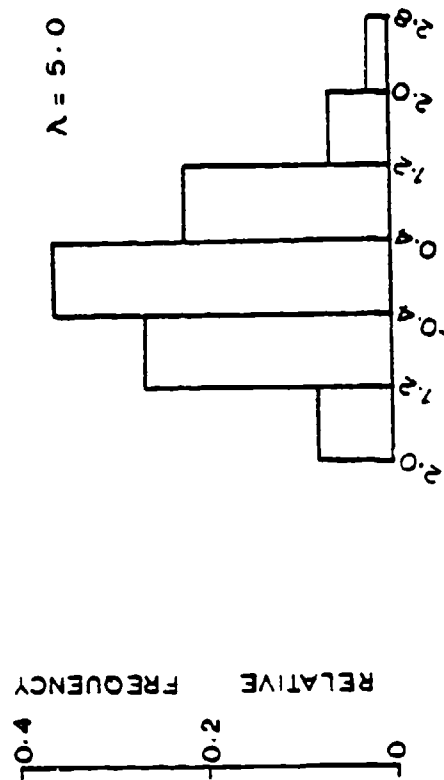
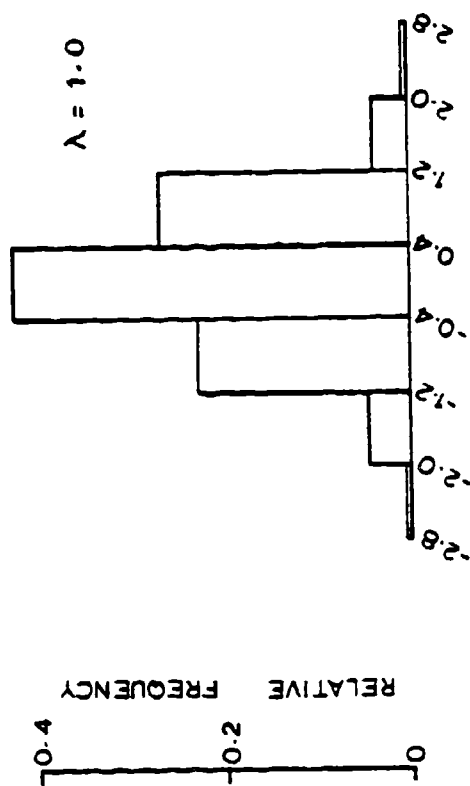


Figure 46. Distributions of sample realizations of two-layer random kernel function for $\alpha = 0.05$.

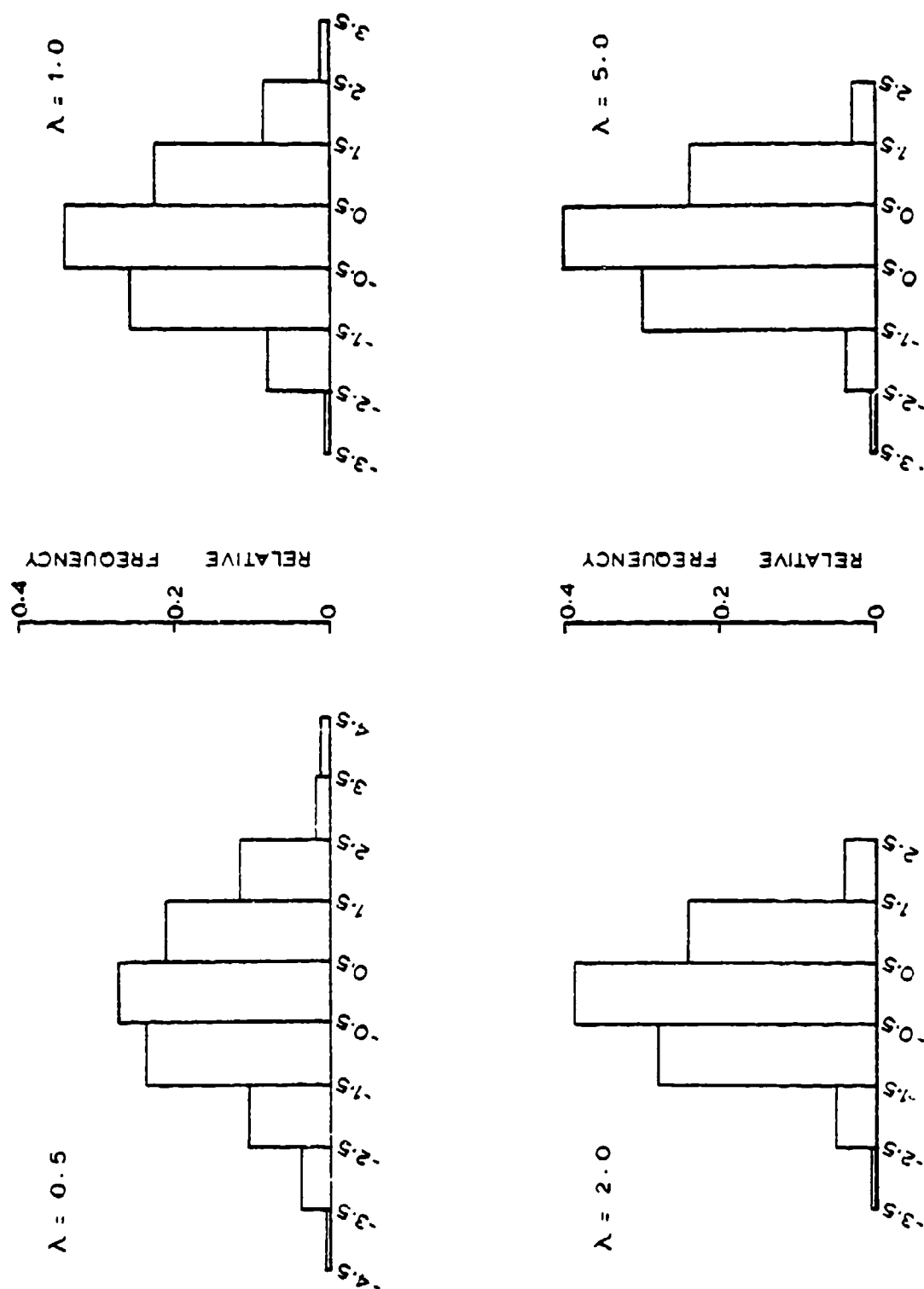


Figure 47. Distributions of sample realizations of two-layer random kernel function for $\alpha = 0.5$.

extent is the interpretation of resistivity data affected? How can these effects be taken into consideration during data interpretation? These and related questions will be discussed in the following paragraphs.

The effect of the random nature of the distribution of conductivities on an apparent resistivity sounding curve is greatest for small electrode spacings. With small spacings we are, effectively, probing only the shallower regions of the earth. It is evident from the results presented previously that as the electrode spacing a decreases the apparent resistivity approaches the resistivity of the near-surface zone, that is,

$$\rho(a) = \rho^0(1 - \epsilon\eta(a))$$

As the spacing a increases more and more information is returned from the deeper regions of the earth and the apparent resistivity approaches the resistivity ρ_2 of the lower layer (basement). In this case, the random conductivity profile in the overburden has a negligible effect. Thus, the net effect of the random conductivity distribution in the overburden is to shift the part of the sounding curve for small a up or down (in the sense of the vertical apparent resistivity axis of the curve) relative to the part of the curve for large a according as $\rho(a)$ is greater or less than the mean overburden resistivity ρ^0 . This relative shift can be considerable depending directly on how much $\rho(a)$ deviates from ρ^0 . As

a practical example, the near-surface zone of a sedimentary section is probably drier than the lower zones. This results in an increase in its resistivity relative to the rest of the section.

The variability in the resistivity profile tends to be smoothed out in the sounding curve. Consequently, the earth may be viewed as a high frequency filter for the noise in the system. The shape of the resulting sounding curve depends to a large extent on the function $\eta(z)$. However, the value $\eta(0)$ has a disproportionate effect on this. The apparent resistivity curve may resemble a two-layer curve, as is usually the case (for example Figures 39 and 40) or there may be distinct indications of an "intermediate layer" as in Figure 37. Such deviations are usually small and are difficult to detect. In addition, measurement noise (which includes instrument noise, human error and lateral inhomogeneities) tends to mask these small deviations. In practice these curves would tend to be considered as two-layer curves with slightly different parameters.

For a semi-quantitative estimate of the magnitude and type of errors introduced in the interpretation of such curves we will resort to standard curve-matching techniques. Several two-layer apparent resistivity curves were traced from the standard curves of Orellana and Mooney (1966). Deviations of $\pm 10\%$ and $\pm 20\%$ were then introduced into the parts of the curves which correspond to small electrode